Characterization of the cis-regulatory regions governing *ojoplano* locus

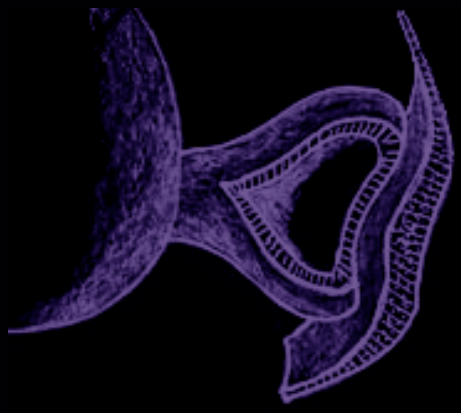

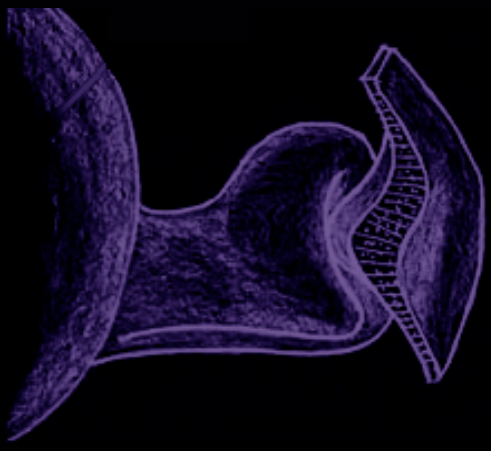

Inês Gago Rodrigues

Never lose a Holy Curiosity

Albert Einstein

Cover: Development of the eye : Optic cup

To my parents

Funding:
Fundação para a Ciência e Tecnologia, Ministério da Ciência, Tecnologia e Ensino Superior – Portugal (ref: SFRH/BD/60489/2009)

Doctoral Thesis

Characterization of the cis-regulatory regions governing *ojoplano locus*

Inês Gago Rodrigues

Director: Juan Ramón Martinez Morales

Centro Andaluz de Biología del Desarrollo

Universidad Pablo de Olavide/ CSIC

October 2013

Contents

Tables and figures

Acronyms

NCRE	non-coding regulatory element
TF	Transcription factor
bp	Base pairs
kb	Kilobase
Mb	Megabase
NR	Neural retina
RPE	Retina pigmented epithelium
RPC	Retina progenitor cell
PNRE	Putative non-coding regulatory element
H1hesc	H1 human embryonic stem cell
Hmec	Human mammary epithelial cells
Hsmm	Human skeletal muscle myocytes
Huvec	Human umbilical vein endothelial cell
Nhek	Natural human epidermal keratinocytes
Nhlf	Natural human lungs fibroblast
hpf	hours *post* fertilization
CNC	Cranial neural crest
CNS	Central nervous system
BS	Binding sites
MO	Morpholino
OFC	orofacial clefting
TS	Tourette syndrome

I. Introduction

1. Regulation of Developmental Genes

During the embryogenesis of multicellular organisms, developmental genes control the regulatory networks responsible for directing the morphogenesis of the different tissues. The transcriptional regulation of these genes requires a precise orchestration of *non*-coding cis-regulatory elements (NCREs), which are genomic sequences often conserved throughout the entire vertebrate's lineage.

NCREs can be active or inactive elements, depending on their interactions with proteins and promoter sequences present in its genomic environment. These elements are found in the same DNA molecule of the gene that they regulate and contain specific binding sites for transcription factors that regulate gene activation or inhibition (Gomez-Skarmeta et al., 2006).

Comparative genomic analyses have revealed recently a collection of approximately 3000 NCREs in vertebrates (Bejerano et al., 2004; Sandelin et al., 2004); the majority of these regions have been found to be in the vicinity of important morphogenetic genes, with essential functions during development (Sandelin et al., 2004; Woolfe et al., 2005). Additionally, functional studies have reported that a large proportion of the NCREs contain either enhancer o silencer elements that regulate the expression of developmental genes in specific domains of the embryo (Gomez Skarmeta, 2009). These findings indicate that the regulatory elements hidden in the non-coding genome play an essential role in gene expression regulation during development.

In this work, I have focussed in the identification of NCREs found in the landscape of a developmental gene called *ojoplano* and in the potential of these NCREs to act as enhancers, activating gene expression.

2. The role of enhancers during embryonic development

Enhancers are major determinants of differential spatio-temporal expression. In other words, they determine where and when a gene promoter will be used, and how much of the gene product will be synthesized. Each of these regulatory elements interact physically with a specific gene promoter to control the efficiency and rate of transcription; they can be specific for one gene or for a group of genes. Additionally, they can activate transcription independently of their location, distance or orientation with respect to the promoter (Banerji et al., 1981) (Figure 1).

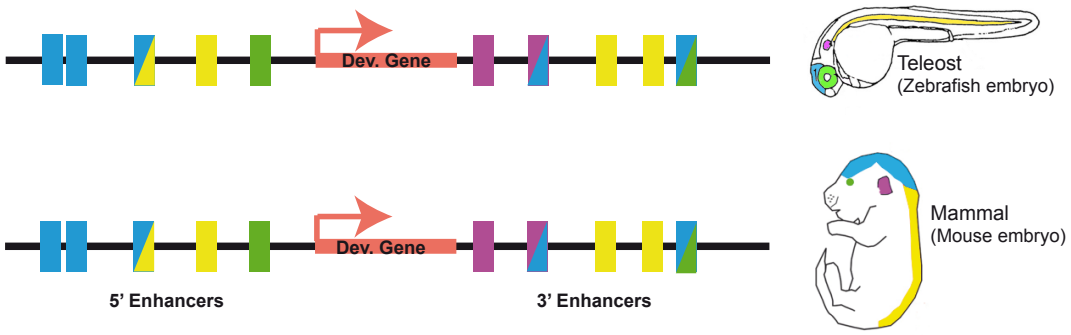

Figure 1. Tissue-specific gene expression is regulated by enhancer activity. Conserved enhancers are represented as rectangular boxes along the DNA sequence (black line) of tow different species: zebrafish (*Danio rerio*) and mouse (*Mus musculus*). The enhancers are distributed upstream and downstream from the gene they regulate (red arrow). Each color represents the activity of an enhancer in a specific domain of the embryo. Enhancers activate the transcription in a combinatorial way (multiple enhancers in the same domains of the embryo) and its activity can be modulated in one or other direction (two-color enhancers).

These regulatory regions are enriched in transcription factor binding sites, which bind to enhancer or promoter regions, activating or repressing the synthesis of mRNA from a particular gene. Transcription factors (TFs) include three major protein domains: the DNA-binding domain that recognizes a specific sequence in the DNA, the trans-activating domain that activates or represses transcription and finally a protein-protein interaction domain that allows the transcription factor activity to be modulated by other TFs and proteins. TFs within the same family share a common framework in their DNA binding sites (Graf and Enver, 2009).

Interestingly, one TF can bind to different enhancers activating the expression of different genes in different cell types. In this sense, it is the combination of several transcription factors acting on several enhancers that causes particular genes to be transcribed. Moreover, a gene can have numerous enhancer elements, each of them turning the gene on in a specific subset of cells (Graf and Enver, 2009) (Figure 2).

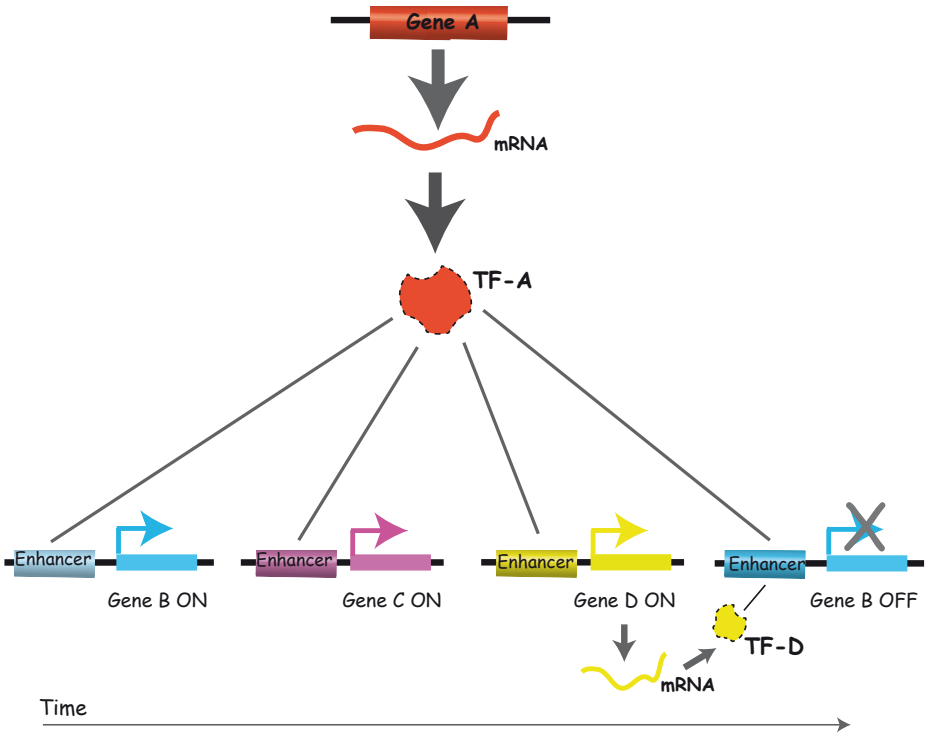

Figure 2. Transcription factors regulate gene expression through enhancer activation/inactivation. Gene A transcribes a transcription factor (TF-A). TF-A turns on genes B, C and D in a particular order. Gene D also encodes a transcription factor, TF-D. Later on in development, TF-A together with TF-D is necessary to stop the expression of gene B.

During gene expression activation, the promoter must be accessible to enhancers, TFs and other protein complexes, and this requires a decompaction of the chromatin fiber. Chromatin is constituted by nucleosomes, which are stretches of DNA, 147 base-pair (bp) long, wrapped around proteins called core histones. In the nucleosomes, core histones form an octamer, which consists of two copies of each core histone (H3, H4, H2A and H2B). The N-terminal tails of core histones are highly conserved between species and can be subjected to post-translational modifications, such as methylation, acetylation and ubiquitylation, which are additions of methyl, acetyl or ubiquitin groups onto the different lysines of histone H3 tail (Bannister and Kouzarides, 2011).

For the regulation of gene expression is required the generation of a nuclesome-free region nearby the gene promoter, which is associated with the distinct modifications in the histone tails. In fact, the localization of histone modification marks usually

indicates the position of enhancers and promoters. Active enhancers can be predicted by the monomethylation of histone H3 in lysine 4 (H3K4me1) and by the acetylation of the histone H3 at lysine 27 (H3K27ac), whereas inactive enhancers only show H3K4me1 mark. The promoters are marked with the trimethylation of histone H3 on lysine 4 (H3K4me3) and normally this histone modification marks transcription activation and subsequent gene expression (Heintzman et al., 2007; Heintzman et al., 2009; Creyghton et al., 2010) (Figure 3).

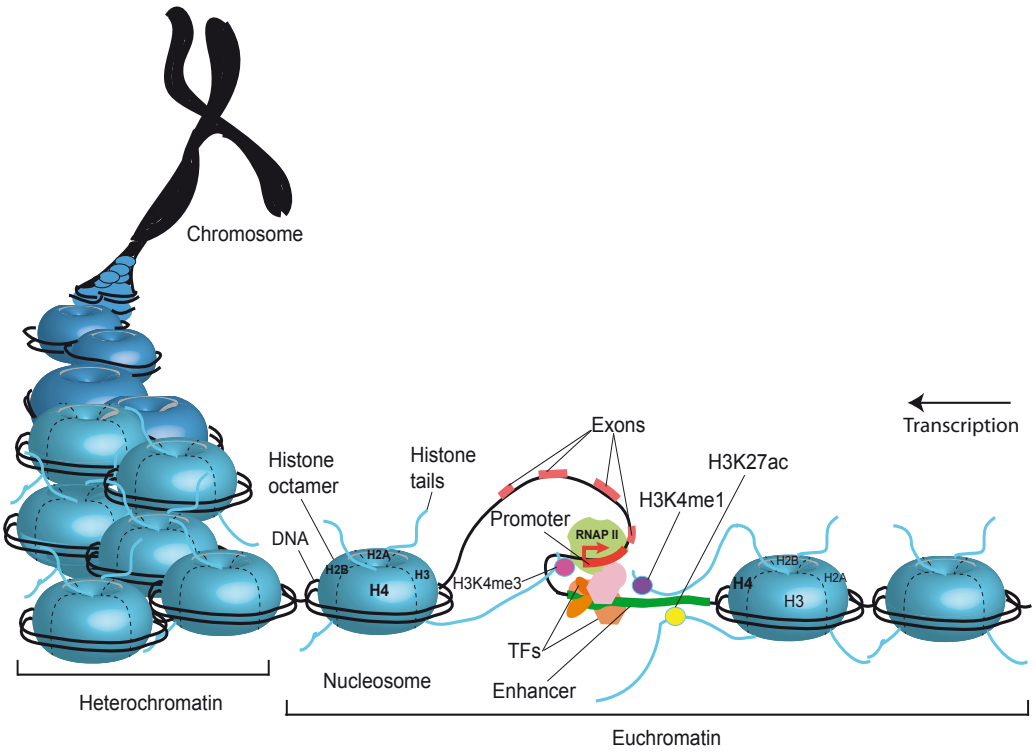

Figure 3. Transcription initiation process. The interactions between histone modification marks, enhancer-TFs and the RNA polymerase II transcription initiation protein complex (RNAP II) are required during gene transcription. For gene expression activation, chromatin must change its conformation from a compact fiber (heterochromatin) to an open fiber (euchromatin), which allows proteins and enhancers to access the gene promoter (red). During gene expression initiation, enhancers (green) marked with H3K4me1 (purple circle) and H3K27ac (yellow circle) are in contact with specific TFs (orange and light pink forms) and together they bind to the gene promoter (red), marked with H3K4me3 (dark pink circle). These interactions favor the binding of the RNAP II protein complex (light green) to the promoter and the transcription is then initiated.

New enhancers can be identified in the non-coding genome through enhancer-screenings (Bessa and Gomez-Skarmeta, 2011). These screenings scan the genome on the bases of sequence conservation and predictive epigenetic marks, elucidating not only the regulation of specific developmental genes, but also uncovering new developmental functions associated to hidden elements in the genome.

Enhancer-screenings can also contribute to the localization of regulatory regions controlling the activity of genes associated with human hereditary diseases, which are frequently developmental genes. These type of diseases caused by deletions, duplications, translocations or point mutations, can occur in either the coding or non-coding genome, as is the case for enhancers.

In this work we study the developmental gene *Ojoplano (opo),* which plays a crucial role during eye morphogenesis in fish (Martinez-Morales et al., 2009) and has been associated with human craniofacial hereditary diseases and schizophrenia (Box 1). We have performed an enhancer screening in the *opo locus* to investigate its regulation and functions during eye morphogenesis and to find out if any of its enhancers is localized in proximity to genetic markers previously associated to hereditary diseases (orofacial clefting and schizophrenia).

However, before discussing the regulation of *opo* during early eye morphogenesis, I will describe below the basic principles behind this developmental event.

Box 1: *opo* and human disease

Opo is a highly conserved developmental gene present in a single copy in vertebrate genomes. Its human ortholog (*ofcc1*) is located at the distal region of chromosome 6p (6p23.4), in a syntenic gene desert of approximately 2 Megabases (Mb). This locus represents only 2% of the chromosome, however it contains 23% of all its *non*-coding *cis*-regulatory elements, which may suggest the existence of complex regulatory logic in the region.

The *opo locus* in humans is associated with hereditary congenital diseases. Breakpoint mutations in patients with orofacial cleft syndrome have been associated with *ofcc1* (Davies et al., 2004). This congenital craniofacial defect is characterized by a deficient development of the palate that leads to the formation of clefts in both the lip and palate (Davies et al., 2004). Additionally, it has been shown that several genetic markers localized in the *ofcc1* region are associated to schizophrenia (Straub et al., 2002). Finally, patients with Tourette syndrome, a common neuro-developmental disorder, revealed the presence of a novel variant in the 5' untranslated region of the *ofcc1* gene (Sundaram et al., 2011).

3. Early eye development: patterning and morphogenesis of the optic cup

The developing brain can be subdivided into three anatomically distinct areas: the forebrain, the midbrain and the hindbrain. The eyes originate from a specialized region of the forebrain called the eye field (Adelmann, 1929).

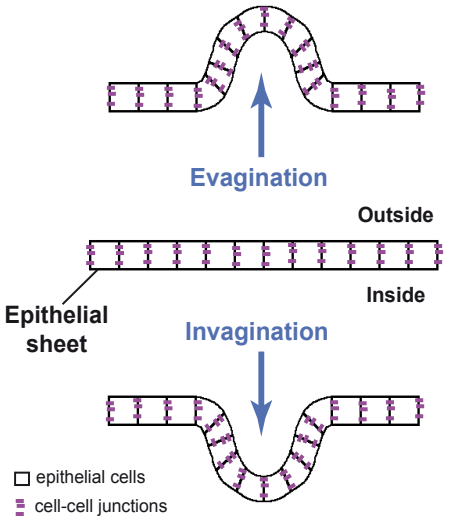

Figure 4. Evagination and invagination processes of an epithelial sheet of cells during development (adapted from http://www.aubrun.edu).

The eye field is composed of neuroepithelial cells that adhere each other through cell-cell junctions forming sheets (Figure 4). These cells have apical-basal polarity defined by distinct 'apical', 'lateral' and 'basal' plasma membrane domains. The apical membrane of the epithelial cells faces the future ventricular surface, the lateral membrane connect the neighboring cells and the basal membrane attach the cells to the basement membrane, which is a thin sheet of extracellular matrix proteins that separates the epithelial sheet from underlying cells (Bryant and Mostov, 2008). Normally epithelial sheets form cavities and surfaces during development along the animal body by evagination and invagination mechanisms (Figure 4).

The neuroepithelial cells from the eye field interact with the surrounding surface ectoderm and the extraocular mesenchyme, which have, respectively, originated from the neural crest and the mesoderm. Following the appearance of the eye field, the cells evaginate from both sides of the forebrain, resulting in the formation of the both bilateral optic vesicles (Figure 5-A).

Each optic vesicle then invaginates at its distal portion to form the optic cup (Figure 5-B and C), with the presumptive neural retina (NR) and retinal pigmented epithelium (RPE) forming the inner and outer walls. The most proximal part develops into the optic stalk, which is the structure that connects the optic vesicle to the forebrain

(Figure 5-D). At the same time, the surface ectoderm adjacent to the retina also invaginates and develops into the lens vesicle, while the rest of the surface ectoderm near the lens becomes the corneal epithelium. Following these morphogenetic events, the RPE and NR cells become specified and also spatially organized (Hilfer, 1983; Chuang and Raymond, 2002; Fuhrmann, 2010).

In summary, the early eye development can be organized in 4 steps: eye field establishment, optic vesicle evagination, optic vesicle patterning (RPE optic stalk and NR) and optic cup morphogenesis. I will next describe these steps in further detail.

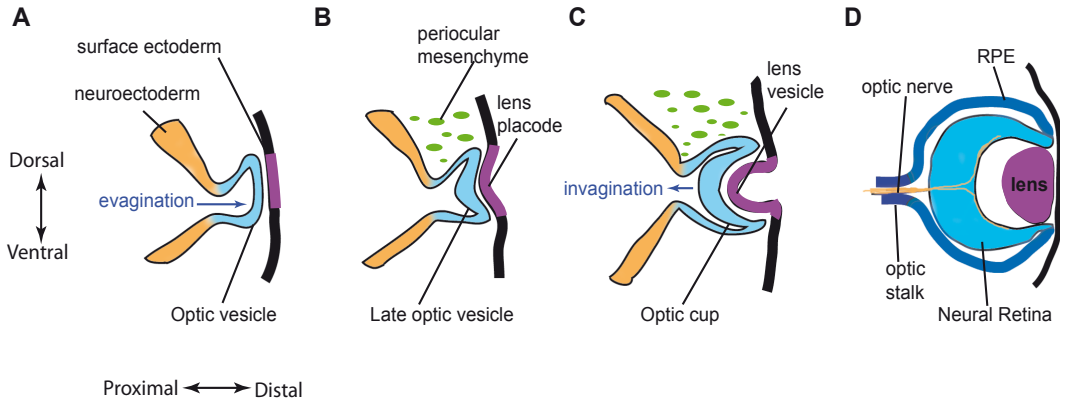

Figure 5. Representation of early eye development in mouse embryo, from E9 to E10.5. A) The optic vesicles (turquoise) evaginate from the forebrain neuroectoderm (orange) and contact with the surface ectoderm (purple). B) and C) the optic vesicles contact with the lens placode and both tissues invaginate to form the optic cup and the lens vesicles. D) After the folding of the optic cup the eye morphogenesis is completed. The optic cup is formed by the presumptive NR (light blue) at its distal part, the RPE (blue), which covers the NR, at its proximal part; the optic stalk (dark blue), which connects the optic vesicle to the forebrain through the optic nerve (orange) is localized at the most proximal part (Adapted from Eiraku et al., 2011).

Step 1: Eye field specification

After the extension of the embryonic body axis, by the convergence-extension movements, the neural plate appears as a regionalized tissue, whit the eye field located in the most anterior part (Wilson and Houart, 2004). The eye field specification and subsequent development into two bilateral optic vesicles depends on the expression of highly conserved homeobox transcription factors; a large group

of genes that share a common DNA sequence (homedomain) (Adler and Canto-Soler, 2007). The homeobox transcription factors: Otx2, Six3, Rx, Pax6, Six6 and Tbx3 are expressed in a dynamic, overlapping pattern in the presumptive eye field (Graw, 2010).

Also expressed in the eye field Sonic hedgehog (Shh) is a ligand of the hedgehog signaling pathway, which plays a key role in the regulation of the tissue growth during organogenesis. The Shh ligand and the TF Six3 are main players during the splitting of the eye field in two optic vesicles (Geng et al., 2008). Geng et al. (2008) showed that Six3 regulates Shh. The loss of either Six3 or Shh leads to holoprosencephaly with cyclopia in zebrafish embryos. Thus showing that without these genes expression the splitting of the eye field into two optic vesicles gets compromised (Geng et al., 2008).

However, eye filed splitting is a complex process that depends also on the interaction between several signaling pathways and tissues. The eye field is surrounded by telencephalic precursors and by cells that will form the hypothalamus (Esteve and Bovolenta, 2006). The prechordal plate mesoderm, which is a cell aggregate located in the anterior end of the notochord, plays a key role in determining the eye field and its subdivision into two separate domains, the future bilateral optic vesicles (Varga et al., 1999). Previous studies reveled that the removal of the prechordal plate mesoderm, which is specified by *One eye pinhead* gene (Schier et al., 1997), led to the formation of a single retina both in chick embryos and Xenopus explants (Li et al., 1997).

Step 2: Optic vesicle evagination

Optic vesicle emergence is a conserved process among vertebrates with many common features amongst species. Teleosts are, however, an exception; as in this group the formation of the optic vesicles is initiated in a different way. Instead of evaginating, as described before in the mouse, fish retinal progenitor cells individually migrate out laterally from the neural tube and form a vesicle by local epithelialization (Rembold et al., 2006).

In both, mammals and teleosts, the optic vesicle formation requires coordinated changes in cell shape and in cellular behavior, the retinal homeodomain transcription factor Rx/RAX is known to modulated these cell behavior (Rembold et al., 2006).

Previous work in medaka and zebrafish revealed that *rx3* is essential optic vesicle evagination (Winkler et al., 2000; Loosli et al., 2003; Stigloher et al., 2006); Figure 5-A). Additionally, Rx/RAX controls neuroepithelial cells movements by activating the non-canonical Wnt signaling pathway, which have been involved in the specification of the eye field in vertebrates (Cavodeassi et al., 2005; Martinez-Morales and Wittbrodt, 2009). Finally, there is evidence also from zebrafish, showing that Rx regulates cell proliferation during optic vesicle evagination (Stigloher et al., 2006; Fuhrmann, 2010). These results indicate the Rx expression is essential for eye field specification and the subsequent evagination of the optic vesicles.

After evagination, neuroepithelial cells are still morphologically and molecularly indistinguishable but do have the capability to develop into different cell types. During optic vesicle patterning multiple signaling molecules act to modify the identity of the cells, and define their differentiation into NR, optic stalk or RPE cells (Martinez-Morales et al., 2004). I will summarize the molecular interactions responsible for the patterning of the optic vesicles in subdomains below.

Step 3: Optic vesicle patterning

The undifferentiated cells from the optic vesicles express a conserved group of TFs, including Rx, Pax6, Hes1, Otx2, Lhx2, Six3, and Six9 (Adler and Canto-Soler, 2007). These genes, which form the nodes of the eye-specific regulatory network, are also responsible for the segregation of the different subdomains (NR, optic stalk and RPE) in the vesicle. (Figure 6).

The main molecular network involved in the patterning of the optic vesicle starts with the LIM homeobox transcription factor Lhx2, which is the earliest patterning gene known for the optic vesicle (Fuhrmann, 2010). This gene is responsible for the specification of both the RPE and the NR (Yun et al., 2009). It activates the bHLH transcription factor Mitf in presumptive RPE and the homeobox transcription factor Vsx2 in the presumptive NR (Burmeister et al., 1996; Green et al., 2003). Initially, *mitf* is expressed throughout the optic vesicle. But as development proceeds, it is

subsequently downregulated at the distal domain of the optic vesicles, where *vsx2* expression is initiated (Nguyen and Arnheiter, 2000). The proximal domain of the optic vesicle, which connects the optic vesicles to forebrain, expresses *pax2* and is thus specified into optic stalk. Previous experiments with *pax2*$^{-/-}$ mice revealed that the interaction between Pax2 and Pax6 is responsible for the establishment of the boundaries between the optic vesicles and the optic stalk (Schwarz et al., 2000) (Figure 6).

During the optic vesicle specification the prospective NR and the RPE are in contact with the surface ectoderm and the periocular mesenchyme, respectively. The signals coming from these exogenous tissues are essential for the initiation and progression of the specification of the optic vesicle into NR and RPE (Esteve and Bovolenta, 2006). I will now explain in more detail the regulation of NR and RPE specification genes by extraocular signals.

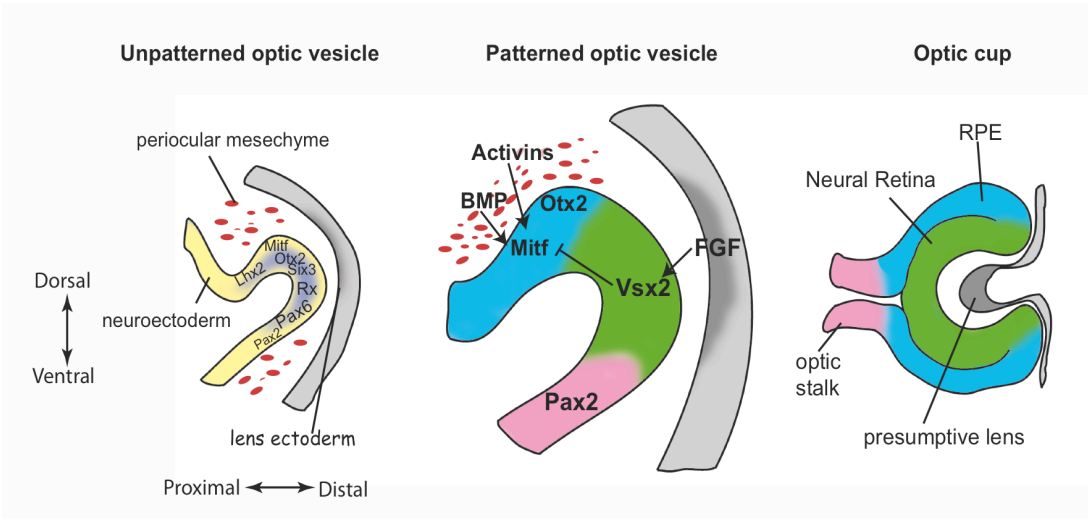

Figure 6. Optic vesicle patterning. In the unpatterned optic vesicle, neuroepithelial cells are indistinguishable and express a common set of transcription factors. In the patterned optic vesicle, activins and BMP signals from the periocular mesenchyme promote the RPE fate (blue), and FGF signals from the lens activate NR identity (green). *Vsx2* expression in the distal optic vesicle defines the NR identity by suppressing *mitf*. At optic cup stage, the three tissues are already specified into RPE, NR and optic stalk (pink).

Step 3.1: The Retinal Pigmented Epithelium (RPE)

RPE specification is controlled fundamentally by the expression of two transcription factors Mitf and *orthodenticle homeobox 2* (Otx2). Otx2 is required for *mitf* expression. Together they specify the RPE domain at optic vesicle stage and later on development they transactivate the expression of pigmentation genes. *mitf* and *otx2* are initially expressed in the eye field; their expression persists to optic vesicle stage and is eventually downregulated as the presumptive NR pattern emerge (Martinez-Morales et al., 2001; Martinez-Morales et al., 2004).

Signaling molecules secreted by the periocular mesenchyme are required for *mitf* expression during the early patterning of the RPE.

Experiments in chick embryos showed that the TGFb family member activin A, expressed in the extraocular mesenchyme, contributes to the specification of the RPE (Feijen et al., 1994). Chick optic vesicle explants cultured separated from the surrounding mesenchyme lose the expression of RPE markers and specific NR markers appear up-regulated (Fuhrmann et al., 2000). Moreover, these phenotypic defects are prevented by the addition of the TGFb family member activin A to the cultured cells (Fuhrmann et al., 2000), thus indicating that optic vesicle cells require signals from the extraocular mesenchyme to differentiate into RPE.

Bone Morphogenetic Proteins (BMP) BMP2, BMP4 and BMP7 are cell cycle regulators expressed in the periocular region and they also participate in the patterning of the optic vesicles (Dudley and Robertson, 1997). Previous studies in chick embryos showed that the overexpression of the BMP antagonist Noggin causes severe alterations in the ventral optic cup, including the loss of expression of RPE markers, which are then substituted by optic stalk markers (Adler and Belecky-Adams, 2002). These results suggest that the BMP signaling pathway expressed in the periocular mesenchyme is also essential for RPE specification (Figure 6).

Step 3.2: The Neural Retina

The presumptive NR is specified by the master gene *vsx2*, which is essential both for the patterning of this tissue at the optic vesicle stage and for the specification of NR cells at later stages. Vsx2 is the first TF expressed in the presumptive NR, in all undifferentiated retinal progenitor cells (RPCs). At this stage its required to maintain

RPCs in a multipotent state (Vitorino et al., 2009). As development proceeds, the RPCs differentiate and *vsx2* expression remains only in bipolar interneurons and Muller glia cells (Burmeister et al., 1996; Belecky-Adams et al., 1997; Chen and Cepko, 2000).

Mutations in *vsx2* are associated with microftalmia in humans (Bar-Yosef et al., 2004) and *vsx2* mutant mice (ocular retardation mutant - or^{J}) also show this phenotype (Truslove, 1962; Osipov and Vakhrusheva, 1983; Burmeister et al., 1996). In these mutants the retinal cells proliferation was decrease and the RPE differentiation genes were up regulated. Additionally, in *vsx2* knock-down zebrafish embryos, it was also observed malformations and morphological defects in early stages of eye development (Barabino et al., 1997). These findings indicate that Vsx2 is necessary for NR patterning.

During presumptive NR specification, signaling molecules derived from extraocular tissues regulate *vsx2* expression within the optic vesicles. Previous studies have shown that FGF signaling, emanating from the presumptive lens ectoderm, activates *vsx2*. The genetic interaction between FGF and *vsx2* is essential for retina patterning in the distal optic vesicle and, at later stages, for retinal neurogenesis (Rowan et al., 2004; Horsford et al., 2005). Furthermore, the conditional inactivation of *shp2* (which is required for complete activation of FGF singling) at the early optic vesicle stage in mouse mutants results in loss of *vsx2* expression. *Shp2* conditional mutants gain *mitf* expression in the NR; the affected part of the optic cup acquires RPE-like morphology and even gains some pigmentation (Cai et al., 2010). This finding suggests that FGF signaling regulates *vsx2* during NR specification, at optic vesicle stage (Figure 6).

In summary, the timely action of conserved transcription factors and inductive signals at optic vesicle stage, directs the initial development of the different compartments of the vertebrate eye. The regionalization of the optic vesicle is accompanied by the differential expression of transcription factors: Pax2 in the prospective optic stalk; Pax6, Rx, Lhx2 and Vsx2 in the prospective NR and Pax6, Otx2 and Mitf in the prospective RPE (Chow and Lang, 2001; Martinez-Morales et al., 2004; Bharti et al., 2006). After patterning has occurred, the optic vesicle undergoes specific morphogenetic movements that make the tissue invaginate forming the optic cup (Figure 4-C and D).

Step 4: Optic cup morphogenesis

The early organogenesis of the vertebrate retina finishes with the folding of the optic cup, leading to a perfectly shaped spherical eye. Geometrically, the invagination of the optic cup is a complex morphogenetic movement, which comprises different cell morphology changes. The invagination process has been examined using histology and life imaging in zebrafish embryos. It begins when the most distal part of the optic vesicle contacts the overlying surface ectoderm. This interaction results in the specification of the lens placodes, at the surface ectoderm, and precedes both tissues invagination (Li et al., 2000).

During invagination, the NR and RPE enwrap the lens as it emerges from the overlying ectoderm. The cells from the presumptive NR extend toward the forebrain, elongate and are subject to an anterior rotation (Kwan et al., 2012). The orientation of these cells at this time point is regulated by the combination of FGF signals along the dorsal-ventral axis of the neural tube (Picker et al., 2009). At the dorsal optic vesicle, the cells from the presumptive RPE follow the extension and elongation movements of the NR cells and after that, they spread dramatically to cover the back of the NR, becoming a flat monolayer where the distance between the cell nuclei is increased (Kwan et al., 2012).

Although there are detailed reports of the morphogenetic movements of the cells during optic cup folding (Li et al., 2000; Kwan et al., 2012), the evidences about the molecular players involved in the initiation and progression of this process started to be investigated only a few years ago.

Step 4.1: Lens ectoderm contributions to the optic cup folding

Previous studies in mouse showed that during the optic cup folding the cells from the surface ectoderm and the cells from the presumptive NR get in contact through F-actin-rich basal filopodia. Basal filopodia are cytoplasmatic projections of the basal membrane of the cells. It has been suggested that the interaction between the filopodia from neuroepithelial cells and from the lens ectoderm act, as a fine-tunning mechanism, to assist the mechanical forces necessary to coordinate the folding of the optic vesicle and the presumptive lens (Chauhan et al., 2009).

Although these findings indicate that the physical interactions between the lens

ectoderm and the optic vesicles may play a role during optic cup folding, several studies demonstrate that this process can also occur without physical contacts from this adjacent tissue. The interaction between retina and lens ectoderm surface also activates signaling pathways that might contribute to the folding of the optic cup facilitating its morphogenesis (Fuhrmann, 2010). Previous studies in chick embryos showed that in the absence of pre-placodal ectoderm (early optic vesicle stage), the invagination of the optic cup is perturbed. However if surface ectoderm ablation occurs later, the optic cup invaginates properly, even without a correct formation of the lens (Hyer et al., 2003; Smith et al., 2009). This result suggests that essential signaling molecules for optic cup folding are expressed in the lens ectoderm at early stages, at the onset of optic vesicle patterning.

More recently, *in vitro* work using mouse embryonic stem cells showed that isolated cell aggregates are able to organize spontaneously into a retina. These cells form a neuroepithelium and bend into hemispherical vesicles that became patterned with retina marker genes along their proximal-distal axis. This tissue could then fold on its own, without interaction with exogenous tissues and in a very similar manner to the folding of the retinal epithelium in the embryo. This work therefore suggests that the optic vesicle contains self-organizing programs, which involve stepwise and domain-specific regulation of the different optic vesicle domains. These programs are responsible for the morphological events and cell identity during optic cup folding (Eiraku et al., 2011).

Step 4.2: Coordination of cell shape changes during optic cup morphogenesis

The morphogenetic events forming the optic cup require the generation of tensional forces to coordinate cell shape changes and movements. Morphogenetic events can occur in animal epithelial sheets either by apical or basal constriction of the cell membranes (e.g. Sawyer et al 2010, Gutzman et al., 2008). Both processes require the recruitment of the actomyosin network, which is responsible for cell contraction (He et al., 2010). Previous work in *Drosophila* embryos showed that apical constriction depends on apical polarity complexes and adherens junctions between cells (Kolsch et al., 2007; Letizia et al., 2011). Basal constriction, which has been studied in *Drosophila* and medaka embryos, depends on integrin-mediated focal adhesions.

Interference with the adhesive function of integrins impairs basal actomyosin recruitment and tissue morphogenesis in both vertebrate and invertebrate epithelia (Martinez-Morales et al., 2009; He et al., 2010). Integrins are well-characterized transmembrane receptor proteins that mediate the attachment between a cell and its surroundings (Hynes, 1992). These proteins, localized within focal adhesion complexes, mediate the regulatory effects of extracellular matrix adhesion on cell behavior, like mechanical forces and signaling transduction (Burridge and Chrzanowska-Wodnicka, 1996).

Previous studies in medaka demonstrate that optic cup folding occurs through basal constriction (Figure 7). This work shows that optic cup folding requires the adhesive function of integrins, which is dependent on the expression of the developmental gene *opo*. During the optic cup folding Opo regulates the localization of the integrins promoting basal constriction of the cells and optic cup folding (Martinez-Morales et al., 2009).

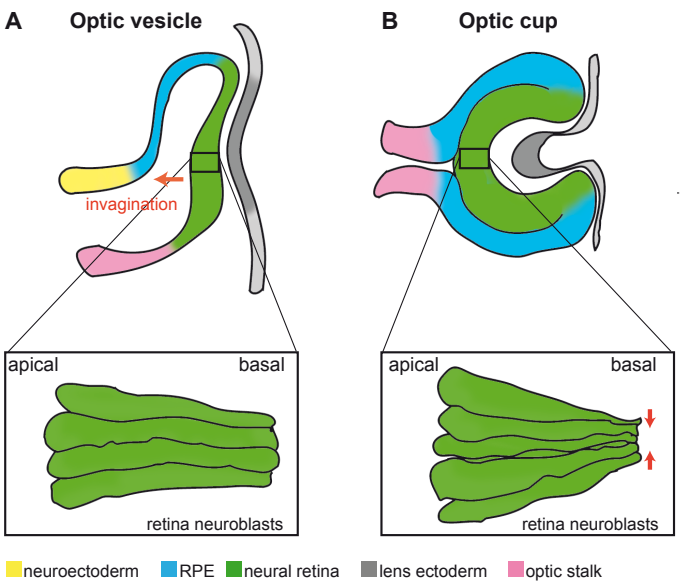

Figure 7. Optic cup folding

A) At optic vesicle stages, retina neuroblasts are organized in a monolayer at its distal part.

B) During the invagination of the optic cup, the basal membrane of the cells is constricted (red arrows) to force the optic cup folding.

4. *Opo* is required for optic cup folding

opo was identified in medaka in a large-scale screening using ENU-mutagenesis (*N*-ethyl-*N*-nitrosourea) as a recessive lethal mutation with full penetrance and low phenotypic variability (Loosli et al., 2004). In *opo* mutants, eye morphogenesis defects became evident during the optic cup folding stage. The expected basal

surface contractions are not observed in the retina neuroblasts, which indicate that tension cannot be exerted properly when *opo* function is damage. Thus, as development proceeds, the optic cup does not fold properly and therefore, the mutants show abnormal morphologies, with large ventral openings in the eyes (Martinez-Morales et al., 2009).

Opo is a developmental gene placed in a gene desert enriched with cis-regulatoty elements. It encodes for a transmembrane protein, localized in the compartments of the secretory pathway and basal end-feet of the neuroepithelial precursors cells. During optic cup development, this protein regulates the asymmetric localization of integrins to the basal surface of the retina epithelium (Martinez-Morales et al., 2009).

The trafficking of integrins along the apical basal axis has been proven to be essential for integrins adhesive function, basal actomyosin recruitment and further a directional cell movement (Ezratty et al., 2009). The endocytosis of integrins is a clathrin-dependent process regulated by members of the phosphotyrosine binding (PTB) family of clathrin adaptors (such as Numb, Dab2 and ARH), which interact directly with integrins and regulate their internalization (Calderwood et al., 2003). This interaction has been shown to provide a directional cell migration in HeLa cells (Nishimura and Kaibuchi, 2007).

Opo functions as a repressor of Numb and hence interferes with clathrin-mediated integrin endocytosis. This antagonism between *opo* and *numb* controls focal adhesions turnover and is specifically required for optic cup folding (Bogdanovic et al., 2012a). Accordingly, in *opo* mutants the lack of adhesive function (i.e. due to an excessive integrin internalization) impairs basal actomyosin recruitment and subsequently optic cup folding.

These findings indicate that the basal constriction mechanism that directs the optic cup folding depends on the molecular antagonism found between Opo and Numb. Future studies will need to address what kind of signals initiate invagination and how conserved is the mechanism mediated by *opo* across vertebrate species.

5. *Opo* role in the development of other tissues.

Besides the optic cup defects, *opo* mutants also show defects in other epithelial tissues like brain, heart, fins and in neural crest-derived craniofacial structures (Martinez-Morales et al., 2009).

The development of the craniofacial region mostly depends on the multipotency and migratory behavior of neural crest cells. This cell population is considered a vertebrate innovation and, accordingly, chordate ancestors lacked neural crest counterparts (Santagati and Rijli, 2003).

In *opo* mutants neural crest cells are correctly specified, however, they fail to migrate/delaminate, as is shown by the severe reduction in the jaw and palate structures. As is the case for the neural crest precursors, fin bud mesenchyme is also correctly specified in *opo* mutants, however the apical ectodermal ridge is misshapen. As a result, pectoral fins fail to grow properly (Martinez-Morales et al., 2009).

Analysis of the *opo* expression pattern in mouse has shown a similar expression pattern to that described in medaka. This includes craniofacial neural crest derivatives, skeletal elements, heart and the eyes (Santagati and Rijli, 2003; Mertes et al., 2009).

In terms of protein conservation, the Opo carboxy-terminal motif is homologous to proteins present in basal chordates, echinoderms, cnidarians (not in protostomes) and in the metazoan basal lineage. The N-terminal motif of the protein can be considered a vertebrate innovation. Taking into account that *opo* has an important role in the development of organs such as the neural crest, the fins or the chamber-shape eye, which are all considered vertebrate novelties, it is likely that *opo* function co-evolved with the emergence of these vertebrate tissues (Shimeld and Holland, 2000; Martinez-Morales et al., 2007; Martinez-Morales et al., 2009).

In summary, *opo* functions as an integrin endocytosis regulator at the basal surface of the retina, during optic cup folding. Interference with its activity impairs optic cup morphogenesis. Given the crucial role that *ojoplano* plays during eye and neural crest development, and the intriguing link that it appears to have with human hereditary diseases, we decided to analyze the enhancers that control its expression. The localization and analysis of these elements allows the investigation of upstream regulators of *opo*. Furthermore, the identification of these enhancers may establish

new links between *opo* and the TF network implicated in early eye development. In addition, it was a challenge to link these new enhancers with *opo* associated hereditary diseases (see Box 1).

To achieve this, I have identified a collection of enhancers within *opo locus* by enhancer screening, using zebrafish as model organism (Bessa and Gomez-Skarmeta, 2011). I generated a collection of stable zebrafish transgenic lines for each enhancer, which were used to characterize its spatio-temporal activity and its potential upstream regulators.

II. Objectives

- To investigate the putative regulatory elements located in *opo* regulatory landscape

- To search for putative up-stream regulators of *opo*

- To explore the link between opo regulatory locus and human hereditary diseases

III. Materials & Methods

1. Selection of non-coding putative regulatory elements

The selection of the highly conserved putative *non*-coding regulatory elements (n=23 conserved PNREs), was carried out using the VISTA Browser (http://pipeline.lbl.gov/cgi-bin/gateway2; (Frazer et al., 2004), taking as a reference the human genome released in March 2006 (NCBI36/hg18) and using the default parameters (regions of al least 100 base pairs (bp) and 70% similarity.

To localize the epigenetic marks H3K4me1 and H3K27ac in the human PNREs, ChIP-seq tracks from six human cell lines were used: embryonic stem cells (H1hesc), mammary epithelial cells (Hmec), skeletal muscle myocites (Hsmm), umbilical vein endothelial cells (Huvec), epidermal keratinocytes (Nhek) and lungs fibroblasts (Nhlf) data (available in UCSC browser: http://genome.ucsc.edu/; (Bernstein et al., 2006; Mikkelsen et al., 2007). Four PNREs showing no conservation between vertebrates, but having high H3K4me1 and H3K27ac signal in human cell lines, were also selected. The PNRES were named according to the genome: human genome (H), chromosome 6 (6), and the first five digits of the element localization (i.e.: the peak localized in chr6:9040802-9041496 is named: *H6:09040;* Supp. Tab. 1).

To investigate if the conserved PNREs were marked with H3K4me1 and H3K27ac signatures during zebrafish developmental stages, previously published ChIP-seq data was used (Bogdanovic et al., 2012b) (Supp. Tab. 2).

2. Cloning into a Tol2-mediated vector

The PNREs were amplified by PCR from human genomic DNA using the primers listed in table 1.

Name	Forward primer (5'-3')	Reverse primer (5'-3')	Localization in human genome (hg18, chromosome 6)		Lenght (bp)
			start	end	
H6:09040	CCATATGGATCATCCTCTTCCC	CTGGAAGCGGTTGTTTGAGG	9040802	9041495	886
H6:09360	TCCTTTCTCCCCAAAACCAC	TTTGTGAATAATGTTTGCACTAAGAAG	9360754	9362917	2360
H6:09510	TTTGAGCTTGCTGCATTATATGG	AATTTGCTTTGGCAGTTGGG	9510079	9512442	2656
H6:09516	GGGGGAAATCTATGTGCATTTG	ACTGTTCATGTGGCTGGGG	9516753	9517809	1216
H6:09536	GCTCAAGGAAGCTGTGATGTC	TCTGTGAATGTGCATTTGTTCG	9536004	9537930	2027
H6:09563	CACAAGGCATCTTACACATCAGC	GCGATCAGGCGGTCTAAATC	9563974	9565999	2148
H6:09601	ATTGCCACATAATGAGTTGCAGTCC	CTGGCCACACATCACAAGTCAAAG	9601172	9602202	1031
H6:09617	GGATGTGCTCCAAGTCACCAAG	AGTGCCAGCAGAGACCATTC	9617863	9618922	1060
H6:09628	CATCTGCTTGGCTTCTGATG	ATGGCTATGGGGGAGATAGG	9628639	9629494	856
H6:09647	GGAGGAGAGAGAGCAGCGAG	AAATGAACTGCAGCCAAGATG	9647690	9648627	1121
H6:09671	TGCTTCATCCCGTAGGTTTGTTTC	AAAGGGGTATGGGAAAAGGTGTCAG	9671795	9672798	1004
H6:09742	CAAACAAGGATTTCTCAAGGGC	CATTAGTCATGATTGAAAAATGGATG	9742877	9745652	2856
H6:09778	AATTGCTTATGGTTGTTCCCG	TCAAAACCCTAACTTGAAGCAAAAC	9778300	9780223	2186
H6:09813	GATCTTCAACATGACTTCTGGC	TTGGGTTAGGTCCTTCAACTGTG	9813174	9814241	1068
H6:09815	GCCCATAAGGTGAGACTATAACTG	ACATCTTGGCTATTGTGAATAATGC	9815794	9816729	936
H6:09892	GTGCTCCAATGCAGTTGCTC	TTAATATCCCAATTTGATACTTGGC	9892240	9894126	2144
H6:09941	TCATGTCTTCCAATGAGTCTGG	GCAAAAAGAAAGAGCCGAGA	9941162	9943190	2029
H6:09949	GGCAACCCAAGTTAGTAGCACCACC	TCAGTAAGGCCAGGCTCCATC	9949629	9950467	839
H6:10043	AGCCTGGGTAACAGAGCGAG	GCATTCAGCCCTACCCAGTC	10043446	10045884	2571
H6:10126	CTGATTTCAAATGCATGCCC	AAATTCCAGAGGGCAGATGG	10126474	10127046	685
H6:10137	CCAAGAAGAGACCTCCAACGAAC	CACTTTTATGAGCTACGTGGTTGTG	10137953	10139056	1104
H6:10258	CTGACAGCTCGCATCGTCCAC	GAGTATAAGGTGAGGTTGGCAAC	10258016	10259047	1032
H6:10309	GTTGCGATGTGTTGTTTTGG	GTCCAGTGGTGGCAGACTA	10309982	10311174	1193
H6:10377	CACATCACAGCCAGAGAAGGGTC	TGGCACGTGCTTACCTATGTAAC	10377252	10378117	866
H6:10422	AGCTTTTCTCCGCTTTGCTG	TTCTTCCCTCCTTCTTCTGGTG	10422720	10424962	2511
H6:10431	ACCTTCCTTTGTGCTTGCCATCC	CTACTGCACCCGACCCTGACTC	10431893	10433099	1207
H6:10455	TAGCACCATTGCACTTCAGC	CTTCTGCTTCATTTGCCACA	10455468	10456853	996

Table 1. Primers used for PNREs amplification.

The PCR fragments were sub-cloned in PCR8/GW/TOPO (Invitrogen) vector and, using the Gateway Technology (Invtrogen, CA, USA), they were then transferred to the destination enhanced green fluorescent protein (eGFP) reporter vector, as described by Bessa and colleagues (Bessa et al., 2009) (Figure 8).

Figure 8. The Zebrafish enhancer detector (ZED) vector. Contains two modules flanked by Medaka Tol2 transposase target sites (orange), that enables efficient transgenesis in zebrafish. The first module contains the minimal GATA promoter (light blue) driving the expression of eGFP (green). Each PNRE was cloned upstream of this module using the Gateway Technology recombination (Gateway *cassette* in yellow), activating or not the GFP expression. Two strong insulators are present in the ends of this first module to reduce the potential influences of the regulatory elements (dark pink). The second module contains the *cardiac actin* promoter (light blue) coupled to a red fluorescent protein (RFP in red), which serves as a positive control for transgenesis. The positive embryos should express homogeneous RFP in somites and heart (*adapted from Bessa et al., 2009*).

3. Maintenance of zebrafish (*Danio rerio*)

Zebrafish was used as a model organism, given their characteristic capacity to deliver large amounts of eggs *per* week, the transparency of their newborn embryos and its fast organogenesis (approximately 3 days). These characteristics are an advantage to investigate morphogenesis and organogenesis during early development.

The wild-type AB/Tuebingen (AB/TU) zebrafish strain was maintained under standard conditions according to the procedures described in Kimmel et al. (1995) and in the Zebrafish Model Organism Database (http://zfin.org; (Sprague et al., 2003). All developmental stages in this study are reported in hours post-fertilization (hpf) at 28.5°C in E3 medium with 0.003% 1-phenyl-2-thiourea, which prevents pigmentation (Figure 9) (Kimmel et al., 1995).

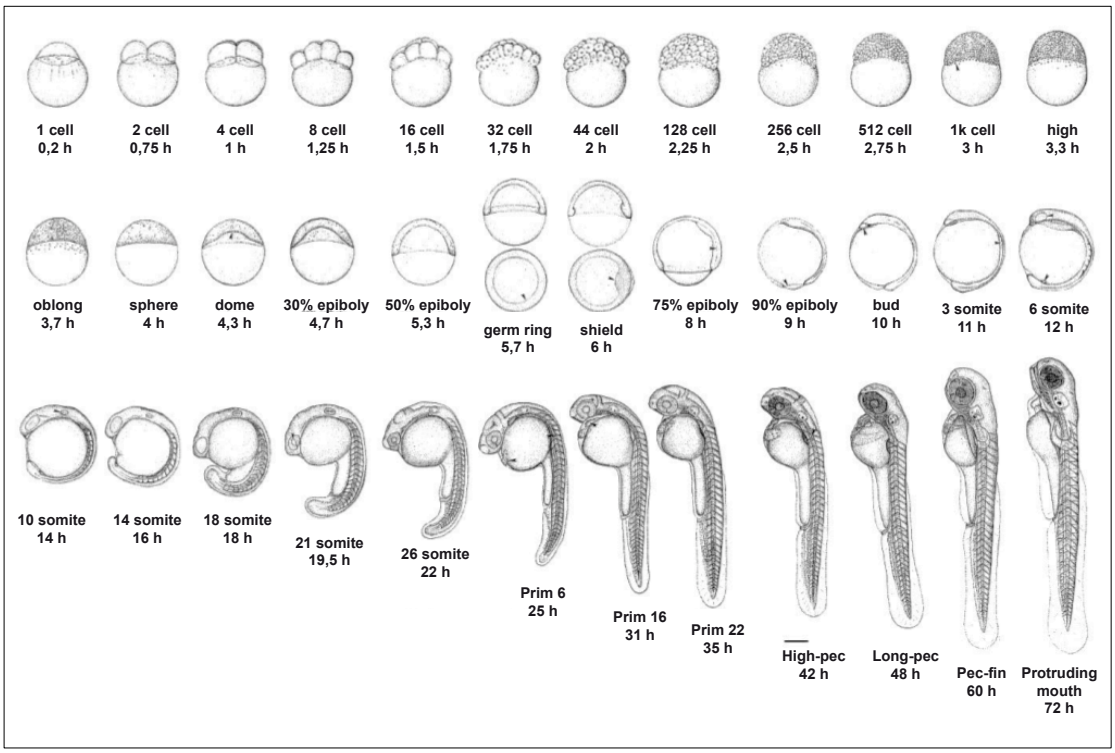

Figure 9. Developmental stages of zebrafish embryo. From one cell stage to 72hpf (*adapted from Kimmel et al., 1995*).

4. Zebrafish Tol2 mediated transgenic assays

The ZED constructs containing the PNREs were microinjected in zebrafish embryos using the following procedures. In the day previous to DNA microinjection, the adult fish were separated according to sex into two different 3 litter (L) tanks. By the

following morning, males and females were placed together in a 5L tank, provided with a grid to separate the adults from the newborn eggs (Kimmel et al., 1995). Minimums of 300 fertilized eggs were injected, at one cell stage, with 3-5 nl of a solution containing 25 nM of PNRE construct, 25 nM of Tol2 mRNA and phenol-red (Sigma-Aldrich) at a final concentration of 0.1%. The microinjected embryos where then incubated at 28°C, during 3 days, and an equal number of un-injected embryos were also incubated as experimental control.

The GFP and RFP patterns of the injected embryos were observed at 24, 48 and 72hpf with a fluorescent stereoscope. Embryos showing homogenous and strong RFP patterns in somites and heart (putative transgenic embryos) were raised to sexual maturity.

5. Tissue specific enhancer screening in F1 generation

Putative transgenic adult fishes (founders) were individually outcrossed with a wild-type zebrafish partners. At least 10 individual fishes were analysed *per* PNRE. The GFP and RFP expression patterns of the first generation embryos (F_1) were observed at 24, 48 and 72 hpf. A PNRE was considered a tissue specific enhancer when three or more founders displayed similar F_1 GFP patterns during development (Bessa et al., 2009). To obtain high-resolution pictures, a fluorescent stereoscope set up with a digital camera coupled was used. Adobe Photoshop was employed to adjust brightness and contrast of the obtained images. Finally, the expression pattern of the new enhancers was compared to the *opo* expression pattern obtained from RNA *in situ* hybridizations and the expression analysis of the *opo* promoter region.

6. Wholemount RNA *in situ* hibridizations and Fluorescent RNA *in situ* hibridizations (ISH & FISH)

To synthesize *opo* riboprobes, total RNA was extracted from wild-type zebrafish strain at 24hpf using Trizol (TRI Reagent: Acid-guanidine thiocyanate, Sigma) followed by phenol-chloroform extraction. Genomic DNA was then digested using TURBO Dnase (DNAseI, *Boehringer Mannheim*) and the mRNA was precipitated with 7.5M of LiCl. Around 1–5 µg/µl of the total RNA was reversely transcribed using a cDNA synthesis Kit (*Invitrogen*). The cDNA was used as template to amplify *opo*

fragments using the following PCR primiers: 5' AAGTTGCAGCAGAAGGCTGTGGAG and 5' ATTTTGCGGAATTGGTTGAG for N-terminal; 5' GTCAGCTAGTGTTTGGCTCAC and 5' ATGCATTAGTGTCAGAATCAT for C-terminal probe. The PCR products were cloned into pCS2+ vector (Addgene), linearized with *NotI (Takara Bio Company*), and transcribed with SP6 (*Roche Applied Science*) using digoxigenin-labelled nucleotides (Digoxigenin-11-UTP, *Roche*). The riboprobes were used at a concentration of 1.5 ng/ul for ISH and FISH. ISH and FISH were preformed as described in (Neto et al., 2012) and (Bogdanovic et al., 2012a) respectively. Embryos processed for ISH were observed with a scope (Leica) and FISH embryos observed with a confocal microscope (Leica SPE). The ISH embryos were then processed for vibratome sectioning, as described in (Martinez-Morales et al., 2009).

7. Cloning of the medaka *opo* promoter region

The genomic DNA was extracted from medaka embryos (*Oryzias latipes*) with phenol:chloroform:Isoamyl alcohol 25:24:1 (Sigma) and washed with 100% ethanol. This DNA was used as a template to amplify a 5,6kb region upstream of *opo* transcription start site (defined using RACE experiments in Martinez-Morales et. al. 2009) with the following primers: 5' GTCAGCTATCACCGCAGTCGTCA and 5' CCTCACTTCCTTGTGCCGACATG 3'. After purification, the 5,6kb PCR product was cloned in PCR8/GW/TOPO vector (Invitrogen), transferred into the destination ZED vector (Bessa et al., 2009) and used for transgenesis in zebrafish as above mentioned, in the sections 3, 4 and 5.

8. Circularized Chromosome Conformation Capture Analysis (4c-seq)

4C-seq assays were performed as described in (Dekker et al., 2002; Hagege et al., 2007; Noordermeer et al., 2011; Splinter et al., 2012). Newborn mice at stage E11.5 were dissociated by collagenase and fixed in 4% formaldehyde. The sample was then treated with lysis buffer (10 mM Tris-HCl pH 8, 10 mM NaCl, 0.3% IGEPAL CA-630 (Sigma), 1X protease inhibitor cocktail (Roche). Nuclei were digested with DpnII endonuclease (New England Biolabs) and ligated with T4 DNA ligase (Promega). Subsequently, Csp6I endonuclease (Fermentas, Thermo Scientific) was used in a second round of digestion, and the DNA was again ligated. Specific primers were

designed near *opo* promoter and H6:10137 enhancer (viewpoints), with the online program primer3 v. 0.4.0 (Rozen and Skaletsky, 2000). Illumina adaptors were included in the primers sequence. The PCRs were performed with Expand Long Template PCR System (Roche) for each viewpoint, pulled together and purified using High Pure PCR Product Purification Kit (Roche). The samples were then quantified using Quanti-iT^{TM} PicoGreen dsDNA Assay Kit (Invitrogen) and submitted to deep sequencing. The analyses of the 4C-seq were performed as described in (Noordermeer et al., 2011). Briefly, raw sequencing data were demultiplexed and aligned using mouse genome released in July 2007 (NCBI37/mm9) as reference. Reads located in fragments flanked by two restriction sites of the same enzyme, or in fragments smaller than 40 bp were filtered out. Mapped reads were then converted to reads-per-first-enzyme-fragment-end units, and smoothed using a mean running window algorithm. To calculate the statistically significant targets for each viewpoint, the average background level was estimated randomizing data in a window of 2 Mb around each viewpoint. The *p*-value for each potential target was calculated by means of Poisson probability function. Smoothed data were uploaded to the UCSC Browser for visualization.

9. Search for up-stream regulators of H6:10137 enhancer

To search for conserved transcription factors DNA-binding sites in H6:10137 sequence it was used the *Mulan* alignments and the *multiTF* search tools were used, which are available in ECR browser, which detects DNA-binding sites based on sequence conservation (TRANSFAC 7.0 *in* http://ecrbrowser.dcode.org/; (Ovcharenko et al., 2004). In this case the binding sites were predicted with a sequence homology of 63% between human and *Xenopus tropicalis.* Additionally it was used the JASPAR database (http://jaspar.genereg.net; (Bryne et al., 2008). JASPAR database contains a collection of DNA-binding sites for transcription factor, modeled as matrices that are compared with a database of experimentally defined transcription factor binding sites (Stormo, 2000; Wasserman and Sandelin, 2004). For JASPAR data, motifs with a sequence homology of 100% and a socre >10 (maximum score=13,5) were considered.
The expression pattern of the founded motifs in ECR and JASPAR was analyzed in the Zebrafish Model Organism Database (http://zfin.org/; (Sprague et al., 2003)). The transcription factors that shared a common expression pattern with the H6:10137

enhancer were then analyzed with multi-species alignments using *ClustalX 2.0* (Larkin et al., 2007).

10. Mutagenesis of Vsx2 DNA-binding sites inside H6:10137 sequence

The Vsx2 DNA-binding sites in the H6:10137-ZED construct were mutated by PCR, using QuikChange Multi Site-Directed Mutagenesis Kit (*Agilent technologies*) with the mutagenic primers: 3'CTATTTTACATTTTCTTAATcgcCAAATCTTAATCTTGACTTTAATG'5 (mutH6:10137del) and 3'CATTATTAGCGGTCTctgCTTGAAGTTATATCAATGTTAGT'5 (mutH6:10137del1), following the manufactures protocol. After sequence disruption confirmation by sequencing, the mutagenic-H6:10137 construct (mutH6:10137) together with the H6:10137 enhancer construct were injected in wild-type zebrafish at one cell stage, as described before. The GFP and RFP activity of both, mutH6:10137 and H6:10137, were compared in F0 (mosaic embryos) at 24hpf.

11. *Vsx2* Morpolinos injections

Vsx2 splicing morpholinos (*vsx2*MOs) were obtained from Gene Tools: I1E2MO: 5'-TCATCTGAATCTGTAACATGGAGGA-3' blocks a splicing acceptor between Intron 1 and Exon 2, E2I2MO: 5'-TTTTCTTTAAGCCCACCTGTGTCGT-3' blocks a splicing donor between Exon 2 and Intron 2.

Both morpholinos were separately injected at one-cell stage in wild-type strain and in the transgenic lines: Tg(H6:10137) and Tg(*vsx3*GFP:caax), in a concentration of 8,5-13ng per embryo. When co-injected in a wild-type strain, the concentrations used were 6-10ng for each *vsx2*MO. *P53* morpholino (*p53*MO: 5-GCGCCATTGCTTTGCAAGAATTG-3 (Langheinrich et al., 2002), was co-injected with *vsx2*MOs in a concentration of 4-6ng per embryo. Control embryos were injected in parallel with water and *p53*MO alone. To assess the morpholino efficiency, cDNA samples were obtained from 24hpf sectioned heads and total embryos, from both, controls and morphants embryos, using Trizol for the mRNA extraction followed by cDNA synthesis, as described before (section 6). The cDNA samples from both morphant and control embryos were also used to quantify *opo* expression levels quantification by RT-qPCR (see section below).

The amplification of the *vsx2* transcripts in both morphant and control cDNAs was

done by RT-PCR using the following primers: I1E2MOfw: 5'-AGCACACTGGACTCCTTCCCCG-3'; E2I2fw 5'- GGGATTAATTGGGCCTGGAGGTAT-3'; I1E2MOrv and E2I2rv: 5'- AGACTCGGGCAGAGGGATAGAGTGA-3'. The PCR products were cloned into StrataClone® vector (Agilent) and sequenced (Secugen) to confirm aberrant splicing events induced by the morpholino.

12. *Opo* RT-qPCRs

The quantification of *opo* expression levels in zebrafish cDNAs by RT-qPCR was done using a forward primer placed in second exon: 5'CGGTCTTCGCTGTAGATGC'3 and a reverse primer placed in third exon: 5'GACGGCGTAGAGGAATAATG'3. The results were normalized with *eif1a*, as a *house-keeping* gene, amplified with 5'-CTTCTCAGGCTGACTGTGC-3' as forward primer and 5'-CCGCTAGCATTACCCTCC-3' as reverse primer.

13. *Vsx2*MOs - Eye phenotype characterization

The eyes of both, *vsx2*MOs injected embryos and its respective controls were observed at 24hpf, using a fluorescent scope coupled with a photo camera (SZX16–DP71, *Olympus*). Photos were taken with the same parameters of magnification, sensitivity and exposition in both transmitted light and fluorescent conditions. The GFP quantifications, the eye ventral openings angles, the retina length and the forebrain height were measured for each embryo with *ImageJ1.45q* (Wayne Rasband, National Institute of Health, USA). The retina length values were normalized with the forebrain size for each individual embryo. Over 100 embryos, including their respective controls were analyzed for each phenotypic condition.

14. *Vsx2* Overexpression

The total RNA extraction and cDNA conversion from zebrafish wild-type embryos were preformed as above mentioned in section 6. The *vsx2* cDNA was amplified by PCR using the primers 5'-GGACCGACTCGAAAGCAAAG-3' and 5'-TTAACGCACAAGCCCAAGTC-3'. The PCR products were cloned into pCS2+ vector (Addgene), generating the Vsx2mRNA:pCS2+ construct. This construct was linearized

with *NotI (Takara Bio Company*), and transcribed with mMESSAGE mMACHINE SP6 Kit (*Ambion*), following the manufacture protocol. After the capped mRNA transcription, the DNA template was eliminated. *Vsx2* mRNA was precipitated with 7.5M LiCl and quantified. The injections of the *Vsx2*mRNA were preformed in zebrafish wild-type at one cell stage (200pg and 340pg *per* embryo). At 24hpf the injected embryos were processed for total RNA extraction followed by cDNA synthesis as mentioned before. The cDNA was used for quantification of *opo* expression levels, by RT-qPCR, as previously described.

15. Chromatin Immuno-precipitation detected by qPCR (ChIP-qPCR)

The physical interaction between H6:10137 and Vsx2 was tested by ChIP-qPCR using the fusion protein *GFPvsx2*mRNA:pCS2+ and the GFP antibodies (Abcam). Briefly: wild-type zebrafish embryos were injected into one cell stage, with 300pg/embryo of *GFPvsx2*mRNA fusion. At 24hpf, 300 heads were dissected, from the injected embryos and fixed in 1% formaldehyde for 15min at room temperature. Following crosslinking, tissues were washed and sonicated (DNA to lengths between 200-300 bp). Half of the samples were stored at -20°C as input and the rest was immuno-precipitated overnight with pre-bounded antiGFP-Dynabeads (Sigma). Then, the immuno-precipitated DNA fragments and the Input sample were subjected to DNA extraction with phenol:chloroform:Isoamyl alcohol 25:24:1 (Sigma) and washed with 100% ethanol. RT-qPCRs were preformed using the following primers: 5´-CAGTGAAGAAGGAAAGCATGG -3´and 5´- TGCATCTTACAGAAGAAGAGA -3´ for H6:10137 enhancer; 5´-GTACCGATTTAATACTGTGG-3´ and 5´-CAGTATAGCATACGCTTTTA-3' for *Vsx1* (positive control obtained from: (Clark et al., 2008)); 5´-CTCTCAAATCCGGAGATGCT-3´ and 5´-GAAGCTCTCCACACACATGG-3´for *Ef1a* (housekeeping gene used as negative control). The recovery of the H6:10137 sequence from the immuno-precipitated sample was compared to the recovery of the positive and negative control sequences, taking the input as control sample.

IV. Results

1. Enhancer screening in the *opo locus*

To explore the regulatory logic within the *opo* landscape, putative non-coding *cis*-regulatory elements (PNREs) were identified on the bases of their conservation in vertebrate genomes as detected by phylogenetic footprinting. The comparison between the genomes of mammals and teleosts allowed the identification of 23 PNREs in the *opo locus*. These elements were selected in the human genome and have a minimum of 70% of sequence homology between *Fugu* and human (Figure 10).

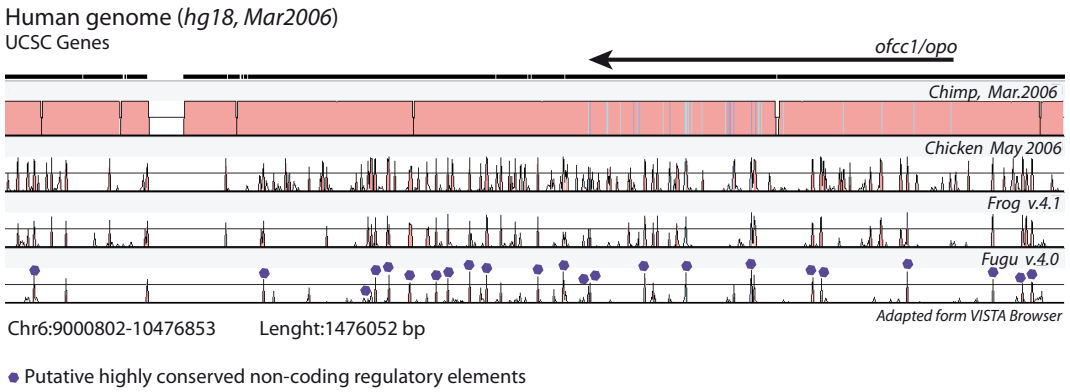

Figure 10. *opo regulatory* landscape. Highly conserved non-coding elements in the *opo locus* are depicted in the figure (purple circles marked in *Fugu* genome).

The majority of the conserved PNREs revealed the presence of typical epigenetic marks for constitutive (H3K4me1) and active (H3K4me1 and H3K27ac) enhancers, when compared to previously published data from chip-seq analyses in human cell lines (Bernstein et al., 2006; Mikkelsen et al., 2007) and zebrafish embryogenesis (Bogdanovic et al., 2012b) (Supp. Tab. 1-2). In 48% (n=11) of the PNREs, H3K4me1 and H3K27ac marks were observed in at least one human cell type and/or during zebrafish embryogenesis; In 43% (n=10) of the PNREs only H3K4me1 was observed in at least one human cell line and/or during zebrafish development and only 9% (n=2) did not shown any epigenetic mark for active or constitutive enhancers (Figure 11).

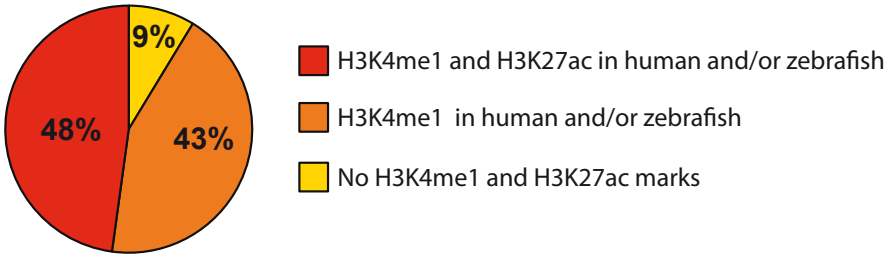

Figure 11. PNREs classification. Classification of the conserved PNREs according to epigenetic marks for enhancer activity in human cell lines and in the developing zebrafish embryo (24hpf and 48hpf).

In addition to the conserved PNREs, other 4 H3K4me1 and H3K27ac positive regions showing no conservation between human and teleosts were selected in the human genome as a reference (Supp. Fig. 1).

The selected elements were analyzed by transgenesis assays in zebrafish using the ZED vector (Bessa et al., 2009), a Tol2 mediated transgenesis shuttle that allows the integration of the humans PNREs in the zebrafish genome. The progeny (F1) of the putative transgenic fish (founders) was screened for reproducible GFP expression patterns between different founders. We observed that 44% (n=12) of the elements were able to activate GFP expression. These elements were all conserved between vertebrates (Supp. Tab. 3). However, from these 12 elements, only 9 behaved like tissue specific enhancers (n=9), meaning that three or more founders showed a reproducible expression pattern in their progeny (Table 2).

GFP + PNREs	Localization in human genome (hg18, chr:6)		n.º of Foundres			Classification
	start	end	Reproducible GFP pattern	Non-reproducible GFP patterns	Total	
H6:09040	9040802	9041495	3	-	13	Enhancer
H6:09516	9516753	9517809	4	-	23	Enhancer
H6:09563	9563974	9565999	8	-	25	Enhancer
H6:09601	9601172	9602202	3	-	13	Enhancer
H6:09617	9617863	9618922	3	1	13	Enhancer
H6:09778	9813174	9814241	-	5	16	Ambiguous
H6:09813	9815794	9816729	-	2	20	Ambiguous
H6:09949	9949629	9950467	3	-	10	Enhancer
H6:10126	10126474	10127046	-	4	20	Ambiguous
H6:10137	10137953	10139056	6	-	12	Enhancer
H6:10377	10377252	10378117	10	3	41	Enhancer
H6:10431	10431893	10433099	4	-	13	Enhancer

Table 2. PNREs with GFP activity. Classification according to the presence of reproducible GFP patterns between founders. If a PNRE shows similar GFP patterns in 3 or more different founders progeny, it is classified as a tissue-specific enhancer (enhancer). If the GFP patterns are different between the founder's progenies for one PNRE, this PNRE is classified as "Ambiguous".

The nine tissue specific enhancers were equally distributed at 5' and 3' from the *opo* sequence. They all showed sequence conservation from human to teleosts, and the majority (7/9) had both epigenetic marks for active enhancers in human cell lines and in zebrafish whole embryos (Figure 12).

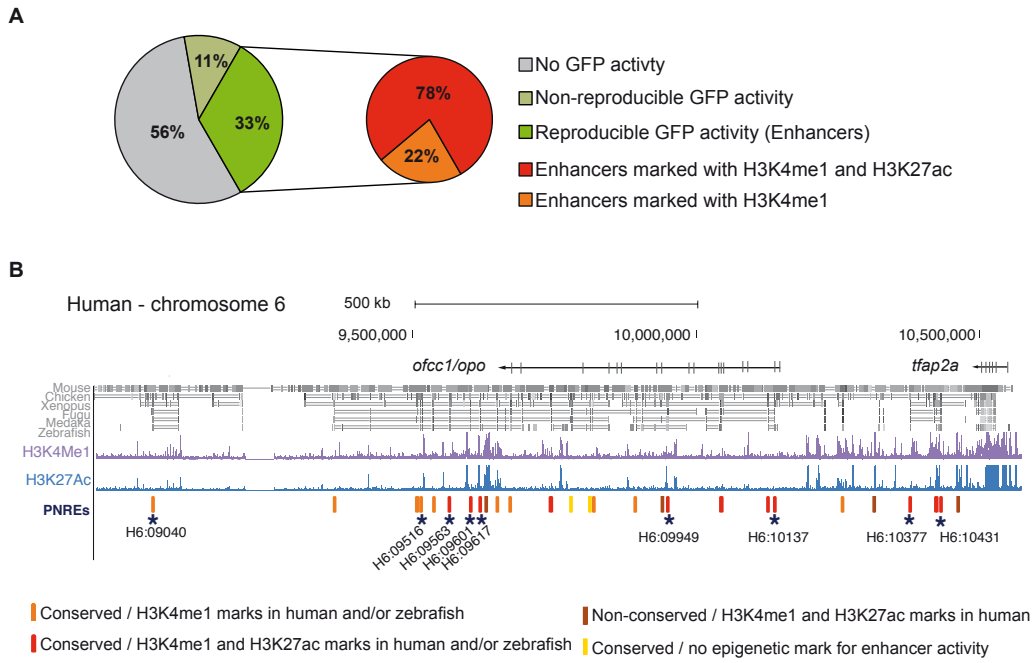

Figure 12. Summary of the enhancer screening within the *opo locus*. A) Percentage of PNREs acting as tissue-specific enhancers B) The *opo* regulatory landscape in the human genome (hg18 - chr6: 8936346-10570697, adapted from UCSC Genome Browser), showing sequence conservation from mammals to teleosts. The sum of H3K4me1 and H3K27ac marks in six human cell types is shown in purple and blue respectively; the last row represents the PNREs collection classified by color, with tissue specific enhancers identified and marked with an asterisk.

The analysis of PNREs in the *opo* landscape revealed that this locus is enriched in conserved non-coding elements that might be regulating the expression of the nearby genes.

2. Expression patterns of the *opo* locus enhancers

The GFP expression patterns of the nine enhancers found in the human *opo locus* were analyzed spatially and temporally, during zebrafish development. The enhancers did not display redundant expression patterns. However, they share common GFP patterns in a number of tissues. The enhancer patterns were distributed mostly within central nervous system (CNS), and craniofacial structures. A full description of them is shown in Table 3 and Figure 13.

***opo locus* Enhancers**	**GFP expression at early stages (16 to 36hpf)**	**GFP expression at late stages (36 to 72hpf)**	**Enhancer regulatory features**
H6:09040	CNS: more intense in the MHB	weak expression	5' from opo; H3K4me1;
H6:09516	FB and BA	FB, PL, BA ears and Jaw	5' from opo; H3K4me1;
H6:09563	CNS, NT and pituitary gland	FB, HB, NT, MHB and OB	5´from opo; H3K4me1 and H3K4ac27
H6:09601	FB	FB	5´from opo; H3K4me1 and H3K4ac27
H6:09617	FB, MHB and CNC	MB, lens, HA and low expression in FB	5´from opo; H3K4me1 and H3K4ac27
H6:09949	FB, DRGs and PF *primordium*	FB and PF	Within opo intronic region; H3K4me1 and H3K4ac27
H6:10137	**Presumptive NR**	**Dorsal NR**	**3' from opo; H3K4me1 and H3K4ac27**
H6:10377	DRGs, Pn, ears, and epidermis	DRG, ears and epidermis	3' from opo; H3K4me1 and H3K4ac27s
H6:10431	FB, BA, DRGs and ears	FB, BA, DRGs, ears, heart chamber	3' from opo; H3K4me1 and H3K4ac27

Table 3. *Opo locus* enhancers expression patterns. GFP expression patterns during zebrafish development, and their putative regulatory influences in tissue development: Central nervous system (CNS); Midbrain hindbrain boundary (MHB); Forebrain (FB); Branchial arches (BA); palate (PL); Neural tube (NT); Hindbrain (HB); Olfactory bulbs (OB); Pectoral fins (PF); Dorsal root ganglia (DRGs); Neural retina (NR); Pronephros (Pn).

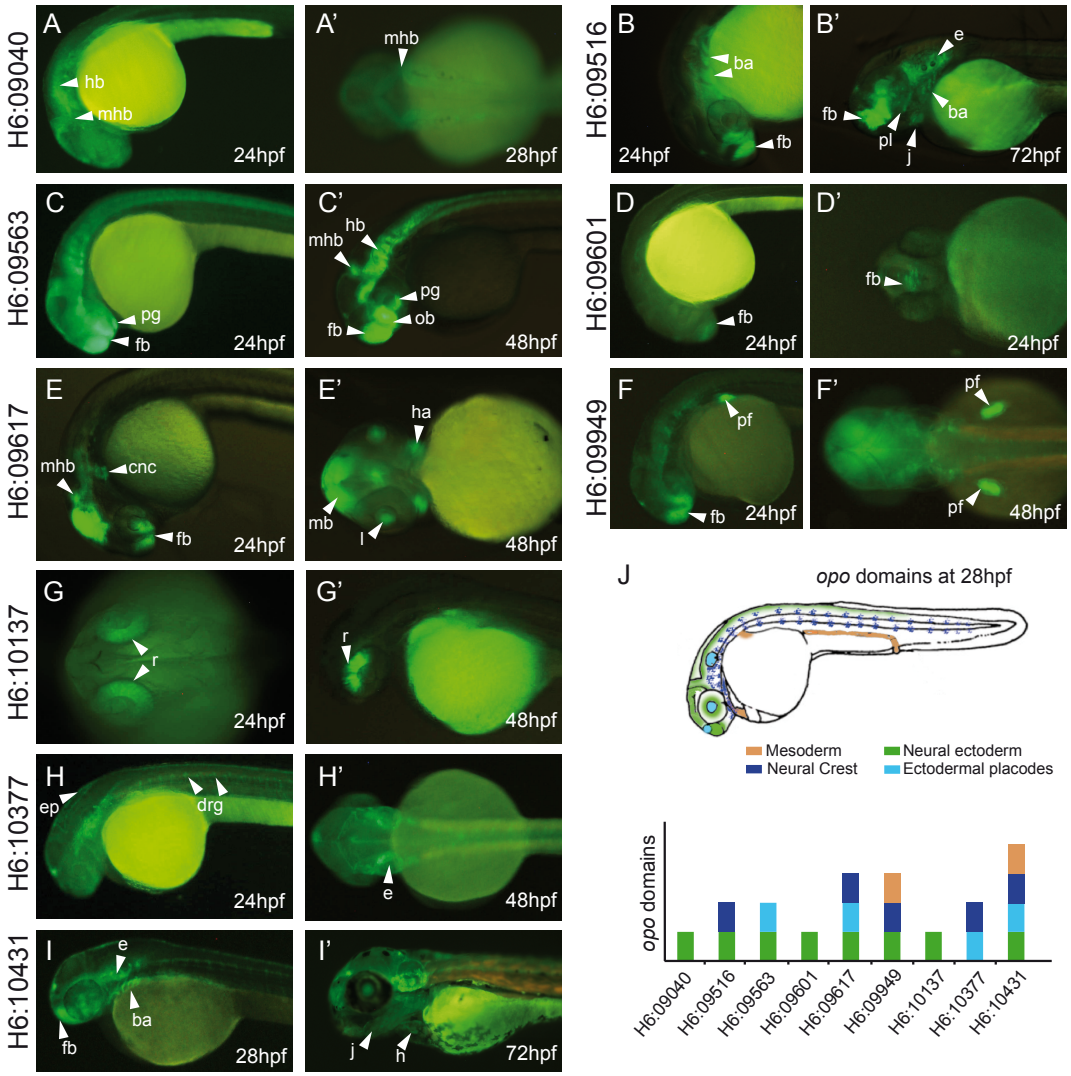

Figure 13. GFP expression pattern of *opo locus* enhancers. A-F) Arrowheads: midbrain-hindbrain boundary (mhb); branchial arches (ba); forebrain (fb); ear (e); palate (pl); jaw (j); hindbrain (hb); midbrain (mb); pituitary gland (pg); olfactory bulbs (ob); hyoid arch (ha); lens (l); pectoral fin (pf); retina (r); dorsal root ganglia (DRG); epidermis (ep); heart (h). J) The zebrafish model is colored according to the sum of the enhancers' GFP patterns. The total sum of the *opo* enhancers patterns appears to recapitulate the *opo* expression pattern as described in medaka (Martinez-Morales et al., 2009; Mertes et al., 2009) and mouse (Mertes et al., 2009).

The expression patterns of the individually isolated enhancers were compared to the *opo* expression pattern during zebrafish development, as revealed by *in situ* hybridization. As an additional reference, a stable transgenic line harboring GFP under the control of the *opo* promoter region (*opo*5kbup:GFP) was generated. This 5 Kb genomic region was isolated from the compact medaka genome, taking advantage of

the precise definition in medaka of the transcription starting site of the gene, as determined by RACE experiments in Martinez-Morales et. al. 2009. The expression patterns obtained from both analyses were similar (Figure 14 and Supp. Fig. 2) although not completely overlapping. Expression starts at around 16hpf in the optic vesicle and central nervous system. At 24hpf, *opo* is expressed in cranial neural crest derivatives, inner ear, pronephros, and particularly in the anterior CNS, including retina, forebrain and midbrain-hindbrain boundary. By 48hpf, *opo* is present in craniofacial structures derived from cranial neural crest; like jaw, palate, and branchial arches. The comparison of the GFP pattern of each enhancer with the global expression *of opo* confirms that, collectively, the enhancers recapitulate *opo* expression during development (Figure 14-J).

1. *opo in situs* Hybridization

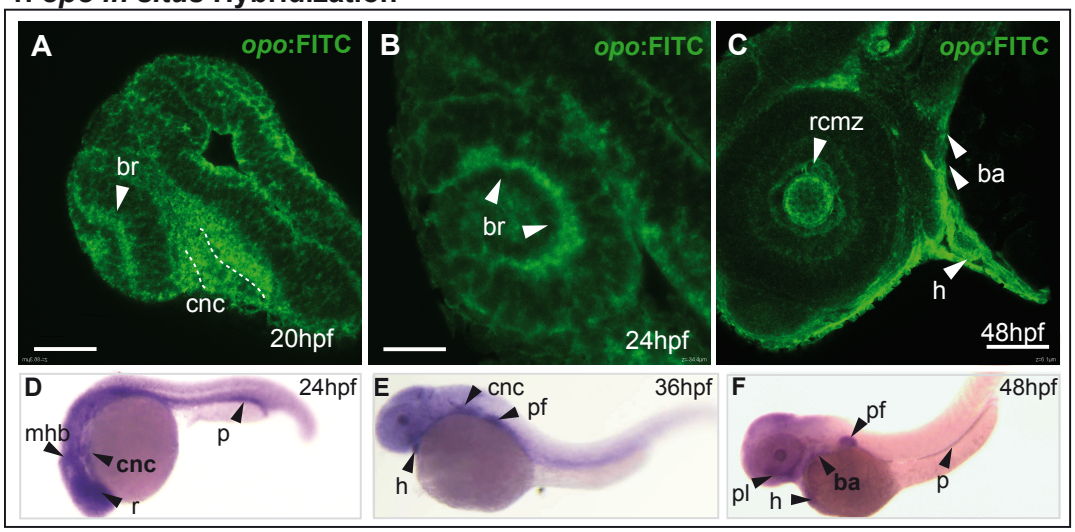

2. *opo* promoter region

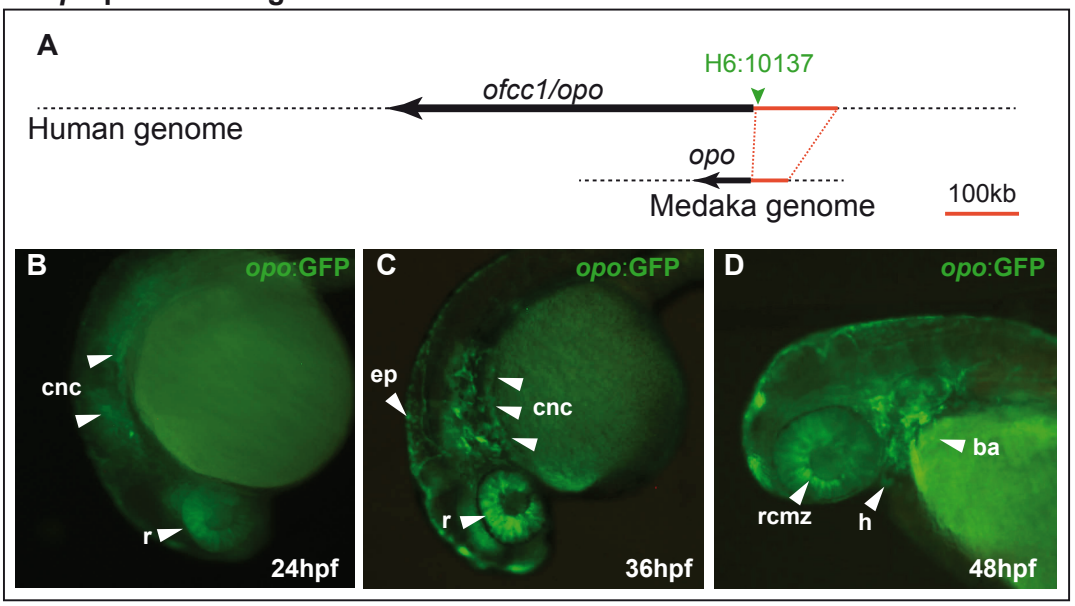

Figure 14. *Opo* expression pattern analyses. Panel 1: A-C) whole mount fluorescent *in situ* hybridizations (FISH); D-F) whole mount *in situ* hybridizations. Dashed lines: cranial neural crest. Arrowheads: (br) basal side of the presumptive neural retina; (cnc) cranial neural crest cells; (ba) branchial arches; (h) heart; (rcmz) retina at ciliar marginal zone; (mhb) midbrain-hindbrain boundary; (p) pronefros; (pf) pectoral fin; (pl) palate. Panel 2: A) *opo* promoter region amplified from the medaka genome contains the H6:10137 enhancer (green). B-D) GFP expression pattern of the *opo* promoter region stable line (Tg(*opo*5kbup:ZED). B) GFP expression in neural retina and in cranial neural crest at 24hpf; C) GFP expression in neural retina cranial neural crest and epidermis at 36hpf; D) GFP expression pattern at retina ciliar marginal zone, branchial arches and heart.

The 5 kb of opo promoter region includes H6:10137 enhancer inside, which is expressed exclusively in the neural retina. Accordingly, *opo* prmoter region displays specific GFP expression in neural retina. Although, this 5kb region also dirves the GFP expression to the cranial neural crest, but not in forebrain, midbrain, pronephros or fins. We could not find any cranial neural crest enhancer in this regions suggesting that we were unable to identify all regulatory elements using phylogenentic footprinting and epigenetic marks criteria.

The majority of the expression patterns associated to the enhancers were not exclusive in one tissue, but were instead expressed in multiple tissues at the same time. Also, multiple enhancers were expressed in the same domains, suggesting a combinatorial activity for the transcriptional control in specific tissues, such as in the forebrain and branchial arches (Figure 15).

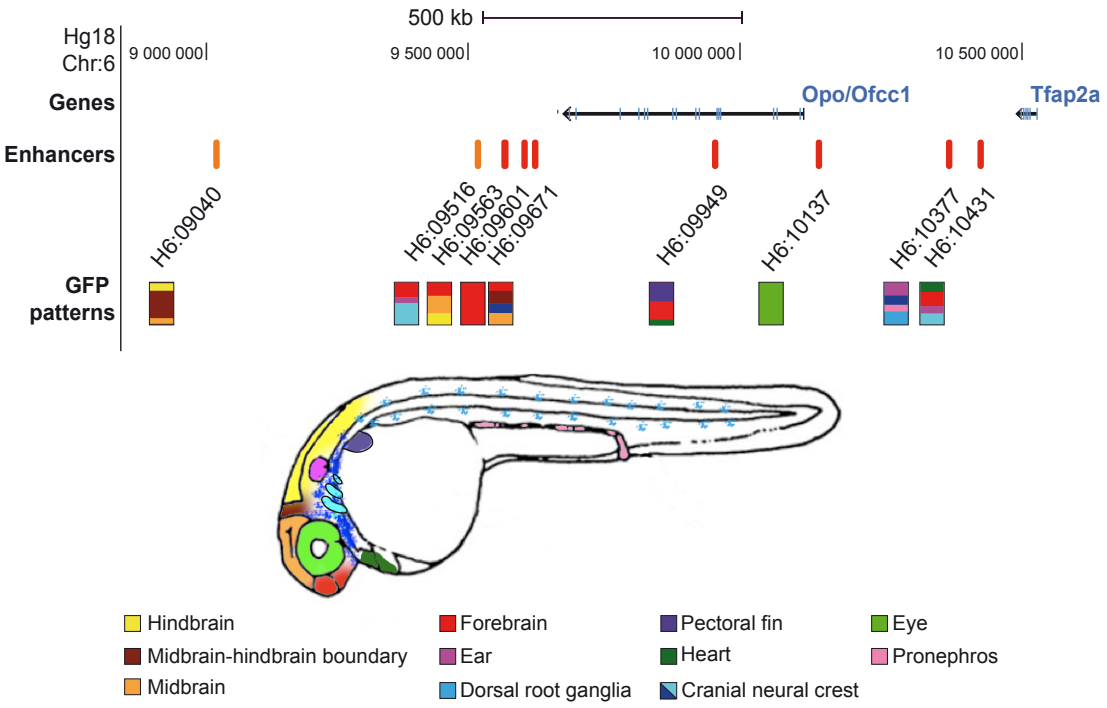

Figure 15. Distribution of the enhancers along the *opo* landscape. Representation of the enhancers GFP expression patterns in zebrafish at 28hpf. Multiple enhancers are expressed in the same embryo domains. Two enhancers (H6:09601 and H6:10137) are expressed in only one tissue.

In summary, the new enhancers found in the *opo locus* drive GFP expression primarily in the CNS and in cranial neural crest derivatives. Interestingly for this thesis, one of the CNS enhancers (H6:10137) was expressed exclusively during the neural retina development. This eye-specific enhancer, H6:10137, is contained within the analyzed *opo* promoter region and drives the expression of the GFP reporter in an remarkable pattern, which appears first at 16hpf, coinciding with the onset of optic cup folding, and remains "active" until 46hpf, when the eye is completely formed.

3. Nuclear environment of *opo* locus

If the enhancers identified in the *opo locus* are indeed regulating *opo* expression, they are expected to establish physical contact with the promoter of the gene. To explore the nuclear environment of *opo locus*, we employed the Circularized Chromosome Conformation Capture technique followed by deep sequencing of the obtained fragments (4c-seq). This technique allows the genome-wide detection of the interactions between *opo* promoter (viewpoint) and its surroundings (Figure 16).

For the 4C analysis we use mouse genetic material at stage E9.5, corresponding to the onset of expression of *opo* during development (Mertes et al., 2009). Ideally we should use genetic material from zebrafish or human, taking in account that our study is done using human sequences and using zebrafsh as model organism. We did not use human genetic material because it is inaccessible. The zebrafish genentic material is available to get, however the annotation of the zebrafish genome is fragmented for the *opo locus*, what impairs the posterior analysis of the results.

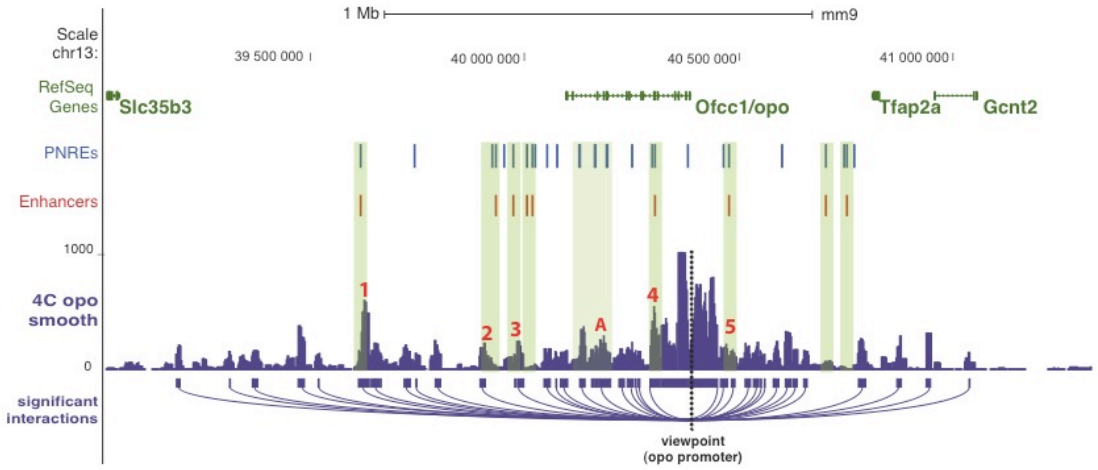

Figure 16. 4C analysis in *opo locus*. 4C analysis with a fixed fragment (dashed black line) in *opo* shows that opo promoter contacts (light green bars) with 5 of the 9 enhancers indentified in *opo locus* (red numbers: 1-H6:09040; 2- H6:09516; 3- H6:09563; 4- H6:09949; 5- H6:10137); Another elements inactive (H6:09815; H6:09892) and with no tissue specific enhancer activity (H6:09813) were also found to contact with *opo* promoter (red letter: A)

The analysis of the 4C data revealed that *opo* promoter establishes contacts with the majority of the previously identified *opo locus* enhancers. A large fraction of the contacts are mapped 3' from *opo* promoter and it was observed that 5 out of the 9 enhancers establish significant contacts with *opo* promoter. Additionally, the global interaction map of the *opo* promoter spands over a 1.5Mb genomic window covering the entire *opo locus* and containing the collection of identified PNREs .

These findings indicate that the majority of the newly identified *opo locus* enhancers maintain physical contacts with *opo* promoter, which suggests a regulatory influence of these elements over *opo* expression.

The 4C analyses were also preformed using the H6:10137 enhancer as viewpoint (Figure 17). The obtained data revealed that H610137 enhancer is contacting the *opo* promoter, two *opo* intronic regions and one enhancer (H6:09601). The fact that H6:10137 enhancer contacts other enhancers at the same time that is contacting the *opo* promoter suggest a complex architecture of the *opo locus*.

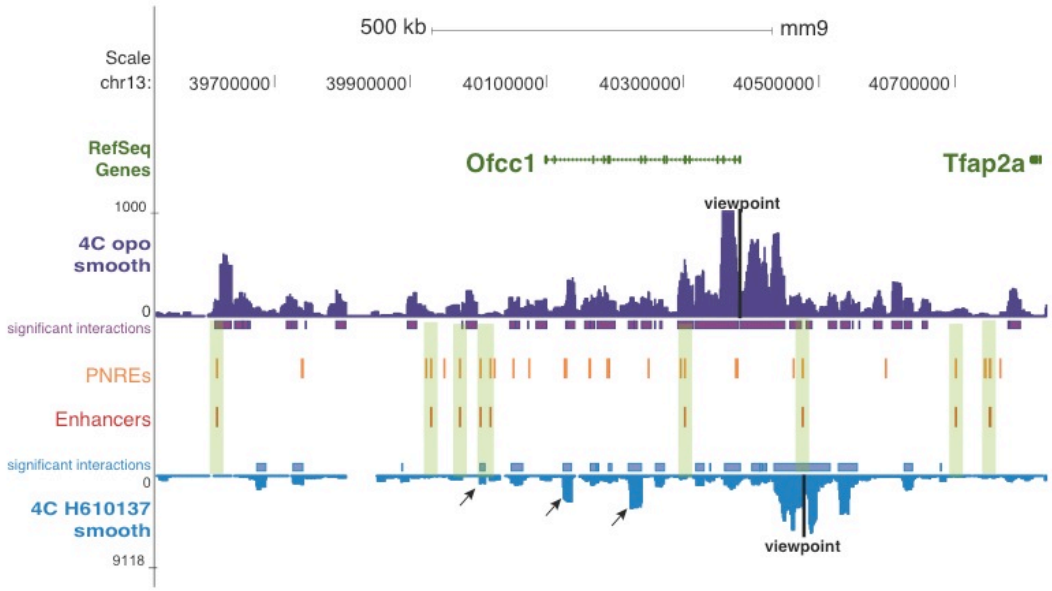

Figure 17. 4C analysis in *opo locus* landscape using *opo* promoter and H6:10137 as viewpoints. Fixed fragments used as viewpoints are represented as black lines. The interactions between the PNREs (orange) and the enhancers (red) with the opo promoter and H6:10137 enhancer are marked with light green bars. The arrows mark the interaction of H6:10137 with both intronic regions and H6:09601 enhancer

Given the known function of *opo* during eye development, the expression of H6:10137 enhancer suggests that it may be a key regulator of *opo* expression in the retina. Thus, in order to identify putative up-stream regulators of *opo*, the H6:10137 sequence was analyzed in detail for the presence of transcription factor (TF) DNA-binding sites.

4. Search for transcription factor binding sites in eye enhancer H6:10137

To search for conserved transcription factor (TF) DNA-binding sites within the H6:10137 sequence, we used MultiTF alignment tool from the ECR browser (Ovcharenko et al., 2004). Through this method, a list of 56 TFs binding sites conserved between human (hg18) and xenopus (*xenopus tropicalis*) was obtained (Supp. Tab. 4). Additionally, the JASPAR Database (Bryne et al., 2008) identified a list of 20 TFs binding sites with a score $\geq$ 10 (Supp. Tab. 5). The combined list of transcription factors was then examined in order to verify which TFs shared a common expression pattern with H6:10137. To this end the expression annotations

described in The Zebrafish Model Organism Database (Sprague et al., 2003) were used as a reference.

These investigations revealed a number of transcription factors expressed in the retinal tissue, such as Vsx2, Rx, Vsx1, Brca. Among them, the homeobox transcription factor *Vsx2* (also called *Chx10* in mammals) showed a neural retina specific expression pattern (Liu et al., 1994; Vitorino et al., 2009) that resembled most the spatio-temporal activation of H6:10137 (Figure 18-A,B). The comparison of the data obtained with ECR and JASPAR databases, indicated the presence of two conserved binding sites for Vsx2 (Zou and Levine, 2012) in H6:10137: BS1:142-151bps, detected both with ECR and JASPAR; and BS2: 678-687bps, detected only with ECR. These binding sites were then aligned for three representative species using *ClustalX*, (Figure 18- C, D). The resulting alignments further confirmed that the two binding sites for Vsx2 in the H6:10137 sequence are conserved from mammals to teleosts.

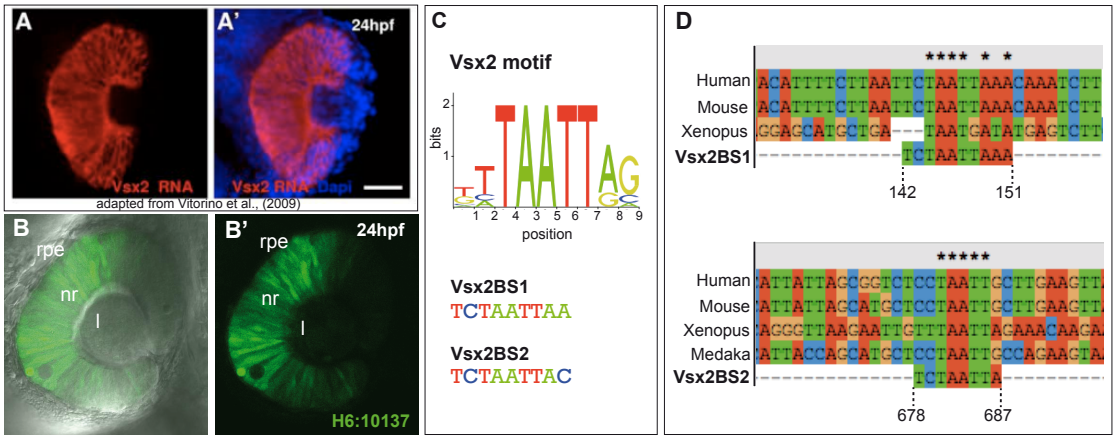

Figure 18. H6:10137 enhancer activity and Vsx2 binding sites. A) *Vsx2* RNA expression in the neural retina at 24hpf (adapted from Vitorino et. al., 2009); B) GFP expression pattern of H6:10137 in the neural retina at 24hpf: (l) lens; (nr) neural retina; (rpe) retina pigmented epithelium; C) Vsx2 motif (Zou and Levine, 2012) and Vsx2 DNA-binding sites within the H6:10137 sequence; D) Multispecies alignment of H6:10137 enhancers show sequence conservation of BS1 and BS2; Genomes versions: Human: Mar. 2006 (NCBI36/hg18); Mouse: July 2007 (NCBI37/mm9); Xenopus: Nov. 2009 (JGI 4.2/xenTro3); Medaka: Oct. 2005 (NIG/UT MEDAKA1/oryLat2).

The presence of these conserved binding sites indicate a possible interaction between the transcription factor Vsx2 and the *opo* eye enhancer, which is also consistent with the specific expression of Vsx2 and H6:10137 in the developing neural retina, but not in the adjacent RPE.

5. Vsx2 DNA-binding sites are necessary for H6:10137 enhancer activity

To investigate if Vsx2 binding sites BS1 and BS2 within the H6:10137 sequence are required for the enhancer activity of H6:10137, both sites were mutated to generate the mutated construct mutH6:10137 (Figure 19).

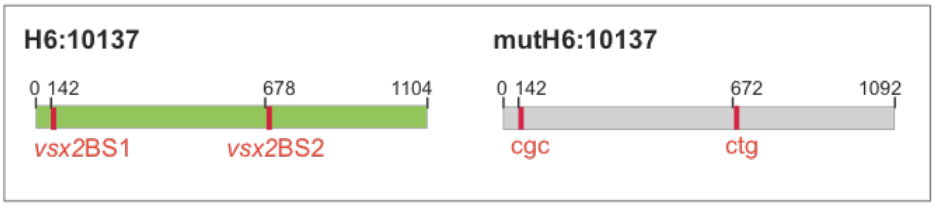

Figure 19. Mutagenesis of H6:10137. Generation of the mutH6:10137 construct by mutagenesis of Vsx2BS1 and Vsx2BS2 sites in the H6:10137 sequence.

The enhancer capacity of mutH6:10137 (activation of GFP expression in the neural retina) was compared with that of H6:10137 in mosaic embryos (F_0) produced in transient zebrafish transgenic assays. As positive control for transgenesis (RFP expression in somites and heart) was observed at 48hpf in both cases (Figure 20) and only positive embryos were scored. While 42% of the H6:10137 embryos positive for transgenesis showed typically elongated GFP positive neuroblasts in this tissue when analyzed at 24hpf, mutH610137 embryos do not present any GFP positive cells in the undifferentiated neural retina (Figure 20).

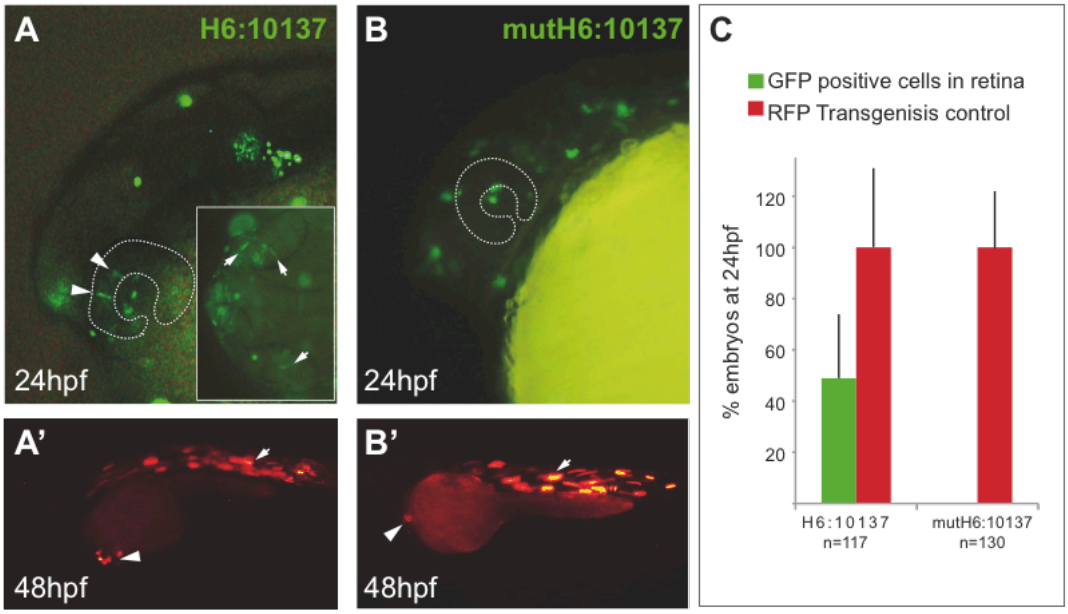

Figure 20. Transgenesis assays of mutH6:10137 and H6:10137. A-A') H6:10137 transgenic embryos (F_0 - mosaic) expressing GFP in two retina cells and RFP in heart and somites, (arrowheads); B-B') mutH6:10137 transgenic embryos (F_0 - mosaic) without GFP activity in retina cells and expressing RFP controls in heart and somites (arrowheads); C) 42% of the H6:10137 transgenic embryos had GFP positive cells in retina at 24hpf. Error bars indicate standard deviation of the mean.

Therefore, the mutation of Vsx2 BSs in the H6:10137 enhancer sequence abolished its enhancer activity in neural retina precursors. This suggests that the activity of the enhancer depends on Vsx2 binding.

6. Vsx2 regulates *opo* expression levels through its binding to H6:10137

We reasoned that if H6:10137 activity depends on Vsx2 binding, loss of *vsx2* function should also affect both H6:10137 activity and *opo* expression levels. To address this point, we designed splicing morpholinos against *vsx2*, to produce a knockdown condition.

Two splicing blocking morpholino oligonucleotides (MO) were designed: I1E2MO and E2I2MO, affecting the splicing of introns 1 and 2 respectively. Both MOs generate aberrant transcripts, as assessed by RT-PCR amplification from morphant embryos cDNA. Sequencing of these transcripts confirmed splicing disruption of Vsx2 mRNA in morphant embryos (Figure 21- A, B).

To evaluate the effects of Vsx2 knockdown on H6:10137 activity, both *vsx2*

morpholinos (*vsx2*MOs) were injected separately into one-cell stage into Tg[H6:10137] embryos (i.e. the stable H6:10137 transgenic line). GFP activity in Tg[H6:10137] morphant and control embryos was examined from 18 to 24 hpf. In addition to conspicuous morphological eye defects, which will be extensively discussed in the next section, *vsx2* morphants showed a dramatic decrease of the levels of GFP signal. In fact, GFP signal could only be detected in 20-30% of the injected embryos (Figure 21-D, G).

These results show that a reduction of functional *vsx2* in the neural retina impinges on the activity of the H6:10137 enhancer; thus indicating that Vsx2 is necessary for its regulation.

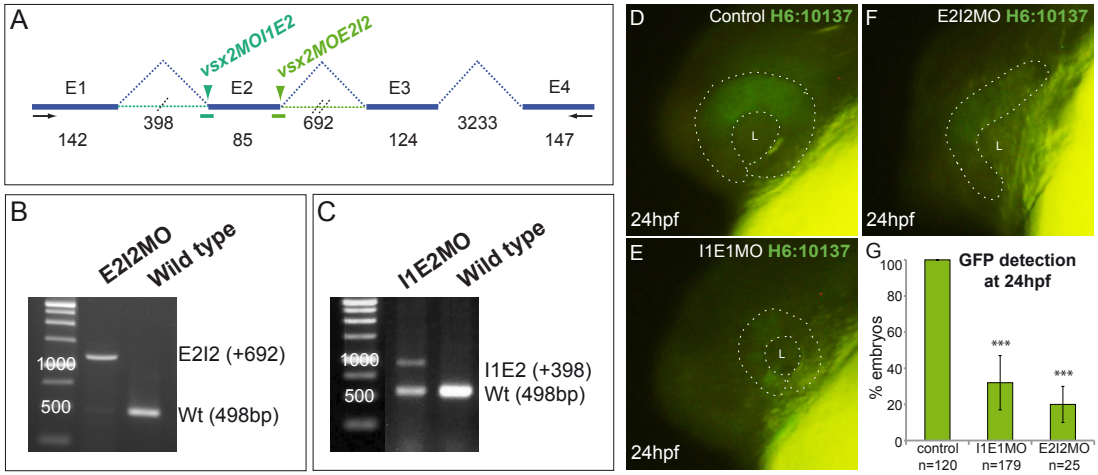

Figure 21. *Vsx2* knockdown using splicing morpholinos. A) The zebrafish *vsx2* transcript. Exon 1 (E1); Exon 2 (E2); Exon 3 (E3); Exon 4 (E4); Introns are represented as dashed lines; the length of both Introns and Exons is represented above. RT-PCR primers are represented as two arrows at transcript ends. Vsx2MOs are represented in green. B-C) RT-PCR of E2I2MO and I1E2MO injected embryos at 24hpf and respective controls (wild type embryos) showing the morphants' aberrant transcripts with the inclusion of Intron 2 in E2I2MO (+692bp), and Intron 1 in I1E2MO (+398bp). In both conditions the amount of native transcript (Wt: 498bp) is reduced when compared to the controls, however the reduction is more evident in the E2I2MO embryos. D-F) GFP activity in *vsx2* morphant embryos is reduced when compared to the controls (the eye is marked with a dashed line). G) GFP detection in morphant embryos is significantly reduced when compared to the controls, using a Student *t*-test (*p*-value <0,0001). Error bars indicate standard deviation of the mean.

Following the previous line of arguments, if Vsx2 is essential for H6:10137 enhancer activity during eye development, and H6:10137 is likely to regulate *opo* expression, it is expected that *opo* expression depend on *vsx2* levels.

To test this, we generated *vsx2* gain and loss of function conditions we either injected zebrafish *vsx2* RNA (0,1 – 0,3 ug/ul *per* embryo) or the above described morpholinos, respectively. Then we used RT-qPCRs to quantify *opo* levels in *vsx2* knockdown and *vsx2* over-expresing embryos at 24hpf. These quantifications showed a significant reduction of *opo* expression in *vsx2* knockdown embryos, when compared to the controls. This reduction was even more evident when only the heads of knockdown embryos were used as sample for the RT-qPCRs. As expected, the expression levels of *opo* were increased in *vsx2* over-expressing embryos with respect to the controls (Figure 22).

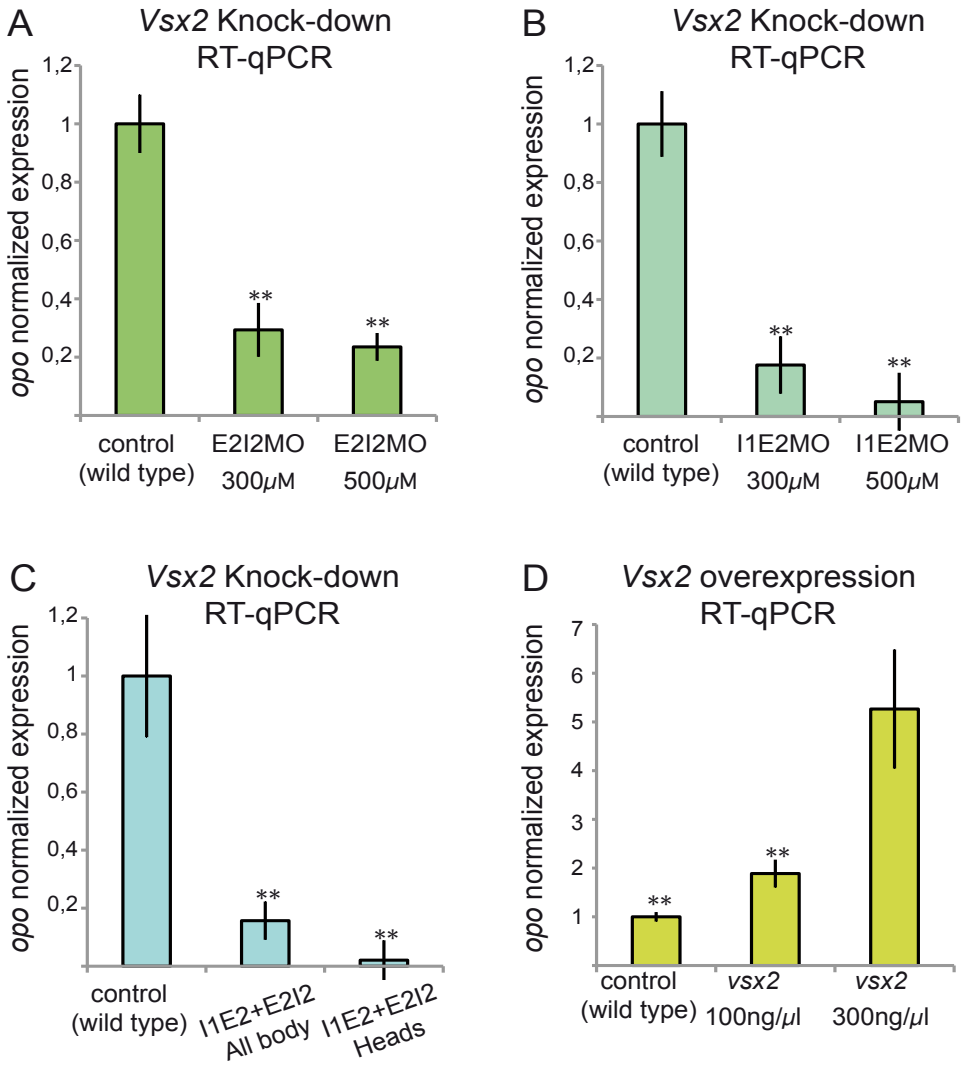

Figure 22. *Opo* expression levels quantifications by RT-qPCR. *Opo* expression levels are significantly reduced in *vsx2* morphant embryos in a dose-dependent manner (A-B). This reduction is more pronounced when only the heads of co-injected embryos with both *vsx2*MOs were used for the quantification (C). *opo* expression levels in embryos over-expressing *vsx2* are significantly higher when compared to controls (D). N=3; Student *t*-tests. Error bars indicate standard error of the mean (SEM).

According to the previous results, Vsx2 regulates the activity of the H6:10137 enhancer and consequently *opo* expression levels. To confirm that this regulation is direct we performed Chromatin Immunoprecipitation followed by quantitative PCRs (ChIP-qPCR assays). To this end we generated a *GFP_Zfvsx2* fusion and its *corresponding* RNA was injected into one-cell stage embryos (see methods). Then ChIP assays were performed using the heads of 300 injected embryos and a ChIP grade antibody against GFP. In qPCRs experiments, primers for the housekeeping *ef1a* gene were used as a negative control, once confirmed that the amplified sequence had no Vsx2 binding sites. As positive control we used primers for the *vsx1* promoter, previously described as a Vsx2 target in Clark et al., (2008). These assays confirmed *in vivo* the binding between Vsx2 and the enhancer H6:10137 (Figure 23).

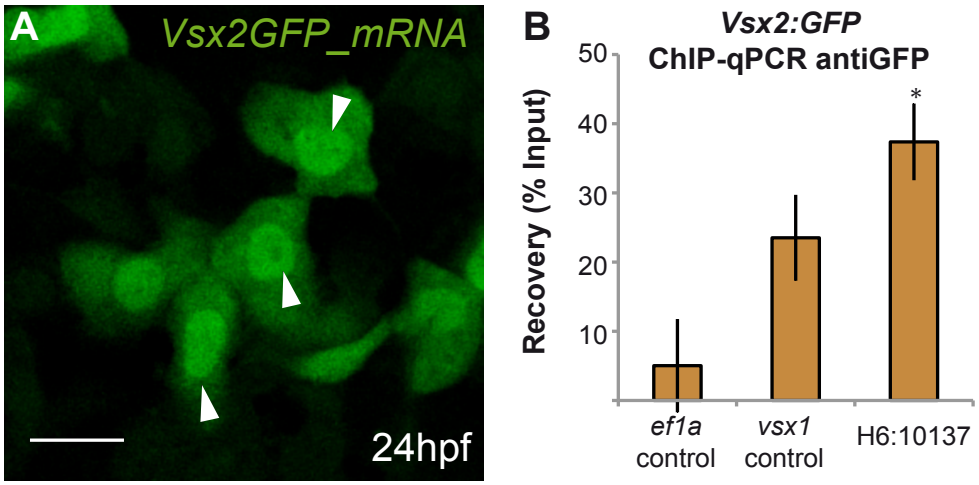

Figure 23. H6:10137 is a direct target of Vsx2. A) Confocal microscopy image of epidermal cells injected with *vsx2*GFP-mRNA, showing the nuclear localization of the mRNA (arrow heads) at 24hpf. B) Using chromatin extracts of *vsx2GFP*-mRNA-injected embryo heads a ChIP-qPCR was performed, using anti-GFP. The recovery of the H6:10137 sequence was significantly increased when compared to the negative control (*ef1a*) (n=2). One Way ANOVA; error bars indicate SEM.

These findings confirm that the H6:10137 enhancer is a direct target of the transcription factor Vsx2 and hence indicate that *vsx2* is an upstream positive regulator of *opo*.

7. *Vsx2* disruption causes optic cup folding defects

To investigate the role of *vsx2* during eye morphogenesis, optic cup folding was analyzed in *vsx2* morphants. Embryos were obtained from several independent injections of the above mentioned *vsx2*MOs (I1E2MO and I2E2MO). The *p53* morpholino (*p53*MO) was co-injected with *vsx2*MOs at 100uM to avoid the reported increased apoptosis artifacts (Langheinrich et al., 2002). Control embryos were either injected with 100uM of *p53*MO or uninjected wild type embryos were used as a reference. Injections were performed on the background of the Tg*(vsx2.2*:GFPcaax*)* line, which was generated in our laboratory using the Medaka *vsx2.2* promoter and GFPcaax as reporter gene. This line, in which neural retina membranes are fluorescently labeled, facilitates the analysis of morphant phenotypes. As a transgenesis control, this line also expresses GFP in the heart (Kwan et al., 2007).

The phenotype analysis shows that both *vsx2*MOs were able to affect eye development when compared to the controls, producing similar eye phenotypic defects. Morphant embryos display two main morphological defects: a reduction of eye size (microftalmia) and the malformation of the optic cup, now displaying large ventral openings. 23% I1E2MO morphant embryos did not show any eye defects, 66% of the morphants showed eye morphological defects and 12% of anoftalmic (n=46, *p*-value <0,0001). For the E2I2MO morphant embryos 28% did not show eye defects, 57% displayed eye morphological defects and 15% were anoftalmic (n=50, *p*-value<0,0001). In the controls it was not observed morphological eye defects (n=40).

Micorftalmia and ventral opening phenotypes overlap in 40%-50% of the affected embryos. The complete absence of the eye (anoftalmia) was observed in the most severe cases (see Figure 23). Interestingly, the E2I2MO morphant embryos showed stronger eye defects than the I1E2MO-injected embryos (see Figure 24- E, F). This correlates with our previous finding showing that in fact E2I2MO induces a deeper knockdown of vsx2 mRNA than I1E2MO.

To test for the specificity of the morphant phenotype, *vsx2*-mRNA was coinjected

with E2I2MO. The morphant phenotype was significantly rescued in 47% of the co-injected embryos (73% No eye defects, 27% Eye morphological defects; N=53) when compared to embryos injected only with E2I2MO (28% of No eye defects, 57% of Eye morphological defects, 15% of anoftalmic, n=50) (Figure 24- E, Supp. Tab. 6).

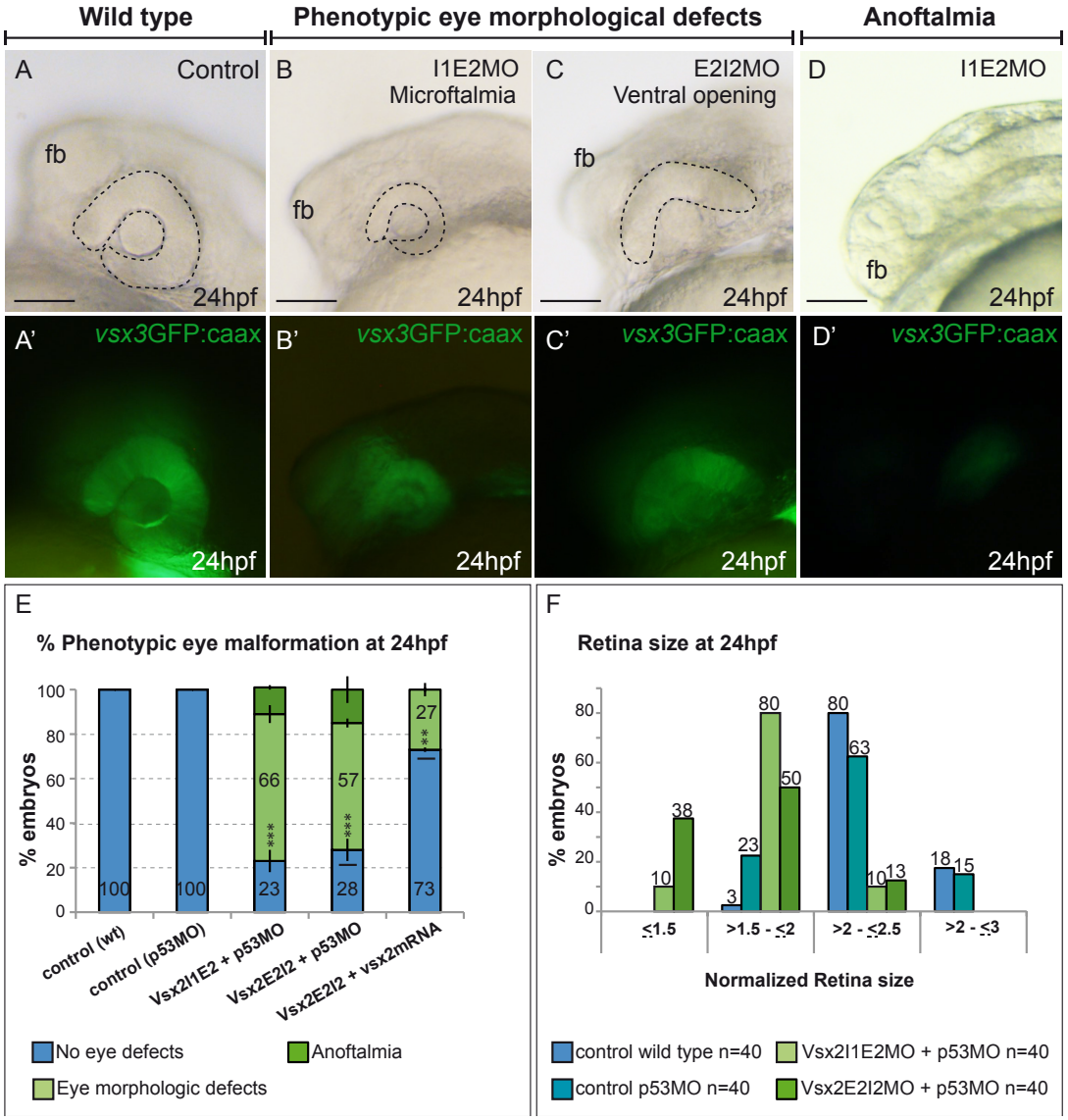

Figure 24. Phenotypical defects of *vsx2*MOs-injected embryos. A-A') wild type control embryos showing no eye defects; B-C) Eye defects in *vsx2*MO-injected embryos (retinas are marked with a dashed line), miroftalmia (B) and ventral opening (C); D) *vsx2*MO-injected embryos with anoftalmia; E) *vsx2* morphant embryos show significant phenotypic eye malformations when compared with controls. In the co-injected embryos with E2I2MO and *vsx2*-mRNA, the % of embryos showing ocular malformations is significantly reduced when compared to embryos injected with E2I2MO; F) In *vsx2* morphants the retina is reduced when compared to the controls. Error bars indicate standard deviation.

The finding that *vsx2* loss can result in microftalmia and anoftalmia had already been observed in previous studies in zebrafish at later stages (Vitorino et al., 2009) and also in *vsx2* Knockout mice models (Burmeister et al., 1996). Although our analysis was performed at earlier stages (20 to 25hpf), when such malformations are harder to identify, we were also able to observe eye reduction defects in over 30% of knockdown embryos (Figure 24, Supp. Tab. 7). Interestingly, retinae in morphant embryos were still ventrally opened at 24hpf, when the folding of the optic cup should be completed (Figure 24-C).

To analyze this phenomenon in a quantitative manner, the angles of ventral openings were measured in over 100 embryos *per* morpholino, at 24hpf. This analysis revealed that around 70% of *vsx2* knockdown embryos displayed ventral openings in the retina, and these openings ranged in angle between 21° to 120°. This is much in contrast to control embryos that showed ventral openings in a range of 0° to 20°. E2I2MO injections produced even stronger phenotypes, with 23% of morphant embryos displaying ventral openings wider than 80° when compared to I1E2MO morphant embryos (12% of ventral openings wider than 80°) (Figure 25, Supp. Tab. 8).

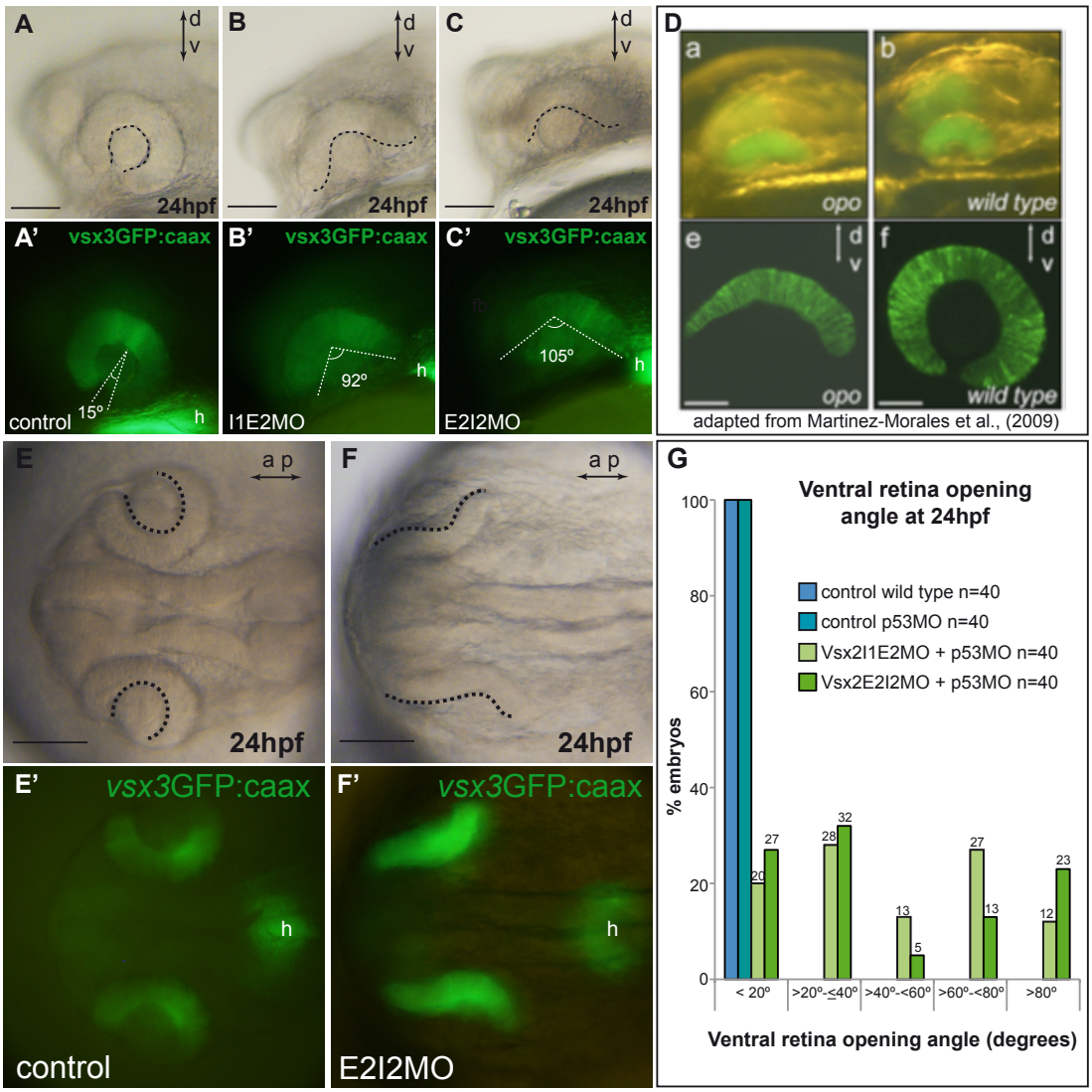

Figure 25. *Vsx2* morphants: Ventral opening retinas measurements. A-A') control wild type embryos; heart (h); B-C') *vsx2*MO morphant embryos showing ventral opening retinas higher than 80°; D) Medaka *opo* mutant expressing *rx2*::mYFP (a and e) wild type *rx2*::mYFP medaka embryo (b and f) (Martinez-Morales et al., 2009); E-E') control wild type embryos (dorsal view). F-F') E2I2MO-injected embryo showing retinae ventral opening (dorsal view). The basal curvature of the retinae is marked with a dashed line. G) Measurements of the ventral opening angles in the *vsx2*MOs morphant embryos and controls at 24hpf.

We can therefore conclude that *vsx2* is necessary for the folding of the optic cup, being the morphological defects produced by its knockdown in the most severe cases similar to the defects observed in *opo* mutant eyes.

Together these results indicate that *vsx2* is an upstream regulator of *opo* via the H6:10137 enhancer. Defects in *vsx2* function result in a down-regulation of *opo* expression, and consequently its function in the folding of the optic cup is compromised. Previous

analyses did not establish a clear connection between the patterning of the optic cup and its morphogenesis. The results here presented show that *vsx2*, by controlling the expression of *opo*, provides an important link between both phenomena.

V. Discussion

This work provides new insight into the regulation of the *opo* gene in vertebrates. Here, we identify and describe a battery of enhancers that regulate *opo* function during craniofacial and eye development. Additionally, we show that during optic cup folding in zebafish, Vsx2 regulates *opo* via the H6:1037 enhancer.

1. The *Opo* regulatory landscape

Organogenesis requires the dynamic control of gene expression, which in turn involves the activity of non-coding *cis*-regulatory elements (NCREs) spread over large genomic distances. The regulatory landscape is defined by the interactions established by the CREs and specific gene promoters. Understanding the logic of regulatory landscapes is essential to interpret how basic genetic programs operate in the context of both development and disease.

In this work we focus on *ojoplano*, a developmental gene essential for both eye morphogenesis and craniofacial development. We dissect out the CREs that regulate its expression during these key developmental events; we make correlations between these new regulatory elements and the control of *opo* expression, and finally we suggest potential links for these new elements with human hereditary diseases.

Our comprehensive expression analysis by transgenesis of a representative collection of human putative non-coding cis-regulatory elements (PNREs) in zebrafish embryos, revealed the presence of nine tissue specific enhancers expressed in the *opo* domain. The majority (six) of these *opo* enhancers were expressed during the development of craniofacial structures such as the jaw and the palate. They were also expressed in the central nervous system, including the eye, and in sensory organs, like the olfactory bulbs and dorsal root ganglia. When the expression of *opo* (Martinez-Morales et al., 2009; Mertes et al., 2009) and its enhancers were analyzed, we observed that when summed together the enhancers expression fully recapitulates the *opo* expression pattern. This indicates that this short collection of enhancers might account for a substantial part of the *opo* gene regulation.

We also analyze the expression of a 5kb region upstream of the *opo* start site (opo_5kbup). This region, that includes the *opo* promoter and the H6:10137 enhancer, was also able to drive GFP expression to the neural retina, thus confirming the

regulatory influence of H6:10137 during eye development. *opo*5kbup:GFP was not able to recapitulate the full expression of the gene (e.g. there was no expression in the CNS, fins or sensory organs), however it was also expressed in the cranial neural crest. This result suggests the presence in this genomic region of cryptic neural crest enhancers, which our combined phylogenetic footprinting and/or epigenetic marks analyses failed to identify. The presence of additional enhancers in this region suggests that the regulatory complexity of the *opo locus* is even higher than anticipated. In addition, it also suggests the presence of shadow enhancers (Hong et al., 2008) that, together with the neural crest enhancers identified in this study, might drive redundant regulatory information.

Once we had defined the enhancers collection in the *opo* landscape, we performed a global analysis of the *opo* promoter interaction map by 4C (Circular Chromosome Conformation Capture). This analysis allows both the examination of the chromosomal architecture of an entire locus in a systematic manner, and also to validate specifically whether the identified enhancers are contacting the *opo* promoter or not. The data we obtained from this validation suggests that the majority of enhancers are establishing physical contacts with the *opo* promoter. Additionally, we found three elements (PNREs) not defined as enhancers in our analysis that also established significant contacts with the promoter: H6:09813, H6:09815; H6:09892 (Figure 13-A). In terms of enhancer activity, at least one of them, H6:09813, drove GFP activity. However, the GFP expression was not tissue-specific in the progenies of the different identified founders (Tab. 2). In these cases, it is possible that the sequences selected for transgenesis were not sufficient to induce tissue-specific enhancer activity, or, alternatively, these elements may need to be in their specific genomic environment to be able to drive tissue-specific activity.

Given the key role for *opo* during eye development that was recently described in our laboratory, we also decided to explore in detail the interaction map of the H6:10137 enhancer; which is expressed exclusively in the neural retina during eye morphogenesis. In agreement with the expression pattern analysis, the resulting data showed significant interactions between the H6:10137 enhancer and the *opo* promoter, suggesting that H6:10137 does directly regulate *opo* expression during eye development. More functional studies need to be performed to clarify if this enhancer is the only region required to control *opo* expression during eye

development. New genome editing tools (Jao et al., 2013; Xiao et al., 2013) open now the possibility to generate chromosomal lesions (insertions/deletions) in the enhancer H6:10137 sequence, and thus observe any resulting effects in *opo* expression and optic cup folding.

2. Opo enhancers and human hereditary diseases

The work presented here may also provide useful information about *opo* regulation in the context of human hereditary diseases. As mentioned before, in humans, *opo* is called *Ofcc1*, which stands for Oro Facial Cleft Candidate 1. The gene was given this name due to its association with orofacial cleft (OFC) syndrome (Davies et al., 2004; Murray and Schutte, 2004), a birth defect caused by abnormal facial development. The fact that *opo* mutant fish show defects in craniofacial structures like jaw, branchial arches and palate (Martinez-Morales et al., 2009), further strengthens the link between *opo* and this birth defect. Previous work form Davies et al., (2004) described three OFC cases in which the patients had independent translocations included within the *opo* locus, which were localized using previously published data and chromosome walking experiments. Importantly, some of these translocations do not compromise the coding region of the gene. They then generated representative clones for each identified breakpoint region: Breakpoint case 1: AL031906 and AL159986; Breakpoint case 2: AL031904; as well as Breakpoint case 3: AL031122 (Davies et al., 2004). With this information available, we have now investigated if any of the *opo locus* enhancers found in this study were localized within the identified translocation breakpoint cases. We established that enhancers H6:09516, H6:09563, H6:09601 and H6:09617 were all localized within the region that includes the breakpoint for case 2, and enhancer H6:10137 within that of the breakpoint for case 3 (Figure 26).

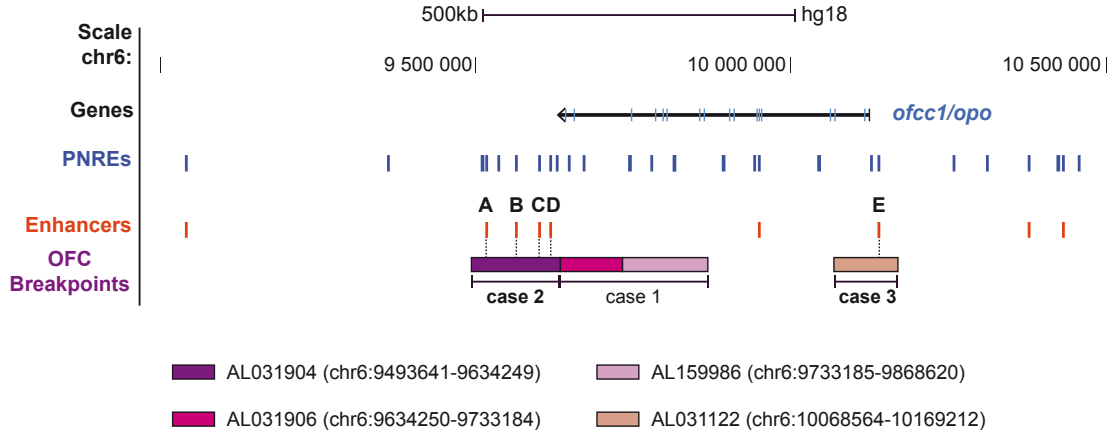

Figure 26. OFC breakpoints in the *opo* regulatory *locus*. Graphic representation of the *opo locus* (hg18 - chr6:8,961,047-10,550,262), showing the localization of the PNREs collection (blue), the newly identified enhancers (red) and the translocation breakpoints reported by Davies et al., in 2004 (pink shades). Enhancers H6:09516 (A), H6:09563 (B), H6:09601 (C) and H6:09617 (D) are localized within the region including the breakpoint corresponding to the OFC patient-case 2 (t(6;9)(p24;q22.3)). Enhancer H6:10137 (E) is localized within the region of the breakpoint corresponding to the OFC patient-case 3 (t(6;9)(p24.3;p23)) (adapted from UCSC Davies et al., (2004) and genome browser http://genome.ucsc.edu). Below, the accession number for each breakpoint-clone and its localization in the human genome is described.

The enhancers H6:09516 and H6:09617 are both expressed in facial derivatives of the neural crest; H6:09563 drives expression in the central nervous system and olfactory bulbs; while H6:09601 and H6:10137 are expressed exclusively in forebrain and neural retina respectively. Cranial neural crest (CNC) derivatives like branchial arches and jaw, as well as the central nervous system and eyes are all essential structures for the correct development of the craniofacial region (Santagati and Rijli, 2003; Kish et al., 2011). The fact that the enhancers H6:09516 and H6:09617 display expression in these structures suggests that they may contribute to craniofacial development. If this is the case, then the translocations between chromosome 6p24 and chromosome 9 would disrupt the cis-regulatory activity of the neural crest *opo* enhancers. Whether this is the causative mechanism explaining why the translocations associate to the craniofacial defects in patients with OFC needs to be formally determined.

As well as with OFC, the *opo locus* has also been associated with mental disorders, such as schizophrenia and Tourette's syndrome (TS) (Straub et al., 2002; Sundaram et al., 2011). There are several genetic markers located within *opo locus* associated with schizophrenia (D6S470; D6S940; D6S340), especially in family cases where the disease is related to cognitive defects (Straub et al., 2002; Hallmayer et al., 2005). Similarly, a novel single nucleotide variant was identified within the *opo locus* in two TS patients with different pedigrees (Comings et al., 1984; Sundaram et al., 2011). Interestingly, many of these genetic landmarks are located in non-coding regions, which suggests that causative mutations for these diseases could occur in cis-regulatory elements spread over the *opo locus*. Here, we observed that the majority of the 3' *opo* enhancers drive a strong GFP expression in the forebrain (H6:09516, H6:09563, H6:09617, H6:09601, H6:09949), suggesting a role for these enhancers in central nervous system development, and opening the possibility that a disruption of their activity could contribute to the development of the mental hereditary diseases. However, more functional and genomic studies need to be performed to investigate in detail the association between the *opo locus* and the development of schizophrenia or Tourette's syndrome.

3. The transcription factor Vsx2 binds to the enhancer H6:10137 to regulate *opo*

Vsx2 is a major gene in neural retina specification (Rowan et al., 2004). This TF is required to initiate the neural retina specification program by suppressing *mitf*, a retina pigmented-epithelium patterning gene, in the neural retina progenitor cells. The *vsx2*-mediated repression of *mitf* expression prevents *mitf* from implementing an RPE differentiation program in the developing neural retina (Horsford et al., 2005).
The mutation of *vsx2* is associated with microftalmia, which has been reported in humans and mice (ocular retardation mutant) and is caused by a decrease in the cell proliferation rate (Burmeister et al., 1996). Despite these observations, no morphogenetic defects have been reported in mammals so far. Previous knockdown studies in zebrafish at 48hpf also reported microftalmia and anoftalmia phenotypes (Barabino et al., 1997; Vitorino et al., 2009). One of these reports (Barabino et al., 1997), tangentially described early (24hpf) morphological defects in the zebrafish retina as a "flattened and triangular eye shape".

In this work, the analysis of the H6:10137 enhancer sequence revealed the presence of two conserved Vsx2 DNA-binding sites. Here, we tested the putative connection between *vsx2* and H6:10137 by mutagenesis assays for H6:101137, as well as with *vsx2* knockdown experiments. Furthermore, we confirmed the association between Vsx2 and the enhancer H6:10137 through the detection of physical interactions by chromatin immunoprecipitation (ChIP)-qPCR. Taken together, these experiments confirmed that H6:10137 enhancer activity depends on Vsx2 binding, and also that H6:10137 is a direct target of Vsx2 during optic cup folding.

In our *vsx2* morphant embryos, microftalmia, anoftalmia and retinal flat morphology were also present at early stages of eye development. This, in addition to previous experiments showing that the expression levels of *opo* were reduced in *vsx2* morphants, further support the hypothesis that *vsx2* plays a key role during optic cup folding, as an upstream regulator of *opo*. The similarities in morphology observed between ventrally-opened *vsx2* morphant and *opo* mutant retinae are also in line with this possibility. The evaluation of *opo* expression levels and eye morphology upon *vsx2* targeted mutation in a teleost model should provide an ultimate demonstration for this hypothesis in the future.

During early eye development, the neural retina precursors activate a genetic program that specify their cellular identity and is responsible for their morphological transformation during optic cup folding. It has been shown that this program acts in a tissue-autonomous manner, being to a large extent independent of neighboring tissues (Eiraku et al., 2011). Previous studies in medaka also demonstrate that optic cup folding occurs through a basal constriction mechanism, which is dependent of *opo* expression (Martinez-Morales et al., 2009). Clonal analysis shows that this folding mechanism depends on the basal constriction of the neural retina precursors, but not on the morphological transformation of the retinal pigmented epithelium precursors that passively fold towards their apical side (Martinez-Morales et al., 2009). Here, we suggest that *vsx2* may not be necessary only to confer identity to the neural retina precursors, but also to specify their morphogenetic behavior. It is likely that this cell identity program also comprises a 'morphogenetic identity' by the activation of effector genes like *opo*. In this sense, *vsx2* would provide the first direct link between

neural retina specification and morphogenesis at the onset of optic cup invagination in teleosts.

In contrast to our observations in zebrafish, eye morphological defects are not observed in *vsx2* mutant mice (Burmeister et al., 1996). Several explanations may account for this discrepancy. It is known that ocular retardation mutants can show a range of variability in the severity of the phenotype, predicting the presence of genetic interactors (Rowan et al., 2004). This observation suggests a complex network of interactions during retinal specification. In line with this, we observe that the overexpression of *vsx2* is not sufficient to induce ectopic expression of the H6:10137 enhancer. This finding may be explained by the fact that the eye enhancer also shows putative binding sites for other well known eye specifiers (i.e. *rx* and *crx*; Supp. Tables 5 and 6). These transcription factors may have different regulatory weight on H6:10137 in teleosts and tetrapods that could explain the phenotypic discrepancy.

VI. Conclusions

1. The analysis of PNREs localized within the *opo* regulatory landscape revealed the presence of nine tissue-specific enhancers.

2. The identified enhancers were distributed equally at the 5´and 3´ sides of the gene; all were highly conserved and the majority (78%) show both H3K4me1 and H3K27ac marks in human cell lines and zebrafish.

3. The total sum of the enhancers' expression patterns recapitulates the expression pattern of the *opo* gene.

4. Only one enhancer was found to be expressed exclusively in early retina (H6:10137); most expression patterns were detected in the central nervous system, neural crest and craniofacial structures.

5. The study of the interaction profile of the *opo* promoter with its genomic neighborhood confirms that most of the identified enhancers contact physically the promoter.

6. The H6:10137 enhancer has two conserved binding sites for *vsx2*, and its activity depends on *vsx2.*

7. Vsx2 interacts physically with the enhancer H6:10137 *in vivo*.

8. *opo* expression itself depends on *vsx2*: it is up-regulated in *vsx2* over-expressing embryos, and down-regulated in *vsx2* knock-down embryos at 24hpf.

9. Knockdown of *vsx2* in zebrafish embryos results in a range of eye defects, including: ventral retina openings, microftalmia, and anoftalmia.

10. The optic cup morphogenetic defects observed upon *vsx2* morpholino interference resemble, in the most severe cases, the ocular phenotype in the medaka *opo* mutants.

VII. Supplementary Material

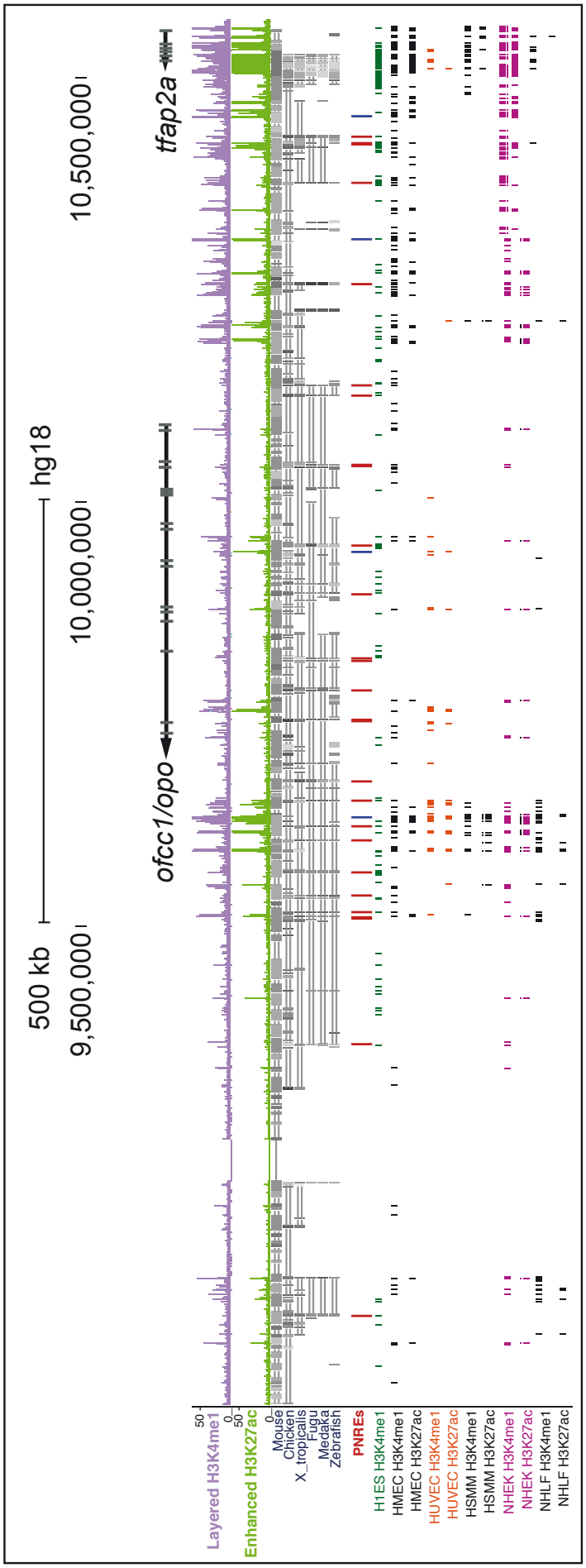
500 kb
hg18
9,500,000
10,000,000
10,500,000
ofcc1/opo
tfap2a
Layered H3K4me1
Enhanced H3K27ac
Mouse
Chicken
X_tropicalis
Fugu
Medaka
Zebrafish
PNREs
H1ES H3K4me1
HMEC H3K4me1
HMEC H3K27ac
HUVEC H3K4me1
HUVEC H3K27ac
HSMM H3K4me1
HSMM H3K27ac
NHEK H3K4me1
NHEK H3K27ac
NHLF H3K4me1
NHLF H3K27ac

Supp. Fig. 1. The *opo* regulatory landscape. Localization: (hg18 2006) in chr6:8936346-10570697. Genes: *ofcc1* and transcription factor *AP2 alpha*. In Purple: H3K4me1 peaks for the sum of the six human cell lines marks. In Green: H3K27ac peaks for the sum of the six human cell lines. In grey conservation between mammals and teleosts. In red: conserved PNREs selected for enhancer screening (in blue: non-conserved PNREs). Last rows: Individual H3K4me1 and H3K4ac marks for each human cell types: embryonic stem cells (H1hesc), mammary epithelial cells (Hmec), skeletal muscle myocites (Hsmm), umbilical vein endothelial cells (Huvec), epidermal keratinocytes (Nhek) and lung fibroblasts (Nhlf). See also STab.1 and Tab1. Adapted from UCSC Genome Browser.

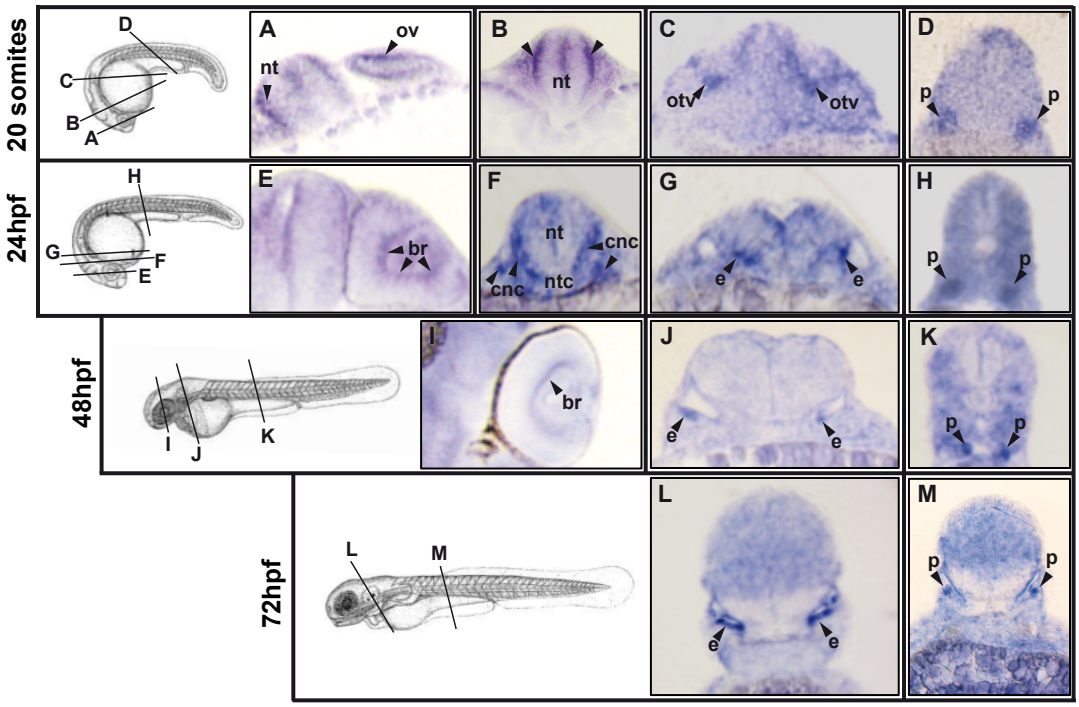

Supp. Fig. 2. The *opo* mRNA expression pattern. ISH sections showing the *opo* mRNA expression pattern from 20 somites to 72hpf. Arrowheads: neural tube (nt); optic vesicle (ov); otic vesicle (otv); pronephros (p); basal retina (br); notochord (nt); cranial neural crest (cnc); ear (e).

Name	Classification			Color code
	Highly conserved	H3K4m1 H3K27ac / human cell line	H3K4m1 H3K27ac in Zebrafish 24hpf and/or 48hpf	
H6:09040	✔	*H1hesc*	✔	
H6:09360	✔	-	✔	
H6:09510	✔	*Hmec;Nhek; Nhlf;*	✔	
H6:09516	✔	*H1hesc; Hmec; Nhlf*		
H6:09536	✔	*Hmec*		
H6:09563	✔	*H1hesc*	✔✔	
H6:09601	✔	-	✔✔	
H6:09617	✔	*Hsmm*	✔✔	
H6:09628		*H1hesc; Hmec; Hsmm; Huvec; Nhlf ;Hmec; Hsmm*	-	
H6: 09647	✔	*Hmec; Huvec; Nhlf;*		
H6:09671	✔	*Huvec*		
H6:09742	✔	-	✔✔	
H6:09778	✔	-		
H6:09813	✔	-	✔	
H6:09815	✔	-		
H6:09892	✔	*H1hesc*		
H6:09941		*Huvec; Huvec*		
H6:09949	✔	*H1hesc*	✔✔	
H6:10043	✔	*Hmec; Nhek*	✔✔	
H6:10126	✔	*H1hesc*	✔✔	
H6:10137	✔	*Hmec*	✔✔	
H6:10258	✔	*Hmec; Nhek*		
H6:10309		*H1hesc; Hmec; Nhek; Hmec; Nhek*	-	
H6:10377	✔	*H1hesc; Hmec; Nhek*	✔✔	
H6:10422	✔	*H1hesc; Hmec; Nhek; Nhlf; Hmec*	-	
H6:10431	✔	*H1hesc; Hmec; Nhek*	✔✔	
H6:10455		*Hmec; Nhek; Hmec; Nhek*	-	

Supp. Tab.1. PNREs characterization. Last column color code- Orange: conserved elements with H3K4m1 marks, in human or zebrafish. Red: conserved elements with H3K4m1 and H3K27ac marks, in human or zebrafish. Brown: non-conserved elements with H3K4m1 and H3K27ac marks in human cell lines. Yellow: conserved elements with any epigenetic mark for enhancer activity.

Name	Localization in Human genome(hg18)			Localization in Zebrafish genome (Zv8)			24hpf		48hpf	
	chr	start	end	chr	start	end	H3K4m1	H3K27ac	H3K4m1	H3K27ac
H6:09040	chr6	9040802	9041495	chr24	8345698	8345778	✔			
H6:09360	chr6	9360754	9362917	Zv8_NA8792	110063	110283	✔		✔	
H6:09510	chr6	9510079	9512442	Zv8_NA543	17616	21052	✔			
H6:09516	chr6	9516753	9517809	Zv8_NA8792	40759	40959				
H6:09536	chr6	9536004	9537930	Zv8_NA8792	31672	31862				
H6:09563	chr6	9563974	9565999	Zv8_NA8792	28994	29489	✔	✔	✔	✔
H6:09601	chr6	9601172	9602202	Zv8_NA8792	14180	14721	✔	✔	✔	✔
H6:09617	chr6	9617863	9618922	Zv8_NA8792	10854	11246			✔	✔
H6: 09647	chr6	9647690	9648627	Zv8_NA2790	5557	5998				
H6:09671	chr6	9671795	9672798	Zv8_NA2790	14478	14714	✔	✔		
H6:09742	chr6	9742877	9745652	Zv8_NA3223	14038	14237			✔	✔
H6:09778	chr6	9778300	9780223	Zv8_NA3223	29292	30058				
H6:09813	chr6	9813174	9814241	Zv8_NA3223	47089	47755			✔	
H6:09815	chr6	9815794	9816729	Zv8_NA1820	29547	29752				
H6:09892	chr6	9892240	9894126	Zv8_NA3223	51807	86254				
H6:09949	chr6	9949629	9950467	Zv8_NA3223	116792	117372	✔		✔	✔
H6:10043	chr6	10043446	10045884	Zv8_NA3223	145737	146467	✔	✔	✔	✔
H6:10126	chr6	10126474	10127046	Zv8_NA941	474	990	✔	✔		
H6:10137	chr6	10137953	10139056	Zv8_NA941	4522	5455	✔	✔	✔	✔
H6:10258	chr6	10258016	10259047	chr24	8404701	8405498				
H6:10377	chr6	10377252	10378117	chr24	8433358	8433511	✔	✔		
H6:10422	chr6	10422720	10424962	chr24	849730	8497649				
H6:10431	chr6	10431893	10433099	chr24	8470504	8470825	✔	✔	✔	✔

Supp. Tab. 2. Localization of the conserved PNREs in human and zebrafish genomes. Annotation of epigenetic marks for enhancer activity based on the data available in (Bogdanovic et al., 2012a).

PNREs Name	n.º Founders analysed	n.º Founders with RFP transmission (transgenisis control)	n.º Founders with GFP transmission (PNRE activity)	GFP activity
H6:09040	**13**	**3**	**3**	**Yes**
H6:09360	19	3	0	No
H6:09510	20	4	0	No
H6:09516	**23**	**5**	**5**	**Yes**
H6:09536	10	3	0	No
H6:09563	**25**	**8**	**8**	**Yes**
H6:09601	**13**	**3**	**3**	**Yes**
H6:09617	**13**	**3**	**3**	**Yes**
H6:09628	10	3	0	No
H6:09647	12	4	0	No
H6:09671	14	3	0	No
H6:09742	10	3	0	No
H6:09778	**16**	**7**	**5**	**Yes**
H6:09813	**20**	**4**	**2**	**Yes**
H6:09815	15	3	0	No
H6:09892	64	6	0	No
H6:09941	53	7	0	No
H6:09949	**10**	**3**	**3**	**Yes**
H6:10043	13	4	0	No
H6:10126	**20**	**7**	**4**	**Yes**
H6:10137	**12**	**6**	**6**	**Yes**
H6:10258	12	8	0	No
H6:10309	10	3	0	No
H6:10377	**41**	**12**	**12**	**Yes**
H6:10422	10	3	1	No
H6:10431	**13**	**4**	**4**	**Yes**
H6:10455	10	4	0	No

Supp. Tab. 3. PNREs transgenic assay in zebrafish. Results from the F_0 outcross and the F_1 generations. Classification of GFP activity in F_1 progeny.

Name	Strand / Position / Motif	Strand / Position / Motif	Expression Pattern
CHX10	- / 36-49 / TCTAATTA	+ / 643-656 / TAATTAGA	Neural Retina
HFH4	- / 41-53 / TAATTAAAC	+ / 639-651 / GTTTAATTA	-
NKX25	- / 77-84 / AATTATG	+ / 609-616 / CATAATT	-
NKX25L	- / 78-84 / AATTA	+ / 609-615 / TAATT	-
XBP1	- / 80-96 / TACTTCA	+ / 597-613 / TGAAGTG	Notocord; Epidermis
TITF1	- / 85-94 / ACTTCATT	+ / 599-608 / AATGAAGT	Forebrain; Neural plate
OCT1	- / 87-99 / TCATTA	+ / 594-606 / TAATGA	CNS
OCT1	+ / 92-103 / TATGTTAAAT	- / 590-601 / ATTTAGCATA	CNS
POU3F2	+ / 93-102 / TTATGTTAAA	- / 591-600 / TTTAGCATAA	CNS
CDC5	- / 93-104 / TATGTTAAATG	+ / 589-600 / CATTTAGCATA	Retina; neural crest
ZEC	+ / 100-112 / AAATGTTAGTTGC	- / 581-593 / GCAACTAACATTT	Whole organism
XFD2	+ / 128-141 / ATAAACA	- / 553-566 / TGTTTAT	-
VMYB	+ / 160-168 / AACTG	- / 526-534 / CAGTT	-
HNF1	- / 168-185 / CTCATTAAC	+ / 509-526 / GTTAATGAG	-
BACH2	- / 170-180 / TTACTCA	+ / 514-524 / TGAGTAA	-
HNF1	- / 170-184 / ACTCATTAAC	+ / 510-524 / GTTAATGAGT	Neural plate
AFP1	+ / 178-188 / ATTAACAAGAT	- / 506-516 / GTCTTGTTAAT	-
ETS2	- / 206-219 / TTCCTC	+ / 475-488 / GAGGAA	Mesoderm
ETS_Q6	+ / 210-217 / TTCC	- / 477-484 / GGAA	-
CRX	+ / 215-227 / TAA	- / 467-479 / TTA	Neural Retina
LPOLYA_B	- / 229-236 / ATTTATT	+ / 459-466 / AATAAAT	-
CDPCR1	- / 339-348 / ATCGAT	+ / 347-356 / ATCGAT	-
CDPCR3H	- / 339-348 / ATCGAT	+ / 347-356 / ATCGAT	-
GATA1	- / 402-411 / ATC	+ / 285-294 / GAT	Hematopoietic system
GFI1	+ / 427-439 / AATC	- / 257-269 / GATT	Gut; liver; pancreas
XFD3	+ / 443-456 / GTGAACA	- / 240-253 / TGTTCAC	Gut; pancreas
FOXO1	- / 443-456 / GTGAACAA	+ / 240-253 / TTGTTCAC	Gut; pancreas
FOXO1	- / 449-462 / AAAAACAA	+ / 234-247 / TTGTTTTT	Gut; pancreas
FOXO4	- / 449-462 / AAAAACAA	+ / 234-247 / TTGTTTTT	-
FOXO1	+ / 451-460 / AAACA	- / 236-245 / TGTTT	Gut; pancreas
AFP1	+ / 452-462 / AAAAACAACAC	- / 234-244 / GTGTTGTTTTT	-
FOXO4	+ / 452-462 / AAACA	- / 234-244 / TGTTT	-
BRCA	- / 457-464 / CAAC	+ / 232-239 / GTTG	CNS; eye; inner ear
MYB	+ / 460-469 / AAC	- / 227-236 / GTT	Myotome
TAACC	- / 469-491 / TTGCAGTTTGATTATTGTTT	+ / 205-227 / AAACAATAATCAAACTGCAA	-
PBX	+ / 476-487 / GTTTGA	- / 209-220 / TCAAAC	CNS; eye; swim bladder
CDP	- / 477-488 / TTTGATTATTGT	+ / 208-219 / ACAATAATCAAA	-
PBX1	- / 478-486 / TGATTATT	+ / 210-218 / AATAATCA	CNS; eye; swim bladder
SRY	- / 481-492 / TTGTT	+ / 204-215 / AACAA	-
FOXO4	- / 482-492 / TGTTT	+ / 204-214 / AAACA	-
FREAC2	- / 482-497 / TGTTTAT	+ / 199-214 / ATAAACA	-
FREAC7	- / 482-497 / TGTTTAT	+ / 199-214 / ATAAACA	-
SOX5	- / 482-491 / ATTGTT	+ / 205-214 / AACAAT	Forebrain; tail bud
XFD2	- / 482-495 / TGTTTAT	+ / 201-214 / ATAAACA	-
XFD3	- / 482-495 / TGTTTAT	+ / 201-214 / ATAAACA	-
HFH1	+ / 483-494 / ATTGTTTATAG	- / 202-213 / CTATAAACAAT	-
FOXO1	- / 484-493 / TGTTT	+ / 203-212 / AAACA	Gut; pancreas
GATA1	+ / 489-502 / GATA	- / 194-207 / TATC	Hematopietic system
NKX62	- / 534-545 / AATTA	+ / 151-162 / TAATT	-
FREAC3	- / 536-551 / ATTATTTAC	+ / 145-160 / GTAAATAAT	-
BACH2	- / 551-561 / AGACTCA	+ / 135-145 / TGAGTCT	Whole organism
OCT1	- / 559-571 / TCATTA	+ / 125-137 / TAATGA	CNS
HOXA3	+ / 578-586 / T	- / 110-118 / A	CNS; pharyngeal arch
VBP	+ / 592-601 / TTAT	- / 95-104 / ATAA	-
ZEC	+ / 599-611 / CAATGTTAGTTGA	- / 85-97 / TCAACTAACATTG	Whole organism
CDC5	+ / 610-621 / GATTTAACACA	- / 75-86 / TGTGTTAAATC	Retina; neural crest

Supp.Tab. 4. ECR Browser results for transcription factor binding sites in H6:10137 enhancer. Transcription Factors Multif alignments in the H610137 conserved sequence between humans (H6:10137 in hg19: chr6:10030070-10030764) and *xenopus tropicalis* (H6:10137 in xenTro3: GL172669:1277890-1278578). Both sequences are similar from the position 104 to 798bps (length: 689bps; sequence homology of 63%). Adapted from: ECR browser: http://ecrbrowser.dcode.org/). Last column: expression patterns at 24hpf in observed in the Zebrafish Model Organism Database (ZFIN).

Model name	Score	Start	End	Strand	Motif
Vsx2	13.491	143	151	-1	TTTAATTAG
Lim1	12.203	144	150	-1	TTAATTA
Scr	11.398	279	285	-1	TTAATGA
Scr	11.398	952	958	-1	TTAATGA
Rx	11.083	143	149	1	CTAATTA
Vsx1	10.888	144	150	-1	TTAATTA
Rx	10.866	144	150	-1	TTAATTA
otp	10.860	144	150	-1	TTAATTA
ap	10.801	143	149	1	CTAATTA
Oct	10.741	144	151	-1	TTTAATTA
exex	10.724	143	149	1	CTAATTA
en	10.719	144	150	-1	TTAATTA
exex	10.536	144	150	-1	TTAATTA
Rx	10.388	682	688	1	CTAATTG
Rx	10.388	819	825	1	CTAATTG
vsx1	10.366	143	149	1	CTAATTA
ap	10.346	144	150	-1	TTAATTA
en	10.312	143	149	1	CTAATTA
Scr	10.175	144	150	-1	TTAATTA
otp	10.093	143	149	1	CTAATTA

Supp. Tab. 5. JASPAR database transcription factor binding sites predictions in H610137 enhancer sequence. 102 putative sites were predicted with 90% sequence homology. In this table, only the results for binding sites with a socre $\geq$10 are shown.

		No eye defects (%)	Phenotipic eye defects (%)	Anoftalmia (%)	*n*
vsx2I1E2 300uM	Exp.1	17	70	13	40
	Exp.2	26	63	11	43
	Exp.3	25	64	11	45
	Mean	**22,7**	**65,7**	**11,7**	***n=128***
	St. Dev	**4,9**	**3,8**	**1,2**	
vsx2E2I2 300uM	Exp.1	22	58	1	40
	Exp.2	29	58	1	77
	Exp.3	32	54	14	87
	Mean	**27,7**	**56,7**	**5,3**	***n=204***
	St. Dev	**5,1**	**2,3**	**7,5**	
vsx2E2I2 + vsx2mRNA	Exp.1	70	29	0	53
	Exp.2	68	25	1	23
	Exp.3	53	47	0	97
	Mean	**63,7**	**33,7**	**0,3**	***n=173***
	St. Dev	**9,3**	**11,7**	**0,6**	
Controls	Exp.1	100	0	0	40
	Exp.2	100	0	0	40
	Exp.3	100	0	0	51
	Mean	**100,0**	**0,0**	**0,0**	***n=131***
	St. Dev	**0,0**	**0,0**	**0,0**	
	Exp.1	100	0	0	35
	Exp.2	100	0	0	38
	Exp.3	100	0	0	42
	Mean	**100,0**	**0,0**	**0,0**	***n=115***
	St. Dev	**0,0**	**0,0**	**0,0**	
	Exp.1	100	0	0	48
	Exp.2	100	0	0	20
	Exp.3	100	0	0	79
	Mean	**100,0**	**0,0**	**0,0**	***n=147***
	St. Dev	**0,0**	**0,0**	**0,0**	

Supp. Tab. 6. Percentage of phenotypic malformations and anoftalmia in *vsx2* morphant embryos. Data obtained from several *vsx2*MO injections, using the Tg(*vsx2.2*GFP:caax) line. St. Dev: Standard Deviation of the Mean.

		Microftalmia - Normalized eye length at 24hpf (% embryos)			
		4 to <6	6 to <8	8 to <10	*n*
vsx2I1E2mo 300uM	Exp1	45	40	15	40
	Exp2	15	76	9	47
	Exp3	19	71	10	21
	Mean	26,3	62,3	11,3	*n*=108
	St. Dev	16,3	19,5	3,2	
vsx2E2I2mo 300uM	Exp1	41	56	3	32
	Exp2	29	59	12	17
	Exp3	28	58	15	40
	Mean	32,7	57,7	10,0	*n*=89
	St. Dev	7,2	1,5	6,2	
Controls	Exp1	0	37	63	40
	Exp2	0	21	79	34
	Exp3	0	0	100	13
	Mean	0	19,3	80,7	*n*=87
	St. Dev	0	18,6	18,6	
	Exp1	0	32	68	31
	Exp2	0	38	62	13
	Exp3	0	26	74	40
	Mean	0	32,0	68,0	*n*=84
	St. Dev	0	6,0	6,0	

Supp. Tab. 7. Microftalmia percentages in *vsx2* morphant embryos. Data obtained from several *vsx2*MOs injections in Tg(*vsx2.2*GFP:caax) line. St. Dev: Standard Deviation of the Mean.

		Ventral opening angle at 24hpf (% embryos)					
		0º - 20º	21º - 40º	41º - 60º	61º - 80º	>80º	*n*
vsx2I1E2 300uM	Exp1	29	0	12	47	12	17
	Exp2	16	24,4	17,6	31	11	45
	Exp3	20,8	6,1	21	29,1	23	48
	Mean	**21,9**	**10,2**	**16,9**	**35,7**	**15,3**	***n*=110**
	St. Dev	**6,6**	**12,7**	**4,5**	**9,8**	**6,7**	
vsx2E2I2 300uM	Exp1	27	32	5	13	23	40
	Exp2	29	12,9	16	22,1	20	31
	Exp3	41	19	10	10	20	58
	Mean	**32,3**	**21,3**	**10,3**	**15,0**	**21,0**	***n*=129**
	St. Dev	**6,2**	**8,0**	**4,5**	**5,1**	**1,4**	
Controls	Exp1	100	0	0	0	0	17
	Exp2	100	0	0	0	0	45
	Exp3	100	0	0	0	0	31
	Mean	**100**	**0**	**0**	**0**	**0**	***n*=93**
	St. Dev	**0**	**0**	**0**	**0**	**0**	
	Exp1	100	0	0	0	0	40
	Exp2	100	0	0	0	0	31
	Exp3	100	0	0	0	0	42
	Mean	**100**	**0**	**0**	**0**	**0**	***n*=113**
	St. Dev	**0**	**0**	**0**	**0**	**0**	

Supp. Tab. 8. Percentage of ventral opening angles in *vsx2* morphant embryos. Data obtained from multiple *vsx2*MOs injections in Tg(*vsx2.2*GFP:caax) line. St. Dev: Standard Deviation of the Mean.

VIII. Appendix

Developmental Cell
Article

Numb/Numbl-Opo Antagonism Controls Retinal Epithelium Morphogenesis by Regulating Integrin Endocytosis

Ozren Bogdanović,[1,5] Mariana Delfino-Machín,[1,5] María Nicolás-Pérez,[1] María P. Gavilán,[2] Inês Gago-Rodrigues,[1] Ana Fernández-Miñán,[1] Concepción Lillo,[3] Rosa M. Ríos,[2] Joachim Wittbrodt,[4] and Juan R. Martínez-Morales[1,5,*]
[1]Centro Andaluz de Biología del Desarrollo (CSIC/UPO/JA), 41013 Sevilla, Spain
[2]CABIMER (CSIC), 41092 Sevilla, Spain
[3]INCYL (University of Salamanca), 37007 Salamanca, Spain
[4]University of Heidelberg, Centre for Organismal Studies, 69120 Heidelberg, Germany
[5]These authors contributed equally to this work
*Correspondence: jrmarmor@upo.es
http://dx.doi.org/10.1016/j.devcel.2012.09.004

SUMMARY

Polarized trafficking of adhesion receptors plays a pivotal role in controlling cellular behavior during morphogenesis. Particularly, clathrin-dependent endocytosis of integrins has long been acknowledged as essential for cell migration. However, little is known about the contribution of integrin trafficking to epithelial tissue morphogenesis. Here we show how the transmembrane protein Opo, previously described for its essential role during optic cup folding, plays a fundamental role in this process. Through interaction with the PTB domain of the clathrin adaptors Numb and Numbl via an integrin-like NPxF motif, Opo antagonizes Numb/Numbl function and acts as a negative regulator of integrin endocytosis in vivo. Accordingly, *numb/numbl* gain-of-function experiments in teleost embryos mimic the retinal malformations observed in *opo* mutants. We propose that developmental regulator Opo enables polarized integrin localization by modulating Numb/Numbl, thus directing the basal constriction that shapes the vertebrate retina epithelium.

INTRODUCTION

In each metazoan group, stereotyped morphogenetic movements shape embryonic tissues into functional organs. During development and tissue remodeling, precursor cells display a number of characteristic behaviors: cells may move freely, migrate as coordinated clusters and chains, or collectively change their shape to force an epithelial sheet to elongate, protrude, bend, or form a tube (Lecuit and Lenne, 2007; Montell, 2008). How cells move and change their shape in a coordinated fashion depends both on the genetic identity of individual cells and on their microenvironment, which conditions cell signaling and adhesion (Papusheva and Heisenberg, 2010). The cytoskeletal machineries that generate and transmit morphogenetic tensions are locally assembled to drive the asymmetric behavior of the cells. This phenomenon is tightly linked to the regulation of general cell polarity and polarized trafficking of receptors and adhesion molecules (Bryant and Mostov, 2008; Nelson, 2009).

During tissue morphogenesis, polarized epithelial sheets bend to form cups, tubes, and cysts, thus providing an important resource for evolutionary plasticity. The best-characterized example among morphogenetic events in animal epithelia is apical constriction (Sawyer et al., 2010). Quantitative imaging studies in *Drosophila* epithelia have shown that this process is driven by the periodic contractions of the actomyosin network at the cell apex (Martin et al., 2009; Solon et al., 2009). In epithelial sheets, bending may also occur toward the basal surface and examples of this behavior are observed in vertebrates during the formation of the midbrain-hindbrain boundary and the folding of the optic cup (Gutzman et al., 2008; Martinez-Morales and Wittbrodt, 2009). Basal cell contraction has also been recently described as the driving force directing the elongation of both the egg chamber in *Drosophila* (He et al., 2010) and the notochord in ascidians (Dong et al., 2011). Together, these studies show that basal constrictions/contractions involve the local recruitment of the actomyosin network. Furthermore, oscillatory actomyosin contractions, similar to those described at the apical surface, have also been recorded at the basal cell surface (He et al., 2010). Although these observations point to common characteristics for the contractile machineries operating at both ends of the apico-basal axis, clear differences also exist. Whereas apical constriction depends on adherens junctions and apical polarity complexes (Kölsch et al., 2007; Letizia et al., 2011), it is integrins within focal adhesions that play a pivotal role in basally driven morphogenetic processes. Thus, interference with the adhesive function of integrins impairs basal actomyosin recruitment and tissue morphogenesis in both vertebrate and invertebrate epithelia (He et al., 2010; Martinez-Morales et al., 2009).

The fundamental role of focal adhesions in tissue morphogenesis has been best characterized in the context of cell migration, where clathrin-dependent trafficking of integrins along the front-back axis has proven to be essential for directional cell movement (Ezratty et al., 2009). Members of the phosphotyrosine binding (PTB) family of clathrin adaptors (such as Numb, Dab2

Developmental Cell
Numbs/Opo Antagonism Controls Optic Cup Formation

and ARH) interact with integrin-β NPxY/F motifs to regulate their endocytosis rate (Calderwood et al., 2003). Accordingly, both Dab2 and Numb regulate integrin-β turnover and directional cell migration in HeLa cells (Nishimura and Kaibuchi, 2007; Teckchandani et al., 2009). Despite the increasing evidence showing that polarized integrin endocytosis is essential for cell polarity and migration (Caswell et al., 2009; Nelson, 2009), the role of PTB clathrin adaptors in tissue morphogenesis is just beginning to be understood. Besides its traditional role in asymmetric cell division (Knoblich et al., 1995), the endocytic adaptor protein Numb has also been implicated in the regulation of different cellular processes including cell adhesion and polarity (Rasin et al., 2007; Wang et al., 2009). Studies using double-knockout mice for *Numb* and *Numb-like* (*Numbl*) have shown in vivo the redundant role of *numb* family members during axonal arborization (Huang et al., 2005) spindle orientation (Wu et al., 2010) and chemotaxis (Zhou et al., 2011). In polarized epithelial cells, Numb asymmetrically localizes to the basolateral cortex (Dho et al., 2006). Both in epithelial and migratory cells, as well as during asymmetric cell divisions, the polarized localization of Numb depends on its phosphorylation by aPKC (Smith et al., 2007). In the context of migratory cells, this polarized distribution has been related to a role in integrin recycling and cell motility (Nishimura and Kaibuchi, 2007). In contrast, although the severe neural tube defects observed in $Numb^{-/-}$ mice suggest a role in epithelial morphogenesis (Zhong et al., 2000), the functional significance of Numb polarized localization in epithelial cells is still unclear.

We previously described the essential role of the transmembrane protein Opo, encoded by the gene *ojoplano/Ofcc1*, during optic cup morphogenesis. Opo regulates the asymmetric localization of focal adhesion components to the basal surface of the retina epithelium and consequently, *ojoplano* loss of function impairs basal constriction in the teleost retina (Martinez-Morales et al., 2009). To further investigate Opo function, we carried out a yeast two-hybrid screen that identified PTB clathrin adaptors as its interacting partners. Here, we show that Opo interacts with the PTB domain of the adaptors, Numb and Numbl, through a conserved NPxF motif located in the amino terminal end of the protein. Using internalization assays and functional studies in mammalian cells and fish embryos, we demonstrate that Opo and Numb/Numbl act antagonistically to regulate integrin-β trafficking and optic cup morphogenesis. Our data indicate that Opo acts as a negative regulator of integrin endocytosis at the basal surface of the retina. These findings highlight the key role of integrin recycling as a developmental mechanism driving basal constriction during epithelial morphogenesis.

RESULTS

Opo Interacts with the PTB Domain of Numb/Numbl through a Conserved NPxF Motif

The morphogenetic gene *opo* encodes a transmembrane protein (Opo) that regulates the polarized localization of focal adhesions in the retinal epithelium through a still uncharacterized molecular mechanism (Martinez-Morales et al., 2009). Besides four putative transmembrane passes (Figure 1A), Opo does not include any annotated protein domains that could suggest its molecular role. To gain insight into Opo molecular function we decided to identify its interacting partners using a yeast two-hybrid approach. As baits, we used the conserved N-terminal (N-Opo) and C-terminal (C-Opo) regions of the protein, both of which face the cytosolic compartment as indicated by topology prediction and also confirmed by epitope tagging (Figure S1 available online). After screening 74 and 64 million interactions, respectively, two members of the PTB family of endocytic adaptors (Numbl and Dab2) were identified as the highest-scoring proteins for the N-terminal bait (Table S1A), whereas the strongest C-terminal interaction was confirmed as Hsc70/Hspa1l (Table S1B), a chaperone belonging to the Hsp70s family. Both the PTB family members as well as Hsc70 are known regulators of clathrin-mediated endocytosis (Chang et al., 2002; Teckchandani et al., 2009; Ungewickell and Hinrichsen, 2007).

Upon closer inspection of the N-Opo sequence, a conserved NPxF motif congruous with the NPxY motif present in integrin-β tails was discovered (Figure 1B). Biochemical interaction of PTB domain proteins and NPxY/F ligands has been well documented in vivo and in vitro (Calderwood et al., 2003; Chen et al., 2006). These observations prompted us to examine the possibility that the Opo NPxF signal might interact with the PTB domain containing proteins: Numb, Numbl, and Dab2, in a similar fashion. To that end, the PTB-containing N-terminal domains of these proteins were recombinantly expressed in bacteria and purified (Figures 1C and 1D). Glutathione S-transferase (GST) pull-downs of radiolabelled full-length Opo confirmed the biochemical interaction of N-Dab2, N-Numb, and N-Numbl with the Opo protein (Figure 1D). Similarly, all three tested PTB proteins interacted in vitro, albeit to different extents, with the Integrin-β1 tail bearing the canonical NPxY sequence (Figure 1D). The converse experiment was also performed, and the immobilized N-Opo was incubated with radiolabelled N-Dab2, N-Numb, and N-Numbl or their corresponding full-length proteins (Figure 1E). Whereas the interaction of N-Opo with N-Numb/N-Numbl was corroborated in this assay, neither N-Dab2 nor Dab2 were recovered after incubation with immobilized N-Opo, suggesting that additional protein domains might play a role in stabilizing this interaction. Moreover, to test the ability of Opo to interact with PTB domain proteins within a physiological context, either a mammalian Opo-GFP fusion or GFP protein alone control were coexpressed with Myc-tagged N-Numbl (*pCS2+:Myc-N-Numbl*) in the immortalized retinal pigment epithelial cell line, RPE-1. Western blotting of cellular extracts immunoprecipitated with anti-GFP antibody resulted in a clear signal identified by anti-GFP and anti-Myc antibodies, thereby confirming the biochemical interaction of Opo and Numbl in a mammalian system (Figure 1F).

These findings are further supported by colocalization experiments performed in HeLa cells where the full-length Opo-GFP fusion was coexpressed with a Numb-Cherry fusion (*pCS2+:zNumb:Cherry*) and analyzed by confocal microscopy (Figure 1G). In spite of their differential routing within the cell, Opo is trafficked through the secretory pathway whereas Numb preferentially localizes to the cell cortex (Knoblich et al., 1995); both proteins overlapped locally at the plasma membrane (Figure 1G).

Finally, to test whether the NPxF sequence present in the Opo N terminus is indeed responsible for the interaction with PTB domain proteins, a point mutagenesis approach was undertaken. It has been previously demonstrated that the tyrosine

Developmental Cell
Numbs/Opo Antagonism Controls Optic Cup Formation

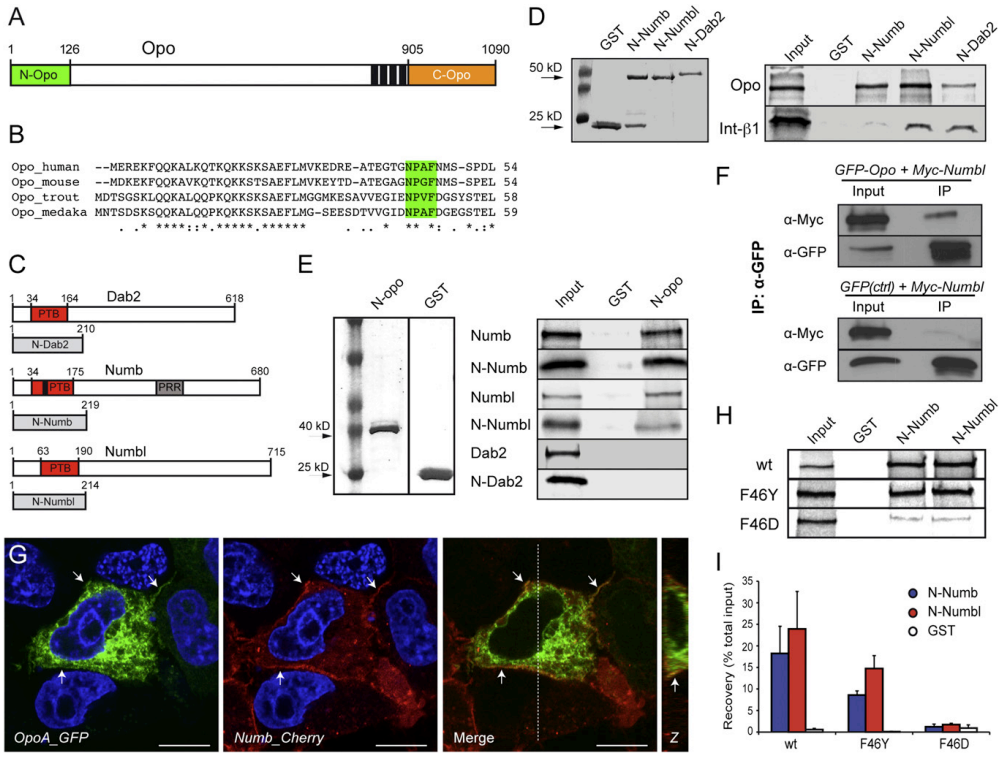

Figure 1. Opo Interacts with Numb/Numbl through a Conserved N-Terminal NPxF Motif

(A) A schematic representation of the medaka Opo protein. The black boxes represent four transmembrane passes.

(B) Conservation of the N-terminal NPxF sequence from teleosts to mammals.

(C) Schematic representation of medaka clathrin adaptors. The PTB containing fragments used for GST pull-downs are indicated.

(D) Coomasie staining (left panel) of recombinantly expressed proteins used for GST pull-downs. Full length Opo interacts with N-Numb, N-Numbl and N-Dab2 in vitro, whereas the Integrin-β1 tail fragment preferentially interacts with Numbl and Dab2 (right panel).

(E) Coomasie staining (left panel) of recombinantly expressed N-Opo used for GST pull-downs of either full length or N-terminal (PTB containing) (S^{35}) Numb, Numbl and Dab2. Both full length and N-terminal Numb and Numbl interact with N-Opo.

(F) Western blotting of RPE-1 cellular extracts immunoprecipitated with anti-GFP antibody. Staining with anti-GFP and anti-Myc antibodies confirms the interaction of GFP-Opo and Myc-Numbl in RPE-1 cells. GFP alone was used as a negative control in parallel experiments.

(G) Colocalization of Numb_Cherry and OpoA_GFP at the cellular cortex in HeLa cells.

(H) GST pull-downs of S^{35}-labeled F46Y and F46D Opo mutants shows reduced interaction with N-Numb and N-Numbl.

(I) Quantification of wild-type Opo, F46Y-Opo and F46D-Opo binding to N-Numb/N-Numbl in GST pull-downs. Input lines contain 10% of the input. Error bars represent SEM of three experiments. Scale bar, 20 μm.

See also Figure S1 and Table S1.

residue present in Integrin NPxY tail sequences is crucial for cell motility and interaction with clathrin adaptors (Chen et al., 2006; Filardo et al., 1995). The phenylalanine present in the Opo motif was therefore mutated to either tyrosine or aspartic acid yielding NPAY or NPAD, respectively. The substitution of phenylalanine to tyrosine led to a modest (~2-fold) reduction in PTB domain binding as assayed by GST pull-down, whereas the substitution to aspartate resulted in a severe (>10-fold) loss of protein interactions (Figures 1H and 1I). Both N-Numb and N-Numbl binding were equally affected by the mutation. Altogether, these data provide evidence for the interaction of Opo with PTB domain proteins and demonstrate the requirement of the NPxF sequence in enabling these interactions.

Opo Localizes to a Subpopulation of Clathrin-Coated Structures

Numb localizes to Ap2α-positive clathrin-coated structures (CCSs) in HeLa cells, preferentially at the adhesion surface (Nishimura and Kaibuchi, 2007; Santolini et al., 2000). To investigate whether Opo shows a similar distribution, we transfected both

Developmental Cell
Numbs/Opo Antagonism Controls Optic Cup Formation

HeLa and RPE-1 cells with either N-terminal (GFP-Opo) or C-terminal (Opo-GFP) fusions (Figures 2 and S2) and examined their subcellular localization. In agreement with our previous observations, Opo localized to different compartments along the secretory pathway including the endoplasmic reticulum, Golgi apparatus, and the plasma membrane, as determined by costaining with BIP, GM130, and F-actin, respectively (data not shown). Opo also colocalized with a subpopulation of Ap2α-positive CCSs both in RPE-1 and HeLa cells, preferentially at the cellular cortex (Figures 2B–2D and S2).

To investigate the specificity of this colocalization, HeLa cells were transfected with either a carboxy-terminal truncation of the protein (Figures 2E–2G) or with OpoB, a mouse protein isoform (Mertes et al., 2009) naturally truncated at the amino terminus (Figures 2H–2J). The truncation of both Opo N- and C terminus resulted in a substantial reduction of its colocalization with Ap2α, suggesting that both protein ends are required for Opo recruitment to CCSs.

Opo Inhibits Integrin Internalization in HeLa Cells

Previous reports in HeLa cells have shown that Numb interacts with the cytoplasmic Integrin-β tails and functions in their endocytosis (Calderwood et al., 2003; Nishimura and Kaibuchi, 2007; Teckchandani et al., 2009). Here we demonstrate that Opo localizes to a subpopulation of endocytic vesicles and interacts physically with Numb and Numbl. These results suggest that Opo may act as a regulator of integrin endocytosis. To functionally address this point we carried out internalization assays in HeLa cells (Figure 3). Transfected cells expressing either control *GFP*, *Opo-eGFP*, or *Numb-Cherry* were incubated with anti-Integrin-β1 antibodies for 30 or 40 min to allow its internalization. Cells were then fixed and the relative rate of integrin endocytosis was calculated as the ratio between neighbor-transfected and nontransfected cells (expressed as a percentage). As expected from the reported role for Numb in endocytosis, Integrin-β1 uptake was significantly enhanced in cells expressing *Numb-Cherry* (Figures 3E, 3F, and 3I). In contrast, it was substantially inhibited in cells expressing *Opo-GFP* (Figures 3C, 3D, and 3I). Interestingly, cells coexpressing both constructs showed a rate of integrin endocytosis that was not significantly different from untransfected cells (Figures 3G–3I) or from cells expressing the control *GFP* construct (Figures 3A, 3B, and 3I). These results show that Opo antagonizes Numb and functions as a negative regulator of integrin endocytosis.

Opo Loss of Function Enhances Integrin Internalization in the Medaka Optic Cup

To further strengthen our observations from HeLa cells, we next set out to investigate the role of Opo in integrin receptor trafficking during optic cup folding. To this end, we carried out in vivo FRAP experiments using the medaka eye-specific transgenic line *Vsx3::Integrinβ1Tail-GFP* (Figure S3A). Benefiting from the strictly polarized architecture of the retinal epithelium, we bleached equivalent volumes either at the basal or apical side of both wild-type and *opo* mutant retinae (Figure S3). Fluorescence recovery, which occurred at the expense of the unbleached half of the columnar neuroblasts, was monitored in a central optical section of the bleached volume until it achieved a plateau, reflecting that forward and reverse transport of labeled

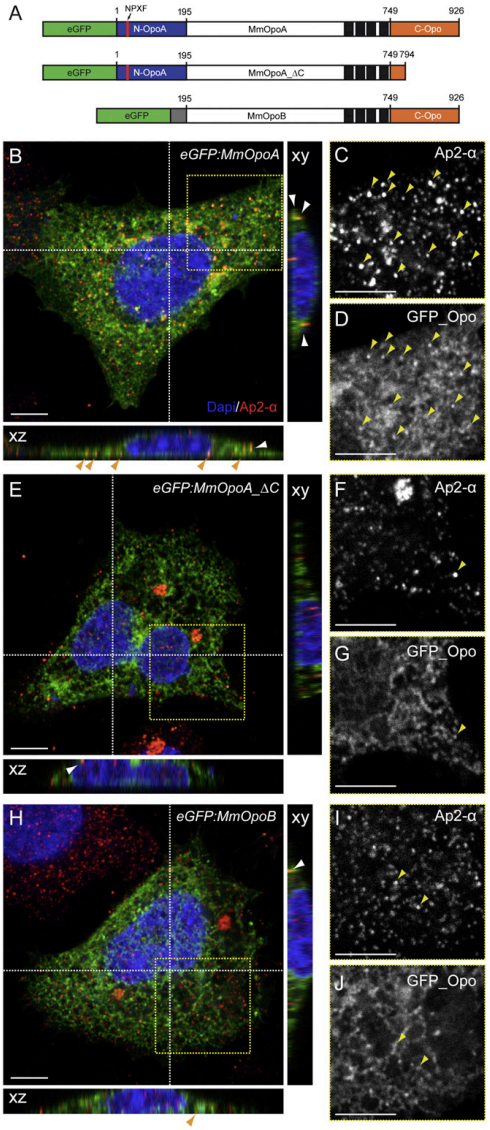

Figure 2. Opo Localizes to Ap2α-Positive Clathrin-Coated Structures

HeLa cells transfected either with mouse GFP-OpoA or C-terminal and N-terminal Opo truncations (A) were stained with anti- Ap2α antibodies to detect CCS. Cells transfected with GFP-OpoA (B–D) show colocalization (arrows) at the cellular cortex (arrows in xz and xy projections). This is reduced when GFP-OpoA_ΔC (E–G) or GFP-OpoB (H–J) are transfected. Scale bars, 5 μm. See also Figure S2.

Developmental Cell
Numbs/Opo Antagonism Controls Optic Cup Formation

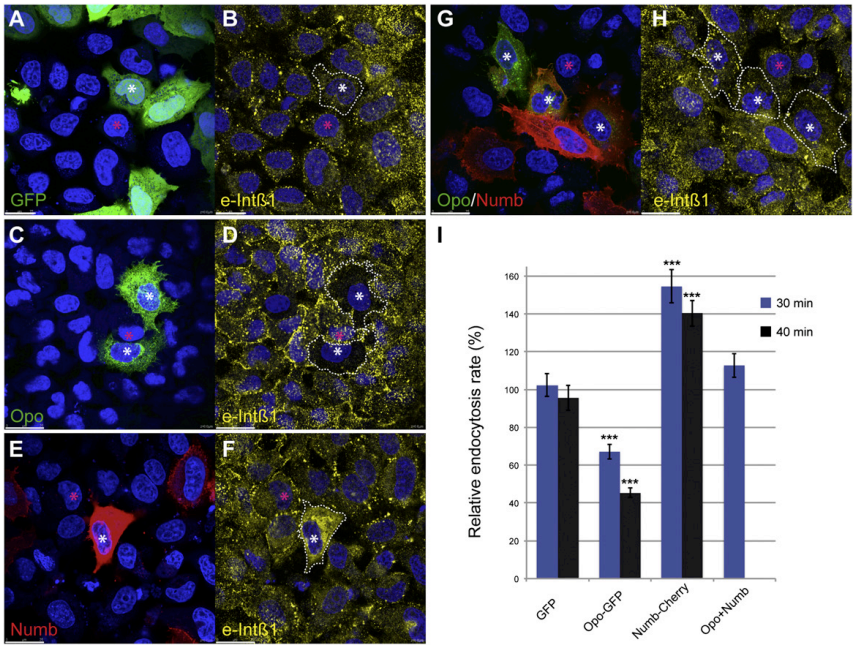

Figure 3. Opo Inhibits Integrin-β1 Internalization in HeLa Cells

(A and B) HeLa cells expressing control GFP (*pCS2+:GFP*) (A) stained with anti-Integrin-β1 antibodies after the internalization assay (B).

(C and D) Opo-GFP expressing cells (C) stained with anti-Integrin-β1 antibodies after the internalization assay display a significant reduction in Integrin-β1 uptake (D).

(E and F) In contrast to (C) and (D), Integrin-β1 uptake is enhanced in cells expressing Numb-Cherry constructs.

(G and H) Cells coexpressing both constructs. Dotted lines represent areas of measured Integrin-β1 turnover. White and pink asterisks denote equivalent transfected and nontransfected cells respectively.

(I) Relative endocytosis rate is expressed as the transfected/nontransfected ratio (%). Data represent the mean and SEM of 24 cells in each condition. Scale bars, 25 μm.

molecules had reached an equilibrium (Figures S3A′ and S3A″). In wild-type tissues, FRAP analyses consistently revealed higher and faster integrin recovery at the basal rather than at the apical side (Figures 4A, 4B, and S3A; Movie S1), thus indicating that integrins are asymmetrically trafficked through the epithelium with a net flux toward the basal side. The analysis of four independent FRAP experiments in mutant tissue showed instead that integrin basal recovery (Figures 4A, 4B, and S3A; Movie S1) is significantly reduced when compared to the wild-type. As a control, the recovery rates for the apical tracer Par3-eGFP (Figures 4C, 4D, and S3B; Movie S2) are not significantly different from those measured in wild-type tissues. These results suggest that *opo* function is specifically required for basal, but not apical, transport of integrins in vivo.

Additionally, electron microscopy (EM) studies also support a role for Opo in trafficking during optic cup morphogenesis. Immunogold analysis of stage 23 *Vsx3::eGFP_Opo* retinae revealed that Opo is associated to basal endosomes (Figures S3C and S3D). Furthermore, morphological electron microscopy analysis of stage 23 wild-type and *opo* mutant retinae revealed a significant accumulation of intracellular vesicles specifically at the basal end of the mutant neuroblasts (Figures 4E, 4F, S3E, and S3F). Although collectively our analyses clearly indicate that Opo acts as regulator of integrin trafficking during optic cup folding, they cannot discriminate whether this is due to an impaired forward transport or an increased endocytic rate.

To address this question, we performed internalization assays in vivo using the *Vsx3::Intβ1Tail-GFP* line, as the GFP tag of the fusion protein is oriented toward the extracellular space (Figures 4G–4O). To establish the rate of integrin uptake in both wild-type and *opo* retinae, dechorionated embryos were incubated with α-GFP antibodies for 30 min before fixation. Fluorescence intensity associated to antibody internalization was then quantified in equivalent areas, both at the basal surface and in medial zones of the retina. We found that in *opo Intβ1Tail-GFP* uptake is significantly enhanced in both areas when compared to wild-type retinae (Figure 4O), indicating that Opo functions as a negative regulator of integrin endocytosis also during optic cup folding.

Developmental Cell
Numbs/Opo Antagonism Controls Optic Cup Formation

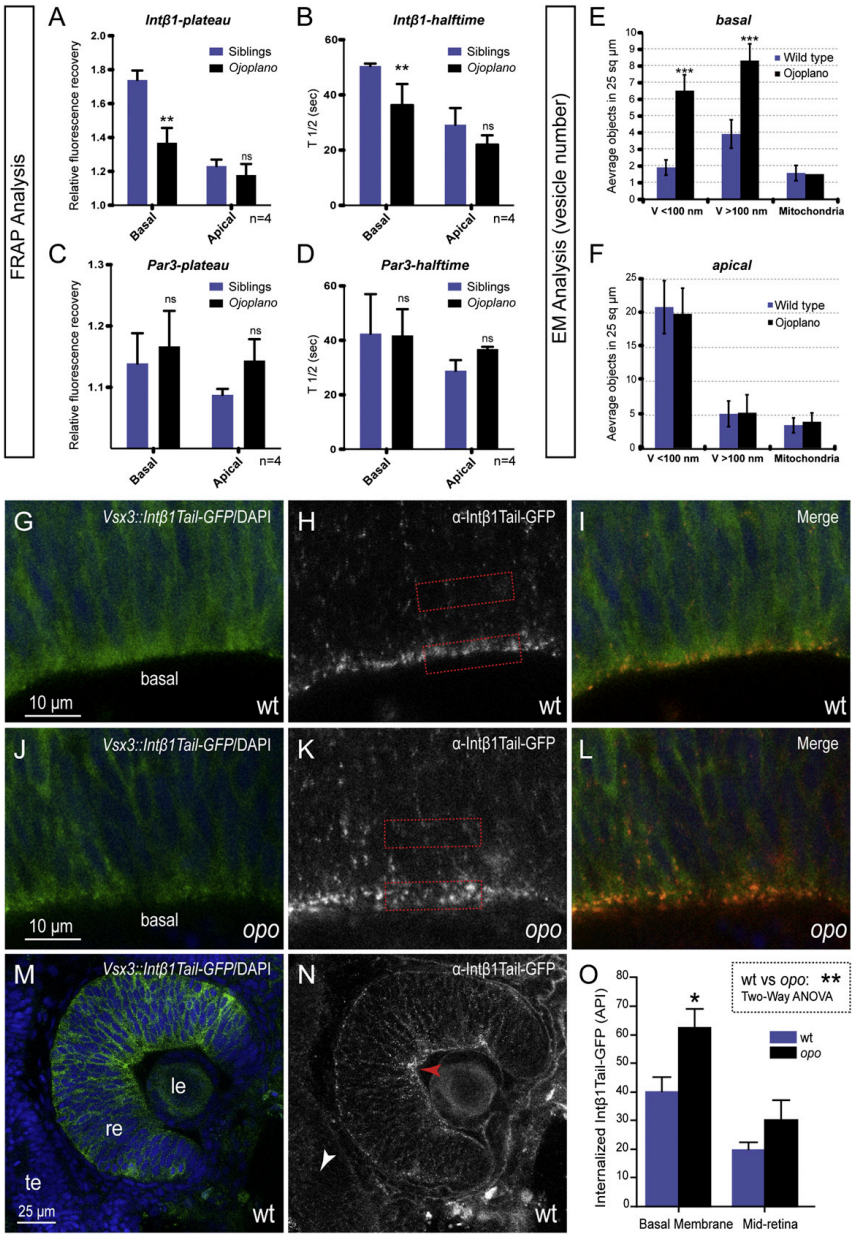

Figure 4. Integrin-β1 Endocytosis Is Enhanced in the *opo* Retina

In vivo FRAP reveals altered integrin-β1 trafficking in *opo* mutants. Equivalent areas were bleached from either basal or apical sides, in stage 24 wild-type and *opo* retinae (see Figure S3 for experimental details).

Developmental Cell
Numbs/Opo Antagonism Controls Optic Cup Formation

Opo and Numb Colocalize to the End Feet of the Neuroepithelial Precursors and Regulate Basal Localization of Integrin-β1

In vertebrates, *numb* and *numbl* have been detected in a wide range of tissues and developmental stages (Wakamatsu et al., 1999; Zhong et al., 1997). In zebrafish embryos, both transcripts are ubiquitously expressed before neurulation and get progressively restricted to the anterior nervous system and in particular to the retina (Niikura et al., 2006; Reugels et al., 2006). The analysis of *numb* and *numbl* expression by qPCR and in situ hybridization showed comparable profiles in medaka and confirmed that both genes are expressed in the developing retina (Figures S4A–S4F). Similarly, both *opo* transcripts and Opo protein are enriched at the basal side of the retinal epithelium in vertebrates (Figures S4G–S4J; Martinez-Morales et al., 2009; Mertes et al., 2009). To investigate in vivo the distribution of Opo and Numb during the folding of the optic cup (stage 24), we examined the medaka transgenic lines *Vsx3::eGFP_Opo* and *Vsx3::Numb_eGFP* (Figures 5A, 5B, and S4; Movies S3 and S4). Confocal microscopy analysis revealed that both proteins are enriched at the basal tip of the neuroblasts in the retina. Numb shows a strong cortical accumulation at the vitreal surface as well as in the baso-lateral cortex of mitotic cells (Figures 5B and 5C), as previously reported for zebrafish and chick neuroepithelial cells (Reugels et al., 2006; Wakamatsu et al., 1999). Finally, the injection of *Numb_Cherry* RNA into *Vsx3::eGFP_Opo* embryos at one-cell stage confirmed in vivo the colocalization of both proteins at the basal surface of the retinal epithelium (Figures 5D–5F). Interestingly, Numb basal localization appeared only mildly reduced in *opo* mutants as visualized in a *Vsx3::Numb_eGFP* background (Figures S4K and S4L), suggesting that its localization does not depend completely on *opo* function.

It has been shown that Numb regulates Integrin-β turnover in vitro (Nishimura and Kaibuchi, 2007; Teckchandani et al., 2009). To determine whether Numb also functions as a regulator of focal adhesions in the retinal epithelium, we generated retinal clones overexpressing *numb* and monitored Integrin-β1 localization (Figures 5G–5P). Integrin-β1 recruitment at the basal side of the neuroepithelium was noticeably reduced in *numb* gain-of-function clones (Figures 5K and 5N) but not in control clones expressing only the *Lyn_tdTomato* tracer (Figure 5H). These results, together with previous findings on *opo* function, suggest that Numb and Opo cooperate to regulate focal adhesions turnover during optic cup formation.

Numb/numbl Gain of Function Impairs Optic Cup Morphogenesis

A logical prediction to be drawn from the functional antagonism observed between Numb/Numbl and Opo would be that *numb/numbl* gain of function should mimic the embryonic phenotype observed in *opo* mutants. To confirm this, and to gain insight into the morphogenetic role of *numb/numbl* during optic cup morphogenesis, we injected medaka *numb* and *numbl* RNAs into medaka embryos at the one-cell stage. Injected embryos developed tissue malformations strikingly similar to those observed in *opo* mutants. The injection of 25 ng/μl of either *numb* (Figures 6A and 6B) or *numbl* (Figures 6C and 6D) RNAs resulted in a proportion of the embryos (19%, n = 76 and 12%, n = 102, respectively; Figure 6E) in which optic cup folding was impaired. The injection of 100 ng/μl of *numb* or *numbl* RNAs resulted in a higher proportion of affected embryos (34.8%, n = 74 and 36%, n = 40, respectively; Figure 6E). Among the morphologic defects observed, large ventral openings of the optic cups (Figures 6F and 6G) as well as strong craniofacial malformations (Figures 6H and 6I) were particularly prominent in hatchlings. Interestingly, a proportion of embryos injected with the highest dose (100 ng/μl) of *numb* (8.7%; Figures 6E and 6J) or *numbl* (10%; Figures 6E and 6K) developed complete cyclopia, a condition also observed in strongly affected *opo* morphants (Martinez-Morales et al., 2009), thus suggesting that Numb and Opo may also cooperate during the bilateralization of the eye field.

To extend our observations to another vertebrate model we also injected *numb* and *numbl* RNAs into zebrafish embryos (evolutionary distance 115–200 Myr (Furutani-Seiki and Wittbrodt, 2004). The injection of either 100 ng/μl of *numb* (n = 228) or 50 and 200 ng/μl of *numbl* RNA (n = 288 and n = 291, respectively) resulted in both a proportion of defects and a phenotypic range of ocular and craniofacial malformations similar to those observed in medaka embryos (Figures S5A–S5F).

Numb/numbl and *opo* Interact Genetically

Given the identified association between Opo and Numb/Numbl proteins, we decided to test whether this interaction was also observed at the genetic level. To this end, *numbl* RNA (25 ng/μl) was injected in the *opo* background. While the percentage of misshapen eyes observed in the progeny of an $opo^{+/-}$ cross is roughly Mendelian (24 ± 0.1%), and the injection of *numbl* RNA (25 ng/μl) into wild-type embryos yields 12% ± 1.1 of retinal defects, when the RNA was injected using the mutant background, ocular malformations increased to 45.8% ± 0.8 (Figure 6L). This percentage was significantly higher than what

(A–D) Statistical analysis of FRAP experiments. The plateau (A and C) and $t_{1/2}$ (B and D) values for the different FRAP experiments are shown. Quantitative data are expressed as mean ± SEM. Significant differences among groups were evaluated by t tests and indicated when relevant. Notice that when wild-type and *opo* data are compared, significant differences were observed only for the basal recovery of *Intβ1Tail-eGFP* (A and B) but not for *Par3-eGFP* (C and D).

(E and F) Electron microscopy analysis of stage 23 wild-type and *opo* retinas reveals an accumulation of intracellular vesicles at the basal feet of the mutant neuroblasts (see Figure S3 for experimental details). Quantitative data at the basal (E) and apical (F) regions are provided for a 25 μm^2 area (n = 15). Vesicles were classified according to their size. As an internal control mitochondria numbers were also recorded. Significant differences among groups were evaluated by t tests (GraphPad Prism) and indicated when relevant. Error bars represent SEM.

(G–O) In vivo internalization of integrins in the retina. Optical sections from WT (G–I, M, and N) and *opo* (J–L) *Vsx3::Int1βTailGFP* retinae stained with: DAPI (G, I, J, L, and M) and anti-GFP antibody (H, I, K, L, and N) after Integrin-β1 uptake assays. Anti-Integrin-β1Tail-GFP staining is significantly increased in *opo* mutants (K, L,and O), indicating an increased endocytic rate. No significant internalization of the antibody was detected in tissues not expressing the construct (compare red and white arrows in N). Dotted lines (H and K) represent areas of measured Integrin-β1 turnover (basal membrane and mid-retina). (O) Relative endocytosis rate is expressed as average pixel intensity (API).

Data represent the mean and SEM of six embryos in each condition. Scale bars, 10 μm. See also Movies S1 and S2.

Developmental Cell
Numbs/Opo Antagonism Controls Optic Cup Formation

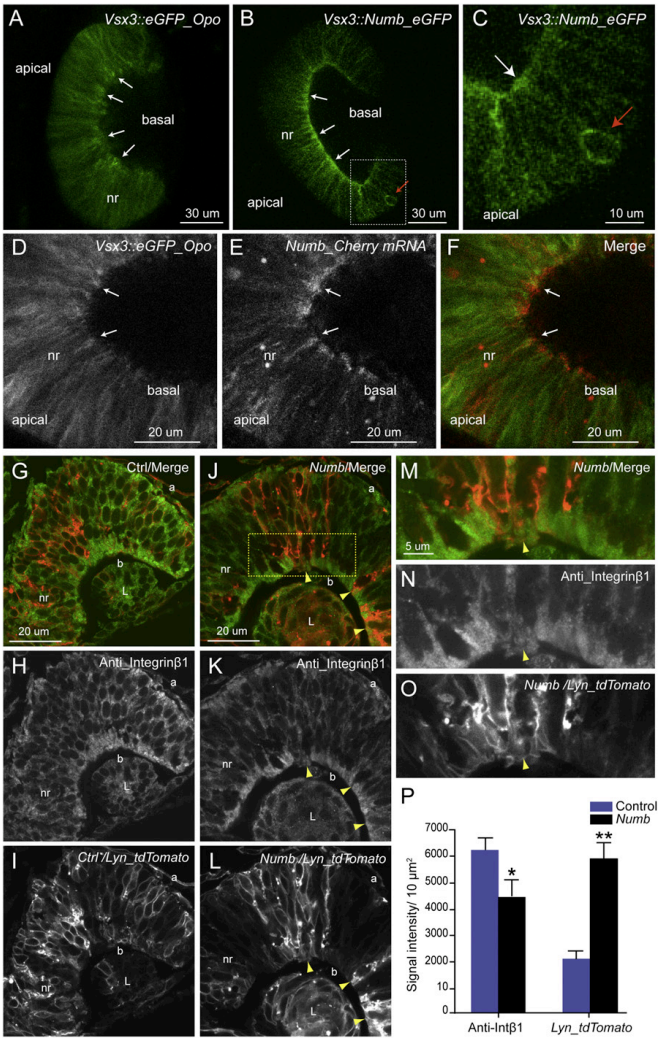

Figure 5. Numb Colocalizes with Opo and Regulates Integrin Recruitment at the Basal Retina

(A and B) Confocal microscopy analysis of transgenic medaka lines *Vsx3::eGFP_Opo* and *Vsx3::Numb_eGFP* shows the localization of both proteins at the basal end of the neuroblast.

(C) Numb_eGFP displays strong accumulation both at the basal surface (white arrow) and the baso-lateral cortex of mitotic cells (red arrow).

(D–F) Transient expression of *Numb_Cherry* RNA in *Vsx3::eGFP_Opo* embryos shows the in vivo colocalization of Numb and Opo at the basal surface.

(G–P) Stage 24 retinal sections showing different clones overexpressing either the linage tracer *Lyn_tdTomato* (G–I) or *numb* together with *Lyn_tdTomato* (J and L). Higher magnification pictures of (J–L) are shown in (M–O). Note that Integrin-β1 basal enrichment is reduced (yellow arrows) in *numb* gain-of-function clones as assessed by immunostaining (K and N). Integrin-β1 and Lyn_tdTomato are quantified (n = 5) in 10 μm^2 basal areas and are expressed as mean ± SEM (P). nr, neural retina; b, basal; L, lens. See also Figure S4 and Movies S3 and S4.

is expected from simple additive effects, as determined after analysis by two-way ANOVA of three independent experiments ($p < 0.0001$; see raw data in Table S2); thus showing a synergistic effect. Moreover, the injection of *numbl* RNA (25 ng/μl) in the *opo* context resulted in a small proportion (3.3% ± 1.7) of cyclopic embryos, a phenotype never observed in a wild-type background.

To further expand our analysis we tested whether a partial inactivation of *numb*/*numbl* function may alleviate *opo* ocular phenotype. To this end, we used splicing morpholinos *Mo_numblI4E5* and *Mo_numbII4E5* to specifically knockdown gene expression (Figures S5G and S5H). In agreement with the severe defects observed in $Numb^{-/-}$ mice (Zhong et al., 2000), the coinjection of both morpholinos at high concentration (300 μM) caused substantial embryo lethality. To overcome this, morpholinos were injected at a lower concentration (50 and 100 μM, respectively) into one blastomere in four-cell stage embryos, both in wild-type and *opo* backgrounds. Morpholino coinjection at this concentration did not interfere with optic cup folding. However, it significantly reduced the percentage of embryos (from the expected Mendelian 25% to 15% ± 3) showing the characteristic flattened optic cups observed in *opo* mutants (Figure 6M). In addition, a proportion of the injected embryos (11.9% ± 0.9) displayed a partial rescue of optic cup morphology, showing an intermediate bending never observed either in *opo* mutants or in wild-type siblings (Figures 6N–6P′). To support this observation, we measured the folding angles of the retinae and found that rescued embryos showed narrower cup folding angles than mutants (Figures 6N–6P′).

Finally, to complement our analyses, we examined optic cup morphogenesis in vivo in wild-type and *numbl*-injected zebrafish embryos. The folding of the retinal epithelium was recorded by time-lapse microscopy in *Vsx3:caaxGFP* embryos, either wild-type (Figure 6Q) or injected with *numbl* RNA (25 ng/μl; Figure 6R).

Developmental Cell
Numbs/Opo Antagonism Controls Optic Cup Formation

Using multiposition image acquisition, tissue morphogenesis was simultaneously monitored in control and injected embryos over approximately 4 hr, starting at 20 high-power fields. While a similar mitotic rate was observed in control and *numbl*-injected retinae, the constriction of the epithelial sheet was retarded in the treated embryos (Figures 6Q and 6R; Movie S5). Collectively, these data indicate that *opo* and *numb/numbl* interact genetically to regulate eye morphogenesis.

DISCUSSION

During organogenesis and tissue remodeling, the regulation of cell adhesive properties determines the morphogenetic behavior of entire epithelial sheets. The basal or baso-lateral localization of integrin receptors in epithelia has long been described as a common theme in vertebrate and invertebrate tissues (Bateman et al., 2001; Schoenenberger et al., 1994). However, the molecular mechanisms controlling the asymmetric turnover of integrin receptors have been poorly explored in the context of epithelial morphogenesis (Schotman et al., 2008).

Taking advantage of the polarized architecture of the vertebrate retina (Figure 7A), we studied the folding of the optic cup as a model system for epithelial basal constriction (Martinez-Morales et al., 2009). Previously, we described that integrin's adhesive function is required for optic cup folding and that the morphogenetic protein Opo plays an essential role during this process, albeit through a still uncharacterized molecular mechanism (Martinez-Morales and Wittbrodt, 2009). Here we show that Opo binds to clathrin adaptors Numb and Numbl, and functions as a negative regulator of integrin endocytosis. Our data suggest that Opo plays an important role in the stabilization of focal contacts at the basal surface. Although it is still unclear how tensional forces are generated and applied during optic cup folding, it is likely that focal contacts are required to transmit tensions basolaterally across the epithelial sheet. A similar requirement has been described during the elongation of the *Drosophila* egg chamber (He et al., 2010).

The PTB domain proteins Numb, Numbl, and Dab2 have been described as essential adaptors for clathrin-mediated integrin endocytosis (Caswell et al., 2009; Teckchandani et al., 2009). Consistently, they belong to the set of proteins recruited to focal adhesions in a Myosin II-dependent manner, as detected by proteomic analysis (Kuo et al., 2011). Our yeast two-hybrid assay has identified the interactions of Opo with Numbl (high confidence) and Dab2 (moderate confidence). Further biochemical analyses confirmed the preferential interaction of Opo with the PTB domains of Numb and Numbl, while showing a much weaker interaction with Dab2. In migratory cells, it has been proposed that Numb and Dab2 may play nonoverlapping roles as integrin endocytosis adaptors; Numb acting at the cell periphery and the leading edge and Dab2 mediating bulk internalization of disengaged integrins (Nishimura and Kaibuchi, 2007; Teckchandani et al., 2009). Both Numb and Opo have been described as basolaterally distributed proteins in epithelia (Martinez-Morales et al., 2009; Smith et al., 2007). Furthermore, here we show that Numb and Opo colocalize in vivo at the basal surface of the retinal epithelium. In contrast, Dab2 localizes preferentially to the apical surface in epithelia (Collaco et al., 2010). All these observations point to Numb and Numbl, rather than Dab2, as the functional partners of Opo.

The data presented here demonstrate that Opo binding to the PTB domain of Numb/Numbl depends on the conserved NPAF motif. In line with previous findings on the functionality of the integrin NPxF motif (Chen et al., 2006; Czuchra et al., 2006), the conservative mutation of the terminal phenylalanine to tyrosine in Opo does not abolish binding to Numb/Numbl. However, the mutation of this residue (1 out of 1090 amino acids) to aspartic acid (NPAD) strongly interferes with this interaction. It has been shown in *Drosophila* that Numb also binds the endocytic regulator Sanpodo through an amino-terminal conserved NPAF motif (Tong et al., 2010). The parallels between the vertebrate-specific protein Opo and the insect-specific protein Sanpodo can be further extended as both are fast-evolving proteins (O'Connor-Giles and Skeath, 2003), which include four transmembrane passes near their C-termini. Despite these similarities, there is no significant sequence homology between the two proteins, which suggests an independent evolutionary convergence phenomenon.

Our biochemical analyses, presented in the context of previous findings, are summarized in Figure 7B. Considering the molecular structures of Opo and its identified partners, two tentative hypotheses can be envisioned to explain Opo function as a repressor of clathrin-mediated integrin endocytosis. The first possibility encompasses a simple competitive binding mechanism involving Numb/Numbl sequestration by Opo, which in turn results in an inhibition of the integrin internalization process. The second possible mechanism would rely on the high-confidence interaction detected between the Opo C terminus and the chaperone Hsc70, which has a central role in clathrin disassembly (Sousa and Lafer, 2006). Opo recruitment to integrin clusters at the plasma membrane could therefore mediate the premature disassembly of clathrin structures. These two mechanisms are not mutually exclusive and can operate in parallel to inhibit integrin endocytosis.

The prominent morphogenetic role of polarized receptor trafficking has been acknowledged for both cell-to-cell and cell-to-extracellular matrix contacts (Nelson, 2009; Ulrich and Heisenberg, 2009). Although substantial crosstalk between cadherin-mediated and integrin-mediated adhesions has been described (Papusheva and Heisenberg, 2010), they have been classically implicated in distinct morphogenetic phenomena. Thus, whereas the asymmetric internalization of E-cadherin at adherens junctions has been involved in cell intercalation/rearrangement in epithelia (Levayer et al., 2011; Shaye et al., 2008), integrin trafficking along the front-rear axis has been primarily studied in migratory cells (Caswell et al., 2009; Ezratty et al., 2009). The Opo/Numb-dependent mechanism that we describe here suggests that integrin trafficking along the apicobasal axis also plays an important morphogenetic role in epithelial tissues, particularly in the context of basally driven constrictions.

EXPERIMENTAL PROCEDURES

Transgenic Lines

The medaka lines *Rx2::mYFP, Vsx3:Intβ1tail_eGFP* and *Vsx3::eGFP_Opo* have been previously described (Martinez-Morales et al., 2009). To generate the

Developmental Cell
Numbs/Opo Antagonism Controls Optic Cup Formation

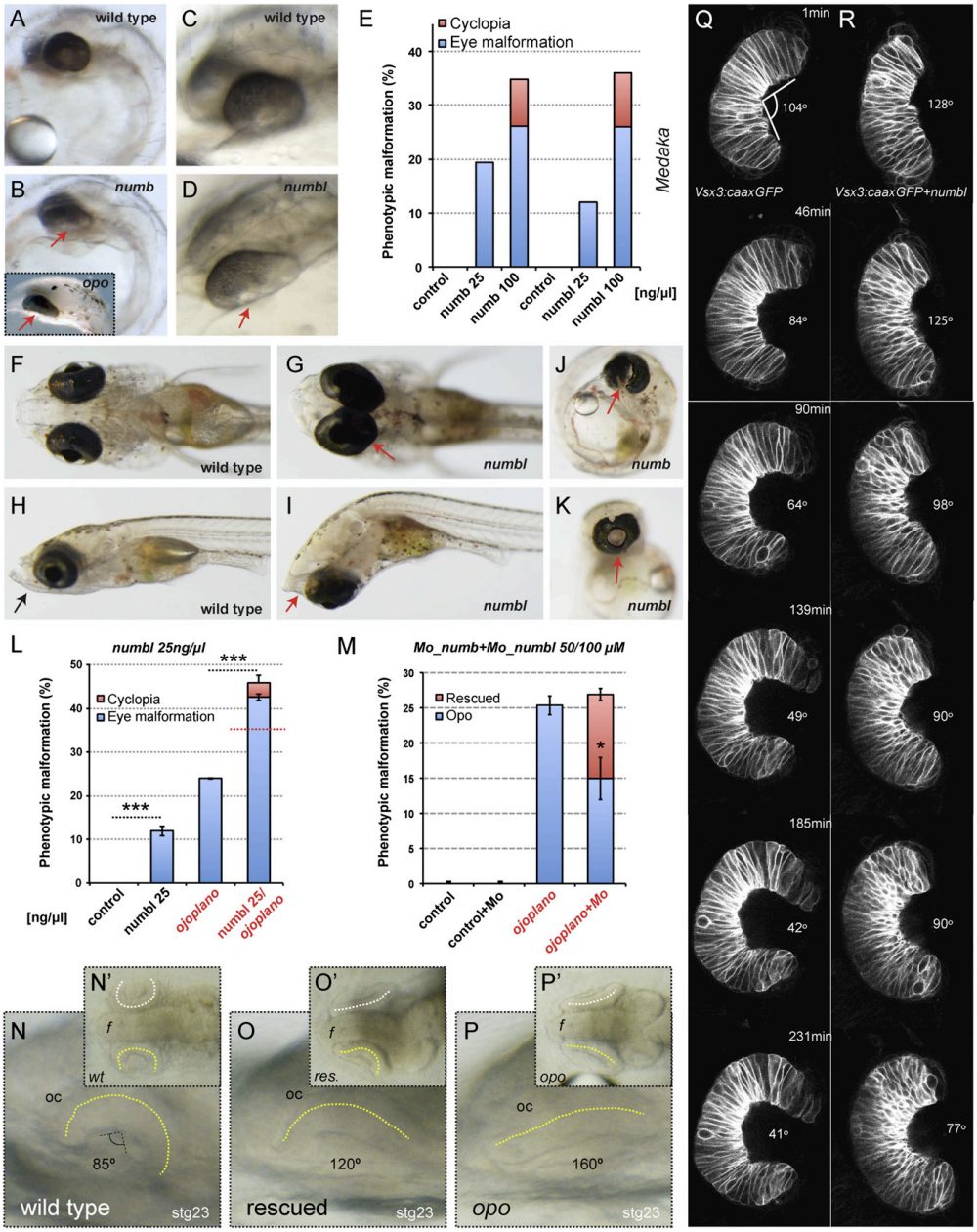

Developmental Cell
Numbs/Opo Antagonism Controls Optic Cup Formation

medaka line *Vsx3::zNumb-eGFP*, the fusion zNumb(PTBL PRRL):eGFP (Reugels et al., 2006) was cloned into a *Vsx3* expression vector. The resulting construct was then injected into one-cell stage embryos following standard protocols (Thermes et al., 2002). Tol2 mediated transgenesis (Kawakami, 2007) in combination with multisite gateway technology (Invitrogen) were used to generate the stable zebrafish line *Vsx3::eGFPcaax*. The medaka *Vsx3* promoter was inserted into a *p5E-MCS* entry vector and recombined with the Tol2kit vectors *pME-EGFPCAAX* and *p3E-polyA* into the Tol2 destination vector (Kwan et al., 2007). For a description of the expression constructs used see Supplemental Experimental Procedures.

Opo Yeast Two-Hybrid Screening

To elucidate Opo biochemical function we performed a yeast two-hybrid screening. The experimental approach used for baits and library construction, the mating methodology employed for screening and the scoring procedure have been previously described (Formstecher et al., 2005; Hybrigenics). Briefly, two different baits corresponding to the conserved amino (amino acids 1–126) and carboxy terminus (amino acids 905–1090) of the protein were generated by fusion to LexA in the vector pB29. The resulting fusions, N-OpoN-LexA-C and N-LexA-OpoC-C, were then used to screen a customized medaka cDNA library, cloned into the plasmid pP6 and built from medaka mRNAs (stages 18, 24, 31, and 34). The number of interactions tested was 74.2 million and 64.8 million for the amino and carboxy baits, respectively. The confidence of these interactions was scored using the Predicted Biological Score program to exclude false-positive results and promiscuous interactions.

GST Pull-Downs

Swollen glutathione agarose beads (Sigma, G4510) were incubated with GST fusion proteins in PBS buffer containing 1 mM DTT and 0.1% NP-40. The mixture was left rotating at 4°C for 3–4 hr with end-to-end mixing. The beads (25 μl) were incubated overnight with 200 μl of pull-down buffer (20 mM HEPES pH 7.9,150 mM NaCl, 0.5 mM EDTA, 10% glycerol, 0.1% Triton X-100, 1 mM DTT), and 20 μl of the S^{35} radiolabeled protein. Beads were washed 3X with pull-down buffer and the bound proteins were eluted in 50 μl Laemmli buffer. The eluted fractions were resolved on a 10% SDS-PA gel. Dried gels were exposed o/n and the signal was quantified with ImageQuant software (GE Healthcare).

Western Blotting and CoIP

Extract preparations, coIP and WB were performed as described (Hurtado et al., 2011). The following antibodies were used: Rabbit polyclonal anti-GFP (ICL); monoclonal anti-c-*myc* at 1:3000 (9E10, Sigma) and monoclonal anti-GFP at 1:1000 (MAB2003, Abnova).

Site-Directed Mutagenesis

The mutagenesis was performed following the manufacturers' protocol (Agilent, QuikChange Lightning Multi Site-Directed Mutagenesis Kit, 210515-5) with the following primers: ggcatagataacccagccgacgatggagaaggaagcac (t47g_t48a-NPAD) and gcatagataacccagcctacgatggagaaggaag (t48a-NPAY).

Cell Culture and Immunofluorescence Analysis

HeLa cells and immortalized human pigment epithelial cells RPE-1 (Takara Bio) were cultured at 37°C in 5% CO2 in DMEM or DMEM/F12 (respectively) supplemented with 10% fetal calf serum. For IF experiments, cells were plated on coverslips the day prior to transfection. Transfections were then performed using Lipofectamine 2000 (Invitrogen) according to the manufacturer's instructions. After 36 hr at 37°C, cells were fixed in 4% PFA for 20 min and permeabilized (when required) with PBS-0.1%, Tween-0.5%, and Triton X-100 containing 5% FCS for 10 min at room temperature. After PBS washes, cells were sequentially incubated with appropriate dilutions of the primary antibodies (12 hr at 4°C) and secondary antibodies labeled with Alexa-568 or Alexa-633 (30 min at room temperature). After PBS washing, cells were mounted and confocal images acquired on a Leica TCS SPE or a Leica TCS SP5 confocal systems using HCX PL APO 63x1.4 Oil objectives. Image processing was carried out using Leica (LAS), Adobe Photoshop, and Image J 10.2 software. The following antibodies were used: rabbit polyclonal anti-GFP at 1:500 (A-11122, Invitrogen), mouse anti-Integrin-β1 at 1:300 (MAB1981, Chemicon), and mouse monoclonal anti-alpha adaptin at 1:300 (ab2807, Abcam).

Internalization Assays

The internalization of integrins was studied in HeLa cells as previously described (Nishimura and Kaibuchi, 2007). Briefly, cultures were grown and transfected on PDL-coated coverslips. At 70% confluence live cells were incubated for 30 or 40 min at 37°C with mouse anti-integrin-β1, diluted 1:300 (MAB1981, Chemicon), to allow internalization. Then cells were rinsed in PBS, fixed in PFA, and permeabilized. Internalized integrins were detected with anti-mouse Alexa633 or Alexa568 secondary antibodies. Parallel negative controls in which cells were treated either without primary antibodies or without permeabilization yielded no significant signal. To quantify integrin internalization, we measured the mean fluorescence intensity per pixel in neighboring transfected and nontransfected cells of the same field (Image J). After background subtraction, relative endocytosis rate was calculated as the transfected/nontransfected ratio (%). Data represent the mean and SEM of 24 cells measured from two independent experiments.

In vivo internalization of integrins in medaka retinae was studied using the transgenic line *Vsx3::Int1βTailGFP*. In this construct the GFP tag is fused N-terminal to the 70 C-terminal amino acids of Integrin-β1, including the transmembrane and intracellular domains. Medaka WT and opo retinae expressing Intβ1tail:eGFP were dissected in cold PBS 1X. Once the overlying ectoderm was removed to facilitate antibody diffusion, embryos were incubated (30 min at 25°C) with polyclonal anti-GFP antibodies (ab290, Abcam) diluted 1:300. After fixation and permeabilization, internalized integrins were detected with anti-rabbit Alexa555 secondary antibodies. No significant internalization of the antibody was detected in neighboring tissues lacking Intβ1tail:eGFP expression.

Figure 6. Numb/Numbl and Opo Interact Genetically in Medaka Embryos

(A and B) Injection of 25 ng/μl of *numb* RNA in medaka embryos results in a flat eye phenotype (red arrows), similar to that observed in *opo* mutants (inset).
(C and D) Overexpression of *numbl* RNA (25 ng/μl) generates similar tissue malformations.
(E) Percentage of phenotypic malformations upon injection of increasing amounts of *numb* or *numbl* RNAs in medaka. Note that some of the embryos injected with 100 ng/μl displayed cyclopia.
(F–I) Medaka embryos injected with *numbl* (100 ng/μl) show large ventral openings of the optic cup and severe cranio-facial malformations (arrows).
(J and K) A small proportion of embryos injected with 100 ng/μl of *numb* or *numbl* developed complete cyclopia.
(L) Statistical analysis showing a synergistic effect when *numbl* RNA (25 ng/μl) was injected into an *opo* mutant background. Note the increased percentage of malformations over the expected 25% from the heterozygous cross.
(M) Statistical analysis showing that coinjection of splicing morpholinos targeting *numb* and *numbl* partially rescues ocular malformations observed in *opo* mutants. (E, L, and M) Error bars represent SEM
(N–P) Ocular morphology in wild-type (N and N′), partially rescued (O and O′), and *opo* (P and P′) medaka embryos from stage 23. Lateral views (N–P). Dorsal views (N′–P′). Ocular morphology is highlighted with dotted lines both for the left (yellow line) and right (white lines) eyes. Optic cup (oc) folding angle is indicated in N–P. f = forebrain. Folding of the retinal epithelium examined by time-lapse confocal microscopy in Vsx3:caaxGFP transgenic embryos. The basal constriction of the epithelial sheet is significantly impaired in embryos injected with 25 ng/μl of *numbl* RNA (Q) when compared to controls (R). Optic cup folding angle is also indicated.
See also Figure S5, Table S2, and Movie S5.

Developmental Cell
Numbs/Opo Antagonism Controls Optic Cup Formation

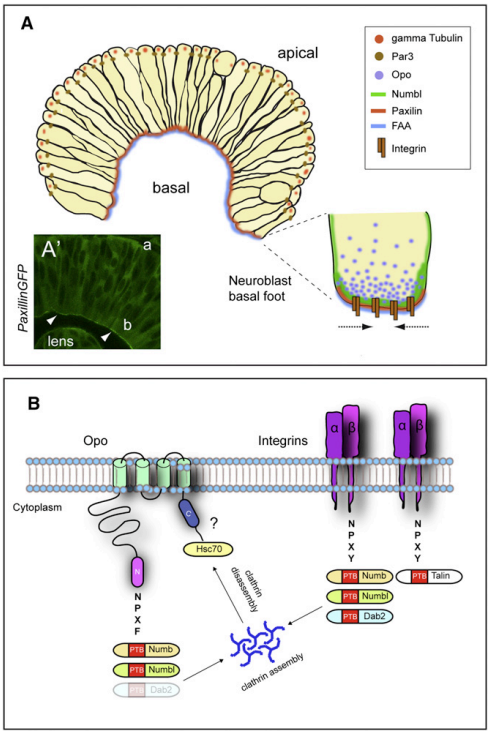

Figure 7. Numb/Numbl and Opo Localization and Function in the Retinal Epithelium

(A) Representation of the polarized retinal organization during morphogenesis. Apical and basal polarity cues are represented. Basal localization of integrins, Opo and Numbl at the basal feet of neuroblast cells is also depicted. Paxillin-eGFP is shown to illustrate the enrichment of focal adhesions (FAA) at the basal retina (A′).

(B) Schematic diagram of the molecular interactions between Opo, clathrin adaptors, and integrins. The PTB domains of talin and clathrin adaptors (Numb, Numbl, and Dab2), as well as the NPxF and NPxY motifs of Opo and Integrins.

In Vivo FRAP Analysis

Stage 24 embryos expressing *Intβ1Tail:eGFP* or *Par3:eGFP* embryos were immobilized and scanned in a Leica SP5 confocal microscope. Retinal cells expressing eGFP-tagged proteins were monitored using the 488 line of the SP5 100 mW argon laser at 20% power and bleached at 100% laser power. The bleaching protocol was as follows: three prebleaching images taken every 3 s; five bleaching pulses taken every 3 s at 100% laser power; 30 postbleaching images taken every 10 s. Equivalent areas in the retina were bleached either at the basal or the apical side of the neuroblasts both for WT and *opo* retinae. Recovery occurring at expenses of the unbleached side was monitored. The average fluorescence intensity per area in each compartment was plotted over time (LAS AF, Leica). To determine the plateau and $t_{1/2}$ values for the different FRAP experiments (n = 4) regression analyses were carried out using a one-phase exponential association function in GraphPad Prism5. To analyze the relative recovery at the plateau, the fluorescence value after bleaching was normalized to 1.

Electron Microscopy Analyses

For morphological EM analyses, stage 23 and 27 embryos were fixed in 0.05 M sodium cacodylate buffer, pH 7.3, containing 2.5% glutaraldehyde and 2% sucrose for 4 hr at 4°C. Samples were washed in cacodylate buffer and treated consecutively with osmium tetroxide 2% for 40 min and uranyl acetate 2% for 30 min. After washing in cacodylate buffer, samples were dehydrated in graded (50%, 70%, 80%, 95%, and 100%) ethanol solutions and embedded in Epon. To quantify vesicle number in EM sections, consecutive 25 μm^2 areas in contact with the basal lamina (n = 15) or the apical surface (n = 6) were analyzed in at least three embryos.

RNA Injections

The vectors *pCS2+:Numb* and *pCS2+:Numbl* were used to synthesize medaka *Numb* and *Numbl* capped RNAs. Similarly, the fusions *ASIP/Par-3:eGFP* and *pEGFPC1-(avian) paxillin WT1-559* (Martinez-Morales et al., 2009) were used to generate capped sense RNAs. After linearization of the vectors, capped sense RNAs were synthesized in vitro using the mMessage Machine Kit (Ambion). Purified RNA (QIAGEN RNeasy) was then injected (25–100 ng/μl) into one-cell stage both in medaka and zebrafish embryos. In clonal analysis experiments, *Numb* RNA (100 ng/μl) together with the lineage tracer Lyn_tdTomato (100 ng/μl), were coinjected into a single blastomere of four- to eight-cell stage medaka embryos. Mosaic embryos were then fixed in 4% PFA at stage 24, cryo-protected and sectioned as described (Martinez-Morales et al., 2009). Rabbit polyclonal anti-Integrin-β1 antibodies were used at 1:300 (Aviva Systems Biology).

Confocal Time-Lapse Analyses

Control and injected 20hpf *Vsx3::caaxGFP* embryos were immobilized in E3 (containing 0.01% tricaine) and embedded in 1% low-melting agarose. Time-lapse analyses were performed on a Nikon A1R microscope with a CFI PlanFluor20xMI N.A.0.75 objective and a 488 nm laser line. Samples were imaged as multiposition time-lapses for 3 hr with a time resolution of 3 min. Several central planes, spanning 40 μm, were selected. Movies were put together with single planes from each Z-stack using ImageJ (NIH).

Statistical Analysis

Quantitative data are expressed as mean ± SEM. Significant differences among groups were evaluated either by t tests or two-way ANOVA followed by Bonferroni post hoc tests (GraphPad Prism) and indicated when relevant.

SUPPLEMENTAL INFORMATION

Supplemental Information includes five figures, two tables, five movies, and Supplemental Experimental Procedures and can be found with this article online at http://dx.doi.org/10.1016/j.devcel.2012.09.004.

ACKNOWLEDGMENTS

We thank A. Gonzalez-Reyes, L. Centanin, F. Loosli, J.L. Gomez-Skarmeta, and P. Bovolenta for their critical input; Pam Halley for proofreading; and Rocío Polvillo, Katherina García, and Corín Díaz for their excellent technical assistance. The programs "Intramural/CSIC" 200920I212, Juan de la Cierva, and FCT (Portugal) supported O.B., M.D.-M., and I.G.-R., respectively. This work was supported by grants BFU2008-04362 and BFU2011-22916.

Received: December 13, 2011
Revised: June 4, 2012
Accepted: September 6, 2012
Published online: October 4, 2012

REFERENCES

Bateman, J., Reddy, R.S., Saito, H., and Van Vactor, D. (2001). The receptor tyrosine phosphatase Dlar and integrins organize actin filaments in the Drosophila follicular epithelium. Curr. Biol. *11*, 1317–1327.

Bryant, D.M., and Mostov, K.E. (2008). From cells to organs: building polarized tissue. Nat. Rev. Mol. Cell Biol. *9*, 887–901.

Developmental Cell
Numbs/Opo Antagonism Controls Optic Cup Formation

Calderwood, D.A., Fujioka, Y., de Pereda, J.M., García-Alvarez, B., Nakamoto, T., Margolis, B., McGlade, C.J., Liddington, R.C., and Ginsberg, M.H. (2003). Integrin beta cytoplasmic domain interactions with phosphotyrosine-binding domains: a structural prototype for diversity in integrin signaling. Proc. Natl. Acad. Sci. USA *100*, 2272–2277.

Caswell, P.T., Vadrevu, S., and Norman, J.C. (2009). Integrins: masters and slaves of endocytic transport. Nat. Rev. Mol. Cell Biol. *10*, 843–853.

Chang, H.C., Newmyer, S.L., Hull, M.J., Ebersold, M., Schmid, S.L., and Mellman, I. (2002). Hsc70 is required for endocytosis and clathrin function in Drosophila. J. Cell Biol. *159*, 477–487.

Chen, H., Zou, Z., Sarratt, K.L., Zhou, D., Zhang, M., Sebzda, E., Hammer, D.A., and Kahn, M.L. (2006). In vivo beta1 integrin function requires phosphorylation-independent regulation by cytoplasmic tyrosines. Genes Dev. *20*, 927–932.

Collaco, A., Jakab, R., Hegan, P., Mooseker, M., and Ameen, N. (2010). Alpha-AP-2 directs myosin VI-dependent endocytosis of cystic fibrosis transmembrane conductance regulator chloride channels in the intestine. J. Biol. Chem. *285*, 17177–17187.

Czuchra, A., Meyer, H., Legate, K.R., Brakebusch, C., and Fässler, R. (2006). Genetic analysis of beta1 integrin "activation motifs" in mice. J. Cell Biol. *174*, 889–899.

Dho, S.E., Trejo, J., Siderovski, D.P., and McGlade, C.J. (2006). Dynamic regulation of mammalian numb by G protein-coupled receptors and protein kinase C activation: Structural determinants of numb association with the cortical membrane. Mol. Biol. Cell *17*, 4142–4155.

Dong, B., Deng, W., and Jiang, D. (2011). Distinct cytoskeleton populations and extensive crosstalk control Ciona notochord tubulogenesis. Development *138*, 1631–1641.

Ezratty, E.J., Bertaux, C., Marcantonio, E.E., and Gundersen, G.G. (2009). Clathrin mediates integrin endocytosis for focal adhesion disassembly in migrating cells. J. Cell Biol. *187*, 733–747.

Filardo, E.J., Brooks, P.C., Deming, S.L., Damsky, C., and Cheresh, D.A. (1995). Requirement of the NPXY motif in the integrin beta 3 subunit cytoplasmic tail for melanoma cell migration in vitro and in vivo. J. Cell Biol. *130*, 441–450.

Formstecher, E., Aresta, S., Collura, V., Hamburger, A., Meil, A., Trehin, A., Reverdy, C., Betin, V., Maire, S., Brun, C., et al. (2005). Protein interaction mapping: a Drosophila case study. Genome Res. *15*, 376–384.

Furutani-Seiki, M., and Wittbrodt, J. (2004). Medaka and zebrafish, an evolutionary twin study. Mech. Dev. *121*, 629–637.

Gutzman, J.H., Graeden, E.G., Lowery, L.A., Holley, H.S., and Sive, H. (2008). Formation of the zebrafish midbrain-hindbrain boundary constriction requires laminin-dependent basal constriction. Mech. Dev. *125*, 974–983.

He, L., Wang, X., Tang, H.L., and Montell, D.J. (2010). Tissue elongation requires oscillating contractions of a basal actomyosin network. Nat. Cell Biol. *12*, 1133–1142.

Huang, E.J., Li, H., Tang, A.A., Wiggins, A.K., Neve, R.L., Zhong, W., Jan, L.Y., and Jan, Y.N. (2005). Targeted deletion of numb and numblike in sensory neurons reveals their essential functions in axon arborization. Genes Dev. *19*, 138–151.

Hurtado, L., Caballero, C., Gavilan, M.P., Cardenas, J., Bornens, M., and Rios, R.M. (2011). Disconnecting the Golgi ribbon from the centrosome prevents directional cell migration and ciliogenesis. J. Cell Biol. *193*, 917–933.

Kawakami, K. (2007). Tol2: a versatile gene transfer vector in vertebrates. Genome Biol. *8* (*Suppl 1*), S7.

Knoblich, J.A., Jan, L.Y., and Jan, Y.N. (1995). Asymmetric segregation of Numb and Prospero during cell division. Nature *377*, 624–627.

Kölsch, V., Seher, T., Fernandez-Ballester, G.J., Serrano, L., and Leptin, M. (2007). Control of Drosophila gastrulation by apical localization of adherens junctions and RhoGEF2. Science *315*, 384–386.

Kuo, J.C., Han, X., Hsiao, C.T., Yates, J.R., 3rd, and Waterman, C.M. (2011). Analysis of the myosin-II-responsive focal adhesion proteome reveals a role for β-Pix in negative regulation of focal adhesion maturation. Nat. Cell Biol. *13*, 383–393.

Kwan, K.M., Fujimoto, E., Grabher, C., Mangum, B.D., Hardy, M.E., Campbell, D.S., Parant, J.M., Yost, H.J., Kanki, J.P., and Chien, C.B. (2007). The Tol2kit: a multisite gateway-based construction kit for Tol2 transposon transgenesis constructs. Dev. Dyn. *236*, 3088–3099.

Lecuit, T., and Lenne, P.F. (2007). Cell surface mechanics and the control of cell shape, tissue patterns and morphogenesis. Nat. Rev. Mol. Cell Biol. *8*, 633–644.

Letizia, A., Sotillos, S., Campuzano, S., and Llimargas, M. (2011). Regulated Crb accumulation controls apical constriction and invagination in Drosophila tracheal cells. J. Cell Sci. *124*, 240–251.

Levayer, R., Pelissier-Monier, A., and Lecuit, T. (2011). Spatial regulation of Dia and Myosin-II by RhoGEF2 controls initiation of E-cadherin endocytosis during epithelial morphogenesis. Nat. Cell Biol. *13*, 529–540.

Martin, A.C., Kaschube, M., and Wieschaus, E.F. (2009). Pulsed contractions of an actin-myosin network drive apical constriction. Nature *457*, 495–499.

Martinez-Morales, J.R., and Wittbrodt, J. (2009). Shaping the vertebrate eye. Curr. Opin. Genet. Dev. *19*, 511–517.

Martinez-Morales, J.R., Rembold, M., Greger, K., Simpson, J.C., Brown, K.E., Quiring, R., Pepperkok, R., Martin-Bermudo, M.D., Himmelbauer, H., and Wittbrodt, J. (2009). ojoplano-mediated basal constriction is essential for optic cup morphogenesis. Development *136*, 2165–2175.

Mertes, F., Martinez-Morales, J.R., Nolden, T., Spörle, R., Wittbrodt, J., Lehrach, H., and Himmelbauer, H. (2009). Cloning of mouse ojoplano, a reticular cytoplasmic protein expressed during embryonic development. Gene Expr. Patterns *9*, 562–567.

Montell, D.J. (2008). Morphogenetic cell movements: diversity from modular mechanical properties. Science *322*, 1502–1505.

Nelson, W.J. (2009). Remodeling epithelial cell organization: transitions between front-rear and apical-basal polarity. Cold Spring Harb. Perspect. Biol. *1*, a000513.

Niikura, Y., Tabata, Y., Tajima, A., Inoue, I., Arai, K., and Watanabe, S. (2006). Zebrafish Numb homologue: phylogenetic evolution and involvement in regulation of left-right asymmetry. Mech. Dev. *123*, 407–414.

Nishimura, T., and Kaibuchi, K. (2007). Numb controls integrin endocytosis for directional cell migration with aPKC and PAR-3. Dev. Cell *13*, 15–28.

O'Connor-Giles, K.M., and Skeath, J.B. (2003). Numb inhibits membrane localization of Sanpodo, a four-pass transmembrane protein, to promote asymmetric divisions in Drosophila. Dev. Cell *5*, 231–243.

Papusheva, E., and Heisenberg, C.P. (2010). Spatial organization of adhesion: force-dependent regulation and function in tissue morphogenesis. EMBO J. *29*, 2753–2768.

Rasin, M.R., Gazula, V.R., Breunig, J.J., Kwan, K.Y., Johnson, M.B., Liu-Chen, S., Li, H.S., Jan, L.Y., Jan, Y.N., Rakic, P., and Sestan, N. (2007). Numb and Numbl are required for maintenance of cadherin-based adhesion and polarity of neural progenitors. Nat. Neurosci. *10*, 819–827.

Reugels, A.M., Boggetti, B., Scheer, N., and Campos-Ortega, J.A. (2006). Asymmetric localization of Numb:EGFP in dividing neuroepithelial cells during neurulation in Danio rerio. Dev. Dyn. *235*, 934–948.

Santolini, E., Puri, C., Salcini, A.E., Gagliani, M.C., Pelicci, P.G., Tacchetti, C., and Di Fiore, P.P. (2000). Numb is an endocytic protein. J. Cell Biol. *151*, 1345–1352.

Sawyer, J.M., Harrell, J.R., Shemer, G., Sullivan-Brown, J., Roh-Johnson, M., and Goldstein, B. (2010). Apical constriction: a cell shape change that can drive morphogenesis. Dev. Biol. *341*, 5–19.

Schoenenberger, C.A., Zuk, A., Zinkl, G.M., Kendall, D., and Matlin, K.S. (1994). Integrin expression and localization in normal MDCK cells and transformed MDCK cells lacking apical polarity. J. Cell Sci. *107*, 527–541.

Schotman, H., Karhinen, L., and Rabouille, C. (2008). dGRASP-mediated noncanonical integrin secretion is required for Drosophila epithelial remodeling. Dev. Cell *14*, 171–182.

Shaye, D.D., Casanova, J., and Llimargas, M. (2008). Modulation of intracellular trafficking regulates cell intercalation in the Drosophila trachea. Nat. Cell Biol. *10*, 964–970.

Smith, C.A., Lau, K.M., Rahmani, Z., Dho, S.E., Brothers, G., She, Y.M., Berry, D.M., Bonneil, E., Thibault, P., Schweisguth, F., et al. (2007). aPKC-mediated phosphorylation regulates asymmetric membrane localization of the cell fate determinant Numb. EMBO J. *26*, 468–480.

Solon, J., Kaya-Copur, A., Colombelli, J., and Brunner, D. (2009). Pulsed forces timed by a ratchet-like mechanism drive directed tissue movement during dorsal closure. Cell *137*, 1331–1342.

Sousa, R., and Lafer, E.M. (2006). Keep the traffic moving: mechanism of the Hsp70 motor. Traffic *7*, 1596–1603.

Teckchandani, A., Toida, N., Goodchild, J., Henderson, C., Watts, J., Wollscheid, B., and Cooper, J.A. (2009). Quantitative proteomics identifies a Dab2/integrin module regulating cell migration. J. Cell Biol. *186*, 99–111.

Thermes, V., Grabher, C., Ristoratore, F., Bourrat, F., Choulika, A., Wittbrodt, J., and Joly, J.S. (2002). I-SceI meganuclease mediates highly efficient transgenesis in fish. Mech. Dev. *118*, 91–98.

Tong, X., Zitserman, D., Serebriiskii, I., Andrake, M., Dunbrack, R., and Roegiers, F. (2010). Numb independently antagonizes Sanpodo membrane targeting and Notch signaling in Drosophila sensory organ precursor cells. Mol. Biol. Cell *21*, 802–810.

Ulrich, F., and Heisenberg, C.P. (2009). Trafficking and cell migration. Traffic *10*, 811–818.

Ungewickell, E.J., and Hinrichsen, L. (2007). Endocytosis: clathrin-mediated membrane budding. Curr. Opin. Cell Biol. *19*, 417–425.

Wakamatsu, Y., Maynard, T.M., Jones, S.U., and Weston, J.A. (1999). NUMB localizes in the basal cortex of mitotic avian neuroepithelial cells and modulates neuronal differentiation by binding to NOTCH-1. Neuron *23*, 71–81.

Wang, Z., Sandiford, S., Wu, C., and Li, S.S. (2009). Numb regulates cell-cell adhesion and polarity in response to tyrosine kinase signalling. EMBO J. *28*, 2360–2373.

Wu, M., Smith, C.L., Hall, J.A., Lee, I., Luby-Phelps, K., and Tallquist, M.D. (2010). Epicardial spindle orientation controls cell entry into the myocardium. Dev. Cell *19*, 114–125.

Zhong, W., Jiang, M.M., Weinmaster, G., Jan, L.Y., and Jan, Y.N. (1997). Differential expression of mammalian Numb, Numblike and Notch1 suggests distinct roles during mouse cortical neurogenesis. Development *124*, 1887–1897.

Zhong, W., Jiang, M.M., Schonemann, M.D., Meneses, J.J., Pedersen, R.A., Jan, L.Y., and Jan, Y.N. (2000). Mouse numb is an essential gene involved in cortical neurogenesis. Proc. Natl. Acad. Sci. USA *97*, 6844–6849.

Zhou, P., Alfaro, J., Chang, E.H., Zhao, X., Porcionatto, M., and Segal, R.A. (2011). Numb links extracellular cues to intracellular polarity machinery to promote chemotaxis. Dev. Cell *20*, 610–622.

IX. References

Adelmann, H. B. (1929) 'Experimental studies on the development of the eye. I. The effect of the removal of median and lateral areas of the anterior end of the urodelan neural plate on the development of the eyes (*Triton teniatus* and *Amblystoma punctatum*)', *Journal of Experimental Zoology* 54: 249-290.

Adler, R. and Belecky-Adams, T. L. (2002) 'The role of bone morphogenetic proteins in the differentiation of the ventral optic cup', *Development* 129(13): 3161-71.

Adler, R. and Canto-Soler, M. V. (2007) 'Molecular mechanisms of optic vesicle development: complexities, ambiguities and controversies', *Dev Biol* 305(1): 1-13.

Banerji, J., Rusconi, S. and Schaffner, W. (1981) 'Expression of a beta-globin gene is enhanced by remote SV40 DNA sequences', *Cell* 27(2 Pt 1): 299-308.

Bannister, A. J. and Kouzarides, T. (2011) 'Regulation of chromatin by histone modifications', *Cell Res* 21(3): 381-95.

Bar-Yosef, U., Abuelaish, I., Harel, T., Hendler, N., Ofir, R. and Birk, O. S. (2004) 'CHX10 mutations cause non-syndromic microphthalmia/ anophthalmia in Arab and Jewish kindreds', *Hum Genet* 115(4): 302-9.

Barabino, S. M. L., Spada, F., Cotelli, F. and Boncinelli, E. (1997) 'Inactivation Of the Zebrafish Homologue Of Chx10 By Antisense Oligonucleotides Causes Eye Malformations Similar to the Ocular Retardation Phenotype', *Mechanisms of Development* 63(2): 133-143.

Bejerano, G., Pheasant, M., Makunin, I., Stephen, S., Kent, W. J., Mattick, J. S. and Haussler, D. (2004) 'Ultraconserved elements in the human genome', *Science* 304(5675): 1321-5.

Belecky-Adams, T., Tomarev, S., Li, H. S., Ploder, L., McInnes, R. R., Sundin, O. and Adler, R. (1997) 'Pax-6, Prox 1, and Chx10 homeobox gene expression correlates with phenotypic fate of retinal precursor cells', *Investigative Ophthalmology & Visual Science* 38(7): 1293-1303.

Bernstein, B. E., Mikkelsen, T. S., Xie, X., Kamal, M., Huebert, D. J., Cuff, J., Fry, B., Meissner, A., Wernig, M., Plath, K. et al. (2006) 'A bivalent chromatin structure marks key developmental genes in embryonic stem cells', *Cell* 125(2): 315-26.

Bessa, J. and Gomez-Skarmeta, J. L. (2011) 'Making reporter gene constructs to analyze cis-regulatory elements', *Methods Mol Biol* 772: 397-408.

Bessa, J., Tena, J. J., de la Calle-Mustienes, E., Fernandez-Minan, A., Naranjo, S., Fernandez, A., Montoliu, L., Akalin, A., Lenhard, B., Casares, F. et al. (2009) 'Zebrafish enhancer detection (ZED) vector: a new tool to facilitate transgenesis and the functional analysis of cis-regulatory regions in zebrafish', *Dev Dyn* 238(9): 2409-17.

Bharti, K., Nguyen, M. T., Skuntz, S., Bertuzzi, S. and Arnheiter, H. (2006) 'The other pigment cell: specification and development of the pigmented epithelium of the vertebrate eye', *Pigment Cell Res* 19(5): 380-94.

Bogdanovic, O., Delfino-Machin, M., Nicolas-Perez, M., Gavilan, M. P., Gago-Rodrigues, I., Fernandez-Minan, A., Lillo, C., Rios, R. M., Wittbrodt, J. and Martinez-Morales, J. R.

(2012a) 'Numb/Numbl-Opo antagonism controls retinal epithelium morphogenesis by regulating integrin endocytosis', *Dev Cell* 23(4): 782-95.

Bogdanovic, O., Fernandez-Minan, A., Tena, J. J., de la Calle-Mustienes, E., Hidalgo, C., van Kruysbergen, I., van Heeringen, S. J., Veenstra, G. J. and Gomez-Skarmeta, J. L. (2012b) 'Dynamics of enhancer chromatin signatures mark the transition from pluripotency to cell specification during embryogenesis', *Genome Res* 22(10): 2043-53.

Bryant, D. M. and Mostov, K. E. (2008) 'From cells to organs: building polarized tissue', *Nat Rev Mol Cell Biol* 9(11): 887-901.

Bryne, J. C., Valen, E., Tang, M. H., Marstrand, T., Winther, O., da Piedade, I., Krogh, A., Lenhard, B. and Sandelin, A. (2008) 'JASPAR, the open access database of transcription factor-binding profiles: new content and tools in the 2008 update', *Nucleic Acids Res* 36(Database issue): D102-6.

Burmeister, M., Novak, J., Liang, M.-Y., Basu, S., Ploder, L., Hawes, N. L., Vidgen, D., Hoover, F., Goldman, D., Kalnins, V. I. et al. (1996) 'Ocular retardation mouse caused by *Chx10* homeobox null allele: impaired retinal progenitor proliferation and bipolar cell differentiation', *Nature Genetics* 12: 376-384.

Burridge, K. and Chrzanowska-Wodnicka, M. (1996) 'Focal adhesions, contractility, and signaling', *Annu Rev Cell Dev Biol* 12: 463-518.

Cai, Z., Feng, G. S. and Zhang, X. (2010) 'Temporal requirement of the protein tyrosine phosphatase Shp2 in establishing the neuronal fate in early retinal development', *J Neurosci* 30(11): 4110-9.

Calderwood, D. A., Fujioka, Y., de Pereda, J. M., Garcia-Alvarez, B., Nakamoto, T., Margolis, B., McGlade, C. J., Liddington, R. C. and Ginsberg, M. H. (2003) 'Integrin beta cytoplasmic domain interactions with phosphotyrosine-binding domains: a structural prototype for diversity in integrin signaling', *Proc Natl Acad Sci U S A* 100(5): 2272-7.

Cavodeassi, F., Carreira-Barbosa, F., Young, R. M., Concha, M. L., Allende, M. L., Houart, C., Tada, M. and Wilson, S. W. (2005) 'Early stages of zebrafish eye formation require the coordinated activity of Wnt11, Fz5, and the Wnt/beta-catenin pathway', *Neuron* 47(1): 43-56.

Chauhan, B. K., Disanza, A., Choi, S. Y., Faber, S. C., Lou, M., Beggs, H. E., Scita, G., Zheng, Y. and Lang, R. A. (2009) 'Cdc42- and IRSp53-dependent contractile filopodia tether presumptive lens and retina to coordinate epithelial invagination', *Development* 136(21): 3657-67.

Chen, C. M. and Cepko, C. L. (2000) 'Expression of Chx10 and Chx10-1 in the developing chicken retina', *Mech Dev* 90(2): 293-7.

Chow, R. L. and Lang, R. A. (2001) 'Early eye development in vertebrates', *Annual Review of Cell & Developmental Biology* 17: 255-96.

Chuang, J. C. and Raymond, P. A. (2002) 'Embryonic origin of the eyes in teleost fish', *Bioessays* 24(6): 519-29.

Clark, A. M., Yun, S., Veien, E. S., Wu, Y. Y., Chow, R. L., Dorsky, R. I. and Levine, E. M. (2008) 'Negative regulation of Vsx1 by its paralog Chx10/Vsx2 is conserved in the vertebrate retina', *Brain Res* 1192: 99-113.

Comings, D. E., Comings, B. G., Devor, E. J. and Cloninger, C. R. (1984) 'Detection of major gene for Gilles de la Tourette syndrome', *Am J Hum Genet* 36(3): 586-600.

Creyghton, M. P., Cheng, A. W., Welstead, G. G., Kooistra, T., Carey, B. W., Steine, E. J., Hanna, J., Lodato, M. A., Frampton, G. M., Sharp, P. A. et al. (2010) 'Histone H3K27ac separates active from poised enhancers and predicts developmental state', *Proc Natl Acad Sci U S A* 107(50): 21931-6.

Davies, S. J., Wise, C., Venkatesh, B., Mirza, G., Jefferson, A., Volpi, E. V. and Ragoussis, J. (2004) 'Mapping of three translocation breakpoints associated with orofacial clefting within 6p24 and identification of new transcripts within the region', *Cytogenet Genome Res* 105(1): 47-53.

Dekker, J., Rippe, K., Dekker, M. and Kleckner, N. (2002) 'Capturing chromosome conformation', *Science* 295(5558): 1306-11.

Dudley, A. T. and Robertson, E. J. (1997) 'Overlapping expression domains of bone morphogenetic protein family members potentially account for limited tissue defects in BMP7 deficient embryos', *Developmental Dynamics* 208: 349-362.

Eiraku, M., Takata, N., Ishibashi, H., Kawada, M., Sakakura, E., Okuda, S., Sekiguchi, K., Adachi, T. and Sasai, Y. (2011) 'Self-organizing optic-cup morphogenesis in three-dimensional culture', *Nature* 472(7341): 51-6.

Esteve, P. and Bovolenta, P. (2006) 'Secreted inducers in vertebrate eye development: more functions for old morphogens', *Curr Opin Neurobiol* 16(1): 13-9.

Ezratty, E. J., Bertaux, C., Marcantonio, E. E. and Gundersen, G. G. (2009) 'Clathrin mediates integrin endocytosis for focal adhesion disassembly in migrating cells', *J Cell Biol* 187(5): 733-47.

Feijen, A., Goumans, M. J. and van den Eijnden-van Raaij, A. J. (1994) 'Expression of activin subunits, activin receptors and follistatin in postimplantation mouse embryos suggests specific developmental functions for different activins', *Development* 120(12): 3621-37.

Frazer, K. A., Pachter, L., Poliakov, A., Rubin, E. M. and Dubchak, I. (2004) 'VISTA: computational tools for comparative genomics', *Nucleic Acids Res* 32(Web Server issue): W273-9.

Fuhrmann, S. (2010) 'Eye morphogenesis and patterning of the optic vesicle', *Curr Top Dev Biol* 93: 61-84.

Fuhrmann, S., Chow, L. and Reh, T. A. (2000) 'Molecular control of cell diversification in the vertebrate retina', *Results & Problems in Cell Differentiation* 31: 69-91.

Geng, X., Speirs, C., Lagutin, O., Inbal, A., Liu, W., Solnica-Krezel, L., Jeong, Y., Epstein, D. J. and Oliver, G. (2008) 'Haploinsufficiency of Six3 fails to activate Sonic hedgehog expression in the ventral forebrain and causes holoprosencephaly', *Dev Cell* 15(2): 236-47.

Gomez Skarmeta, J. L. (2009) 'Non-coding regulatory regions in genomes. Editorial', *Brief Funct Genomic Proteomic* 8(4): 213-4.

Gomez-Skarmeta, J. L., Lenhard, B. and Becker, T. S. (2006) 'New technologies, new findings, and new concepts in the study of vertebrate cis-regulatory sequences', *Dev Dyn* 235(4): 870-85.

Graf, T. and Enver, T. (2009) 'Forcing cells to change lineages', *Nature* 462(7273): 587-94.

Graw, J. (2010) 'Eye development', *Curr Top Dev Biol* 90: 343-86.

Green, E. S., Stubbs, J. L. and Levine, E. M. (2003) 'Genetic rescue of cell number in a mouse model of microphthalmia: interactions between Chx10 and G1-phase cell cycle regulators', *Development* 130(3): 539-52.

Hagege, H., Klous, P., Braem, C., Splinter, E., Dekker, J., Cathala, G., de Laat, W. and Forne, T. (2007) 'Quantitative analysis of chromosome conformation capture assays (3C-qPCR)', *Nat Protoc* 2(7): 1722-33.

Hallmayer, J. F., Kalaydjieva, L., Badcock, J., Dragovic, M., Howell, S., Michie, P. T., Rock, D., Vile, D., Williams, R., Corder, E. H. et al. (2005) 'Genetic evidence for a distinct subtype of schizophrenia characterized by pervasive cognitive deficit', *Am J Hum Genet* 77(3): 468-76.

He, L., Wang, X., Tang, H. L. and Montell, D. J. (2010) 'Tissue elongation requires oscillating contractions of a basal actomyosin network', *Nat Cell Biol* 12(12): 1133-42.

Heintzman, N. D., Hon, G. C., Hawkins, R. D., Kheradpour, P., Stark, A., Harp, L. F., Ye, Z., Lee, L. K., Stuart, R. K., Ching, C. W. et al. (2009) 'Histone modifications at human enhancers reflect global cell-type-specific gene expression', *Nature* 459(7243): 108-12.

Heintzman, N. D., Stuart, R. K., Hon, G., Fu, Y., Ching, C. W., Hawkins, R. D., Barrera, L. O., Van Calcar, S., Qu, C., Ching, K. A. et al. (2007) 'Distinct and predictive chromatin signatures of transcriptional promoters and enhancers in the human genome', *Nat Genet* 39(3): 311-8.

Hilfer, S. R. (1983) 'Development of the eye of the chick embryo', *Scan Electron Microsc*(Pt 3): 1353-69.

Hong, J. W., Hendrix, D. A. and Levine, M. S. (2008) 'Shadow enhancers as a source of evolutionary novelty', *Science* 321(5894): 1314.

Horsford, D. J., Nguyen, M. T., Sellar, G. C., Kothary, R., Arnheiter, H. and McInnes, R. R. (2005) 'Chx10 repression of Mitf is required for the maintenance of mammalian neuroretinal identity', *Development* 132(1): 177-87.

Hyer, J., Kuhlman, J., Afif, E. and Mikawa, T. (2003) 'Optic cup morphogenesis requires pre-lens ectoderm but not lens differentiation', *Dev Biol* 259(2): 351-63.

Hynes, R. O. (1992) 'Integrins: versatility, modulation, and signaling in cell adhesion', *Cell* 69(1): 11-25.

Jao, L. E., Wente, S. R. and Chen, W. (2013) 'Efficient multiplex biallelic zebrafish genome editing using a CRISPR nuclease system', *Proc Natl Acad Sci U S A* 110(34): 13904-9.

Kimmel, C. B., Ballard, W. W., Kimmel, S. R., Ullmann, B. and Schilling, T. F. (1995) 'Stages of embryonic development of the zebrafish', *Dev Dyn* 203(3): 253-310.

Kish, P. E., Bohnsack, B. L., Gallina, D., Kasprick, D. S. and Kahana, A. (2011) 'The eye as an organizer of craniofacial development', *Genesis* 49(4): 222-30.

Kolsch, V., Seher, T., Fernandez-Ballester, G. J., Serrano, L. and Leptin, M. (2007) 'Control of Drosophila gastrulation by apical localization of adherens junctions and RhoGEF2', *Science* 315(5810): 384-6.

Kwan, K. M., Fujimoto, E., Grabher, C., Mangum, B. D., Hardy, M. E., Campbell, D. S., Parant, J. M., Yost, H. J., Kanki, J. P. and Chien, C. B. (2007) 'The Tol2kit: a multisite gateway-based construction kit for Tol2 transposon transgenesis constructs', *Dev Dyn* 236(11): 3088-99.

Kwan, K. M., Otsuna, H., Kidokoro, H., Carney, K. R., Saijoh, Y. and Chien, C. B. (2012) 'A complex choreography of cell movements shapes the vertebrate eye', *Development* 139(2): 359-72.

Langheinrich, U., Hennen, E., Stott, G. and Vacun, G. (2002) 'Zebrafish as a model organism for the identification and characterization of drugs and genes affecting p53 signaling', *Curr Biol* 12(23): 2023-8.

Larkin, M. A., Blackshields, G., Brown, N. P., Chenna, R., McGettigan, P. A., McWilliam, H., Valentin, F., Wallace, I. M., Wilm, A., Lopez, R. et al. (2007) 'Clustal W and Clustal X version 2.0', *Bioinformatics* 23(21): 2947-8.

Letizia, A., Sotillos, S., Campuzano, S. and Llimargas, M. (2011) 'Regulated Crb accumulation controls apical constriction and invagination in Drosophila tracheal cells', *J Cell Sci* 124(Pt 2): 240-51.

Li, H., Tierney, C., Wen, L., Wu, J. Y. and Rao, Y. (1997) 'A single morphogenetic field gives rise to two retina primordia under the inluence of the prechordal plate', *Development* 124: 603-615.

Li, Z., Joseph, N. M. and Easter, S. S. J. (2000) 'The morphogenesis of the zebrafish eye, including a fate map of the optic vesicle', *Developmental Dynamics* 218: 175-188.

Liu, I. S. C., Chen, J. D., Ploder, L., Vidgen, D., Vanderkooy, D., Kalnins, V. I. and Mcinnes, R. R. (1994) 'Developmental expression of a novel murine homeobox gene (Chx10): Evidence for roles in determination of the neuroretina and inner nuclear layer', *Neuron* 13(2): 377-393.

Loosli, F., Del Bene, F., Quiring, R., Rembold, M., Martinez-Morales, J. R., Carl, M., Grabher, C., Iquel, C., Krone, A., Wittbrodt, B. et al. (2004) 'Mutations affecting retina development in Medaka', *Mech Dev* 121(7-8): 703-14.

Loosli, F., Staub, W., Finger-Baier, K., Ober, E., Verkade, H., Wittbrodt, J. and Baier, H. (2003) 'Loss of eyes in zebrafish caused by mutation of chokh/rx3', *EMBO Reports* 4: 894-899.

Martinez-Morales, J. R., Henrich, T., Ramialison, M. and Wittbrodt, J. (2007) 'New genes in the evolution of the neural crest differentiation program', *Genome Biol* 8(3): R36.

Martinez-Morales, J. R., Rembold, M., Greger, K., Simpson, J. C., Brown, K. E., Quiring, R., Pepperkok, R., Martin-Bermudo, M. D., Himmelbauer, H. and Wittbrodt, J. (2009) 'ojoplano-mediated basal constriction is essential for optic cup morphogenesis', *Development* 136(13): 2165-75.

Martinez-Morales, J. R., Rodrigo, I. and Bovolenta, P. (2004) 'Eye development: a view from the retina pigmented epithelium', *Bioessays* 26(7): 766-77.

Martinez-Morales, J. R., Signore, M., Acampora, D., Simeone, A. and Bovolenta, P. (2001) 'Otx genes are required for tissue specification in the developing eye', *Development* 128(11): 2019-30.

Martinez-Morales, J. R. and Wittbrodt, J. (2009) 'Shaping the vertebrate eye', *Curr Opin Genet Dev* 19(5): 511-7.

Mertes, F., Martinez-Morales, J. R., Nolden, T., Sporle, R., Wittbrodt, J., Lehrach, H. and Himmelbauer, H. (2009) 'Cloning of mouse ojoplano, a reticular cytoplasmic protein expressed during embryonic development', *Gene Expr Patterns* 9(8): 562-7.

Mikkelsen, T. S., Ku, M., Jaffe, D. B., Issac, B., Lieberman, E., Giannoukos, G., Alvarez, P., Brockman, W., Kim, T. K., Koche, R. P. et al. (2007) 'Genome-wide maps of chromatin state in pluripotent and lineage-committed cells', *Nature* 448(7153): 553-60.

Murray, J. C. and Schutte, B. C. (2004) 'Cleft palate: players, pathways, and pursuits', *J Clin Invest* 113(12): 1676-8.

Neto, A., Mercader, N. and Gomez-Skarmeta, J. L. (2012) 'The Osr1 and Osr2 genes act in the pronephric anlage downstream of retinoic acid signaling and upstream of Wnt2b to maintain pectoral fin development', *Development* 139(2): 301-11.

Nguyen, M. T. and Arnheiter, H. (2000) 'Signaling and transcriptional regulation in early mammalian eye development: a link between FGF and MITF', *Development* 127: 3581-3591.

Nishimura, T. and Kaibuchi, K. (2007) 'Numb controls integrin endocytosis for directional cell migration with aPKC and PAR-3', *Dev Cell* 13(1): 15-28.

Noordermeer, D., Leleu, M., Splinter, E., Rougemont, J., De Laat, W. and Duboule, D. (2011) 'The dynamic architecture of Hox gene clusters', *Science* 334(6053): 222-5.

Osipov, V. V. and Vakhrusheva, M. P. (1983) '[Variation in the expressivity of the ocular retardation gene in mice]', *Tsitol Genet* 17(4): 39-43.

Ovcharenko, I., Nobrega, M. A., Loots, G. G. and Stubbs, L. (2004) 'ECR Browser: a tool for visualizing and accessing data from comparisons of multiple vertebrate genomes', *Nucleic Acids Res* 32(Web Server issue): W280-6.

Picker, A., Brennan, C., Reifers, F., Böhli, H., Holder, N. and Brand, M. (1999) 'Requirement for zebrafish *acerebellar*/FGF8 in midbrain polarization, mapping and confinement of the retinotectal projection', *Development* 126: 2967-2978.

Picker, A., Cavodeassi, F., Machate, A., Bernauer, S., Hans, S., Abe, G., Kawakami, K., Wilson, S. W. and Brand, M. (2009) 'Dynamic coupling of pattern formation and morphogenesis in the developing vertebrate retina', *PLoS Biol* 7(10): e1000214.

Rembold, M., Loosli, F., Adams, R. J. and Wittbrodt, J. (2006) 'Individual cell migration serves as the driving force for optic vesicle evagination', *Science* 313(5790): 1130-4.

Rowan, S., Chen, C. M., Young, T. L., Fisher, D. E. and Cepko, C. L. (2004) 'Transdifferentiation of the retina into pigmented cells in ocular retardation mice defines a new function of the homeodomain gene Chx10', *Development* 131(20): 5139-52.

Rozen, S. and Skaletsky, H. (2000) 'Primer3 on the WWW for general users and for biologist programmers', *Methods Mol Biol* 132: 365-86.

Sandelin, A., Wasserman, W. W. and Lenhard, B. (2004) 'ConSite: web-based prediction of regulatory elements using cross-species comparison', *Nucleic Acids Res* 32(Web Server issue): W249-52.

Santagati, F. and Rijli, F. M. (2003) 'Cranial neural crest and the building of the vertebrate head', *Nat Rev Neurosci* 4(10): 806-18.

Schier, A. F., Neuhauss, S. C., Helde, K. A., Talbot, W. S. and Driever, W. (1997) 'The one-eyed pinhead gene functions in mesoderm and endoderm formation in zebrafish and interacts with no tail', *Development* 124(2): 327-42.

Schwarz, M., Cecconi, F., Bernier, G., Andrejewski, N., Kammandel, B., Wagner, M. and Gruss, P. (2000) 'Spatial specification of mammalian eye territories by reciprocal transcriptional repression of Pax2 and Pax6', *Development* 127: 4325-4334.

Shimeld, S. M. and Holland, P. W. (2000) 'Vertebrate innovations', *Proc Natl Acad Sci U S A* 97(9): 4449-52.

Smith, A. N., Miller, L. A., Radice, G., Ashery-Padan, R. and Lang, R. A. (2009) 'Stage-dependent modes of Pax6-Sox2 epistasis regulate lens development and eye morphogenesis', *Development* 136(17): 2977-85.

Splinter, E., de Wit, E., van de Werken, H. J., Klous, P. and de Laat, W. (2012) 'Determining long-range chromatin interactions for selected genomic sites using 4C-seq technology: from fixation to computation', *Methods* 58(3): 221-30.

Sprague, J., Clements, D., Conlin, T., Edwards, P., Frazer, K., Schaper, K., Segerdell, E., Song, P., Sprunger, B. and Westerfield, M. (2003) 'The Zebrafish Information Network (ZFIN): the zebrafish model organism database', *Nucleic Acids Res* 31(1): 241-3.

Stigloher, C., Ninkovic, J., Laplante, M., Geling, A., Tannhauser, B., Topp, S., Kikuta, H., Becker, T. S., Houart, C. and Bally-Cuif, L. (2006) 'Segregation of telencephalic and eye-field identities inside the zebrafish forebrain territory is controlled by Rx3', *Development* 133(15): 2925-35.

Stormo, G. D. (2000) 'DNA binding sites: representation and discovery', *Bioinformatics* 16(1): 16-23.

Straub, R. E., MacLean, C. J., Ma, Y., Webb, B. T., Myakishev, M. V., Harris-Kerr, C., Wormley, B., Sadek, H., Kadambi, B., O'Neill, F. A. et al. (2002) 'Genome-wide scans of three independent sets of 90 Irish multiplex schizophrenia families and follow-up of selected regions in all families provides evidence for multiple susceptibility genes', *Mol Psychiatry* 7(6): 542-59.

Sundaram, S. K., Huq, A. M., Sun, Z., Yu, W., Bennett, L., Wilson, B. J., Behen, M. E. and Chugani, H. T. (2011) 'Exome sequencing of a pedigree with Tourette syndrome or chronic tic disorder', *Ann Neurol* 69(5): 901-4.

Truslove, G. M. (1962) 'A gene causing ocular retardation in the mouse', *J Embryol Exp Morphol* 10: 652-60.

Varga, Z. M., Wegner, J. and Westerfield, M. (1999) 'Anterior movement of ventral diencephalic precursors separates the primordial eye field in the neural plate and requires cyclops', *Development* 126(24): 5533-46.

Vitorino, M., Jusuf, P. R., Maurus, D., Kimura, Y., Higashijima, S. and Harris, W. A. (2009) 'Vsx2 in the zebrafish retina: restricted lineages through derepression', *Neural Dev* 4: 14.

Vogel-Hopker, A., Momose, T., Rohrer, H., Yasuda, K., Ishihara, L. and Rapaport, D. H. (2000) 'Multiple functions of fibroblast growth factor-8 (FGF-8) in chick eye development', *Mech Dev* 94(1-2): 25-36.

Wasserman, W. W. and Sandelin, A. (2004) 'Applied bioinformatics for the identification of regulatory elements', *Nat Rev Genet* 5(4): 276-87.

Wilson, S. W. and Houart, C. (2004) 'Early steps in the development of the forebrain', *Dev Cell* 6(2): 167-81.

Winkler, S., Loosli, F., Henrich, T., Wakamatsu, Y. and Wittbrodt, J. (2000) 'The conditional medaka mutation eyeless uncouples patterning and morphogenesis of the eye', *Development* 127(9): 1911-1919.

Woolfe, A., Goodson, M., Goode, D. K., Snell, P., McEwen, G. K., Vavouri, T., Smith, S. F., North, P., Callaway, H., Kelly, K. et al. (2005) 'Highly conserved non-coding sequences are associated with vertebrate development', *PLoS Biol* 3(1): e7.

Xiao, A., Wang, Z., Hu, Y., Wu, Y., Luo, Z., Yang, Z., Zu, Y., Li, W., Huang, P., Tong, X. et al. (2013) 'Chromosomal deletions and inversions mediated by TALENs and CRISPR/Cas in zebrafish', *Nucleic Acids Res* 41(14): e141.

Yun, S., Saijoh, Y., Hirokawa, K. E., Kopinke, D., Murtaugh, L. C., Monuki, E. S. and Levine, E. M. (2009) 'Lhx2 links the intrinsic and extrinsic factors that control optic cup formation', *Development* 136(23): 3895-906.

Zou, C. and Levine, E. M. (2012) 'Vsx2 controls eye organogenesis and retinal progenitor identity via homeodomain and non-homeodomain residues required for high affinity DNA binding', *PLoS Genet* 8(9): e1002924.

X. Acknowledgements

Os primeiros nesta lista de agradecimentos são e sempre o serão a minha família. Mãe, Pai e Ana Lúcia, obrigado por todo o apoio e carinho ao longo destes 4 anos (e de toda a minha vida), sem vocês isto não teria sido possível. Obrigado por apoiarem as minhas ideias loucas, que neste caso em especial, até acabou bem!

Obrigado ao meu querido Bruno, o meu companheiro em tudo. Nesta luta tu desempenhaste um papel especial e tu sabes disso! Obrigado por me aturares nos bons e maus momentos, por me obrigares a descansar, por me ajudares com tudo, em casa no lab, onde quer que fosse.

Gracias a todos los miembros de los grupos de JL Gómez Skarmeta y de Juan Martínez que me habéis ayudado a aprender, a investigar, a leer, a ser crítica, a ser autónoma y a seguir adelante. Vosotros me habéis formado como doctora y os agradezco toda la paciencia, cariño y apoyo a lo largo de estos 4 años. En especial a: Ana Neto, JL Royo, Renata, Ze, Ozren, Ana Miñán, Juan Tena, y Mariana. Mariana a ti te doy especialmente las gracias por todo el tiempo que has dedicado a la construcción de esta tesis! Gracias por enseñarme a escribir un "decent english".

María, Rocío y Ozren, gracias especialmente por aguantarme diariamente (sabéis de lo que hablo). Gracias por vuestra amistad, confianza y cariño. María Ángeles, Adela, Manolo, Mario, Carlitos y Ariza, lo mismo. Os agradezco vuestra amistad y cariño. Todos vosotros habéis contribuido para que lo haya pasado bien aquí.

Gracias a los jefes JL Gómez Skarmeta y en especial a Juan Ramón por la oportunidad que me habéis dado de formarme como doctora, por todo lo que me habéis enseñado, por toda la confianza y motivación que siempre supisteis transmitirme a lo largo de este tiempo.

The End

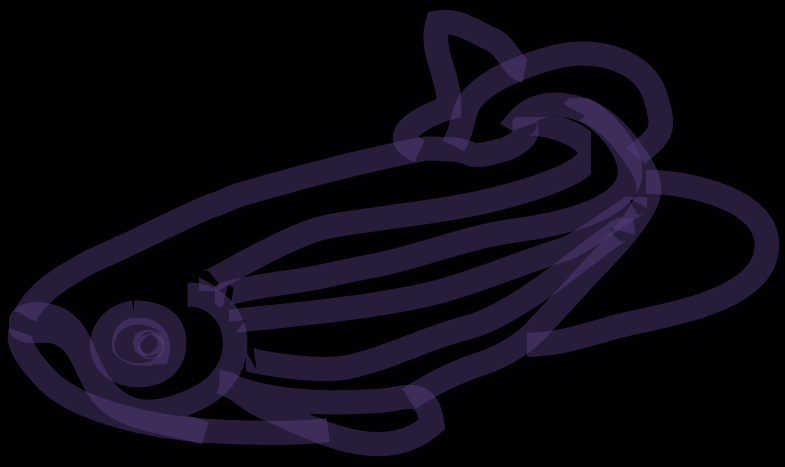

October 2013